MOUNTAIN-PLAINS CONSORTIUM

MPC 22-478 | K. Ng, N. Masud, O. Oluwatuyi, and S. Wulff

DEVELOPMENT OF LRFD RECOMMENDATIONS OF DRIVEN PILES ON INTERMEDIATE GEOMATERIALS

MOUNTAIN-PLAINS CONSORTIUM REGION 8

A University Transportation Center sponsored by the U.S. Department of Transportation serving the Mountain-Plains Region. Consortium members:

Colorado State University
North Dakota State University
South Dakota State University
University of Colorado Denver
University of Denver
University of Utah
Utah State University
University of Wyoming

Technical Report Documentation Page

1. Report No.	2. Government Accession No.	3. Recipient's Catalog No.
MPC-651		

4. Title and Subtitle	5. Report Date
Development of LRFD Recommendations of Driven Piles on Intermediate Geomaterials	August 2022
	6. Performing Organization Code

7. Author(s)	8. Performing Organization Report No.
Kam Ng, Nafis Masud, Opeyemi Oluwatuyi, Shaun S. Wulff	MPC 22-478

9. Performing Organization Name and Address	10. Work Unit No. (TRAIS)
University of Wyoming Dept of Civil & Architectural Engineering and Construction Management Dept of Mathematics & Statistics 1000 E. University Avenue Laramie, Wyoming 82071	11. Contract or Grant No.

12. Sponsoring Agency Name and Address	13. Type of Report and Period Covered
Mountain-Plains Consortium North Dakota State University PO Box 6050, Fargo, ND 58108	Final Report
	14. Sponsoring Agency Code

15. Supplementary Notes

Supported by a grant from the US DOT, University Transportation Centers Program

16. Abstract

This study aims to improve the efficiency of driven piles in intermediate geomaterials (IGMs) to increase the reliability of pile foundations for bridge structures. Test pile data collected from the seven state DOTs and total 223 pile load test data are evaluated to provide recommendations for driven piles in IGMs. A classification method to differentiate fine-grained soil from fine-grained IGMs (FG-IGMs) is established. Shales are classified depending on their weathering conditions, mechanical properties, and measured pile resistances. Newly static analysis (SA) methods for predicting unit shaft resistance (q_s) and unit end bearing (q_b) are proposed and validated for both FG-IGMs and shales. The statistical assessment concludes that the proposed SA methods provide more accurate predictions of q_s and q_b and yield higher LRFD resistance factors than those of the existing SA methods. A back-calculation procedure is adopted to yield recommended dynamic parameters for shale, which are incorporated into a proposed Wave Equation Analysis Program (WEAP) method. An economic study reveals that the proposed WEAP method yields the least excess steel weight, on average, during construction, which will alleviate construction challenges encountered in the current practice, such as higher construction cost and longer construction duration.

17. Key Word	18. Distribution Statement
Driven piles, Intermediate GeoMaterials, Static Analysis Methods, LRFD	Public distribution

19. Security Classif. (of this report)	20. Security Classif. (of this page)	21. No. of Pages	22. Price
Unclassified	Unclassified	102	n/a

Form DOT F 1700.7 (8-72) Reproduction of completed page authorized

DEVELOPMENT OF LRFD RECOMMENDATIONS OF DRIVEN PILES ON INTERMEDIATE GEOMATERIALS

Prepared by:

Kam Ng, Ph.D., P.E., Associate Professor[1]
Nafis Masud, Ph.D. Candidate[1]
Opeyemi Oluwatuyi, Ph.D. Candidate[1]
Shaun S. Wulff, Ph.D., Professor[2]

[1]Department of Civil & Architectural Engineering and Construction Management
[2]Department of Mathematics & Statistics
University of Wyoming
1000 E. University Avenue
Laramie, Wyoming 82071

August 2022

Acknowledgements

The authors would like to thank the Mountain Plains Consortium (MPC) for funding this research project. The authors would like to specially thank the following agencies: the Wyoming Department of Transportation as the lead agency, Colorado Department of Transportation, Iowa Department of Transportation, Kansas Department of Transportation, North Dakota Department of Transportation, Idaho Transportation Department and Montana Department of Transportation under the Grant RS05219.

Disclaimer

ABSTRACT

This study aims to improve the efficiency of driven piles in intermediate geomaterials (IGMs) to increase the reliability of pile foundations for bridge structures. Test pile data collected from the seven state DOTs and total 223 pile load test data are evaluated to provide recommendations for driven piles in IGMs. A classification method to differentiate fine-grained soil from fine-grained IGMs (FG-IGMs) is established. Shales are classified depending on their weathering conditions, mechanical properties, and measured pile resistances. Newly static analysis (SA) methods for predicting unit shaft resistance (q_s) and unit end bearing (q_b) are proposed and validated for both FG-IGMs and shales. The statistical assessment concludes that the proposed SA methods provide more accurate predictions of q_s and q_b and yield higher LRFD resistance factors than those of the existing SA methods. A back-calculation procedure is adopted to yield recommended dynamic parameters for shale, which are incorporated into a proposed Wave Equation Analysis Program (WEAP) method. An economic study reveals that the proposed WEAP method yields the least excess steel weight, on average, during construction, which will alleviate construction challenges encountered in the current practice, such as higher construction cost and longer construction duration.

TABLE OF CONTENTS

LIST OF TABLES

LIST OF FIGURES

EXECUTIVE SUMMARY

The American Association of State Highway and Transportation Officials (AASHTO) Load and Resistance Factor Design (LRFD) Bridge Design Specifications (2020) provide various static analysis (SA) methods for the determination of geotechnical pile resistances in soils for driven piles. In the Rocky Mountain region and some states in the Appalachian region, pile foundations are often driven into intermediate geomaterials (IGM) to support civil infrastructures like bridges due to shallow bedrock stratigraphy. Thus, pile foundations of this region rely on the resistance contributed from the IGM layers. However, IGM is a transitional geomaterial between soil and rock, which is not well defined for the design and construction of driven piles. AASHTO (2020) suggests treating the IGM in the same manner as soil. However, Ng and Sullivan (2017) conducted a recent study on 15 steel H-piles driven on IGMs in Wyoming and concluded that SA methods developed for soil resulted in an inconsistent and conservative estimation of geotechnical resistances. Mokwa and Brooks (2008) also investigated the conventional methods of determining the axial capacity of driven piles in IGMs. They concluded that considerable variation existed between the predicted resistances and resistances determined using a pile driving analyzer (PDA) with a subsequent signal matching technique using the Case Pile Wave Analysis Program (CAPWAP). Thus, there is a critical need to improve the current design construction practices for driven piles in IGMs by establishing representative engineering properties of IGM, developing new SA and constriction control methods, and developing LRFD resistance factors for piles driven into IGM. In the absence of such techniques for IGM, reliable and economical design and construction of driven piles cannot be accomplished.

This study aims to improve the efficiency of driven piles in IGM, which will increase the system reliability of civil infrastructures, especially bridge structures. The objectives of this proposed research are to develop advanced SA methods for pile resistance estimation in IGMs, validate and improve the accuracy of dynamic analysis methods, develop LRFD resistance factors for piles in IGMs, and recommend changes and improvements to current pile design and construction practices. The objectives of the study are achieved by completing these six key tasks: 1) pile data collection, 2) establishment of electronic database, 3) geotechnical and pile data assessment, 4) pile resistance prediction, 5) development of LRFD resistance factors, and 6) LRFD recommendations.

A total of 393 test piles are collected from seven state DOTs: WYDOT, CDOT, KDOT, IADOT, ITD, MDT, and NDDOT. These pile load test data are evaluated to identify their usability and added to an electronic database developed in this study. A total of 223 test piles are usable. The breakdown of these usable piles by DOTs shows that 207 piles are driven in IGMs, and the most common IGM is shale and hard soil with high SPT N-values. In addition, a few test piles are driven into siltstone, granite, breccia, granodiorite, and quartzite. Fine-grained soil-based IGM (FG-IGM) is categorized into clay-IGM and silt-IGM based on their grain size and plasticity. A classification boundary between fine-grained soil and FG-IGM is established at undrained shear strength (s_u) of 2.7 ksf. SA methods for unit shaft resistance (q_s) are recommended based on s_u while SA methods for unit end bearing (q_b) are established using the combination of s_u, pile size, and pile penetration. The proposed SA methods are compared against the existing α-methods developed for soil and validated using 33 independent test pile data. The statistical indices conclude that the proposed SA methods provide a more accurate estimation of q_s and q_b than the α-method. Higher LRFD resistance factors and efficiency factors are determined for the proposed SA methods than those developed for fine-grained soils. An average 48% increase can be considered in the q_s prediction of steel H-piles in FG-IGM at one day after the EOD. However, pile setup should be neglected in the q_b prediction, and potential pile relaxation in q_b should be accounted for during the design and construction of piles in FG-IGM. Shales are classified based on weathering conditions, mechanical properties, and measured pile resistances. Failure behaviors of soil- and rock-based shales are discussed. Prediction equations are developed based on shale properties. Properties of rock-based shales decrease with the increase in weathering. New SA methods are proposed to predict q_s and q_b of piles in shales and

are validated using an independent pile dataset. This study yields higher resistance and efficiency factors for the proposed SA methods developed for piles in shales than existing SA methods developed for piles in soils. The q_s in the soil-based shale exhibits pile setup while the q_s in rock-based shales experience both setup and relaxation. The q_b in both soil-based and highly weathered shales is likely to experience pile setup. However, the q_b in the moderately and slightly weathered shales experience both setup and relaxation.

The development of improved WEAP methods for steel H-piles driven in shale include LRFD recommendations. A back-calculation procedure is adopted to yield recommended dynamic parameters for shale, which are incorporated into two proposed WEAP methods. A range of damping factors from 0.008 to 0.297 s/ft are recommended for two proposed WEAP methods, shale types, and weathering conditions. The accuracy and efficiency of the proposed methods and default WEAP method are validated and compared using 44 dynamic load test results and two static pile load test (SLT) data at the end of driving (EOD). Furthermore, 49 dynamic test results at the beginning of restrike (BOR) condition are also used for comparison. The LRFD resistance and efficiency factors are calibrated for the three WEAP methods for analyzing pile resistances in shale. An economic study reveals that the three WEAP methods, on average, overpredict the weight of steel pile per load demand ranging from -0.31 lb/kips to -0.54 lb/kips. Among the three methods, the proposed WEAP method yields the least excess steel weight, on average, during construction, which will alleviate construction challenges encountered in the current practice, such as higher construction costs and longer duration.

IGM is a transitional material that acts between soil and hard rock, and they are not well defined for the design and construction of driven piles. This study intends to establish the proper definition for IGMs so that IGMs will not be treated as soils during the driven pile design suggested by AASHTO (2020). The heterogeneity of IGMs is considered through the proposed classification criteria for FG-IGMs, which will help design engineers to differentiate different geomaterials in the design of driven piles. The newly developed SA methods yield more accurate pile resistance estimation than the existing SA methods; the discrepancy between measured and estimated resistance based on the existing method will be minimized. Calibrated resistance factors are developed for the proposed SA methods and construction control methods to improve the reliability of pile design and construction. Finally, economic driven pile design and construction can be achieved, which will minimize additional costs, avoid construction delays, and avoid unnecessary conflicts between contractors and owners.

1. INTRODUCTION

1.1 Background

Due to a relatively shallow bedrock stratigraphy in the Rocky Mountain region and some states in the Appalachian region, pile foundations are often driven on and into rock to support structures like bridges. The pile foundation must rely on the resistance contributed from the rock-bearing layer to attain the increasing demand in capacity from structures and to satisfy the load and resistance factor design (LRFD) strength limit state. However, this rock-bearing layer usually has high natural variability, and the associated engineering characteristics may not be fully characterized. Furthermore, intermediate GeoMaterial (IGM), also known as soft rock, is a transitional geomaterial between soil and hard rock, which is not well defined for the design and construction of driven piles. This variability creates challenges in identifying, sampling, and quantifying of IGM materials (Long and Horsfall 2017). In fact, the American Association of State Highway and Transportation Officials (AASHTO) (2020) acknowledges that there are currently no acceptable approaches to differentiate soft from hard rocks for the design of driven piles. Local experience with driving piles on soft rocks shall be applied to define their quality. However, limited test results are available to describe the characteristics and engineering properties of IGM (Adhikari et al. 2020c).

Reliable static analysis methods have not yet been developed to estimate the pile resistance in IGMs. AASHTO (2020) suggests that piles driven on soft rock shall be treated in the same manner as soil. However, a past research study based on 15 steel H-piles driven in IGMs in Wyoming concluded that static analysis methods originally developed for soil provided inconsistent and conservative geotechnical resistance estimations (Ng and Sullivan 2017a). The pile load tests conducted by Long (2016) found large differences between estimated and measured pile resistances. The limitation on the estimation of pile resistances creates challenges during the pile design stage.
The resistances of piles driven in IGMs are currently determined using dynamic analysis or static load tests during construction. AASHTO (2020) recommends that piles be driven based on locally developed criteria to prevent pile damage. The Wisconsin Department of Transportation (WisDOT) revealed that steel H-piles have been found to either run longer than the design length or be damaged during driving when a higher pile driving criterion is established (Long and Horsfall 2017). WisDOT acknowledged that there are still unknowns with both the design and construction of steel H-piles in IGMs. In Wyoming, pile driving will be terminated when a target nominal pile resistance is achieved at the planned depth as determined from the wave equation analysis method (WEAP) on all production piles. The Pile Driving Analyzer (PDA), with subsequent signal matching analysis using the Case Pile Wave Analysis Program (CAPWAP), is used as a construction control method on about only 2% of the production piles. PDA/CAPWAP tests are recommended in bridge projects experiencing relatively high load demand and soft rock bearing. For bridge projects with piles driven in IGMs in Wyoming from 2012 and 2015, the performance of some production piles is considered unacceptable in accordance with the LRFD strength limit state recommended by AASHTO (Ng and Sullivan 2017b).

These limitations exaggerate the uncertainty of the subsurface condition, the discrepancy between estimated and measured pile resistances, and the difficulty in establishing criteria to differentiate IGM from hard rocks. These factors reduce the accuracy of pile resistance estimation, result in lower LRFD resistance factors, and eventually increase the construction cost.

1.2 Objectives

This research project is proposed to accomplish the following objectives:

1) Develop advanced static analysis methods for pile resistance estimation in IGMs
2) Validate and improve the accuracy of dynamic analysis methods
3) Develop LRFD resistance factors for piles in IGMs
4) Recommend changes and improvements to current pile design and construction practices

1.3 Tasks

The research program is established based on the aforementioned research objectives. The research objectives are achieved by the following major tasks.

1.3.1 Task 1–Pile Data Collection

High quality and usable data containing subsurface, pile, hammer, installation, and load test information are identified and collected from seven DOTs: WYDOT, CDOT, KDOT, IADOT, ITD, MDT, and NDDOT. These pile load test data are evaluated to identify usability, added to an electronic database developed in Task 2, and included for subsequent analyses described in Tasks 3 through 6.

1.3.2 Task 2–Electronic Database

All usable pile data are compiled and stored in an electronic database similarly developed for WYDOT using Microsoft Office Access™. This electronic database enables the delivery of an organized storage facility with a user-friendly interface. This database has the capability of performing efficient filtering, sorting, and querying procedures on the amassed pile dataset. This electronic database allows for the efficient performance of reference and analysis procedures on the comprehensive dataset.

1.3.3 Task 3–Geotechnical and Pile Data Assessment

Using the pile data collected in Task 1, subsurface profiles are constructed, pile embedded length and penetration into the IGM are determined, soil and IGM characteristics are identified, and pile, driving, hammer, restrike and load test information are interpreted. Technical reports are reviewed to determine properties of the overburden soils and underlying IGM as well as pile information necessary for pile resistance estimation in Task 4.

1.3.4 Task 4–Pile Resistance Prediction

Shaft resistance, end bearing, and total resistance of driven piles are predicted using static analysis methods and dynamic analysis methods. Advanced static analysis methods are developed to improve resistance prediction of piles driven in IGMs during the design stage. Using the measured pile resistances obtained from static load tests or CAPWAP, regression analysis is performed to develop static analysis methods for pile resistance prediction. The new static analysis methods are validated using independent pile data obtained from the seven DOTs and literature. Pile resistances are estimated using WEAP at the EOD and BOR events. Estimated resistances from a bearing graph analysis are compared with resistances determined from load tests. Procedures to improve pile resistance estimations using WEAP are established.

1.3.5 Task 5–Development of LRFD Resistance Factors

The predicted pile resistance from proposed static analysis methods and WEAP in Task 4 are compared with the measured pile resistance from the load test methods. Resistance bias is determined by comparing the predicted pile resistance to the observed pile resistance. LRFD resistance factors are determined using the probability-based reliability methods: the first-order reliability method (FORM), first-order second moment (FOSM) method, and Monte Carlo simulation. The reliability methods will ensure that the regionally calibrated resistance factors satisfy the LRFD framework as required by AASHTO (2020). The LRFD resistance factors are developed based on the assumptions made in the reliability methods such as those recommended numerical values for probabilistic characteristics of loads (Paikowsky et al. 2004; Allen 2005). Reliability indices of 2.33 and 3.00 for a redundant pile group (i.e., a group of five or more piles) and a non-redundant pile group are used in the calibration. Finally, a set of resistance factors for both design and construction control methods are recommended.

1.3.6 Task 6–LRFD Recommendations

Upon completion of Tasks 1 through 5, LRFD recommendations are established to facilitate the design and construction of driven piles in IGMs. The LRFD recommendations in terms of the following deliverables are summarized as follows:

1) An electronic database of pile data
2) A catalog of representative IGM properties for pile designs
3) A catalog of unit shaft resistance and end bearing to facilitate pile designs
4) An improved classification of geomaterials for piles driven in IGMs
5) Recommendation of calibrated static analysis methods for the improved estimation of shaft resistance and end bearing of piles driven in different IGMs
6) Recommendation for improving pile resistance estimation by WEAP
7) A set of recommended LRFD resistance factors for design and construction control methods
8) Recommended best design and construction practices for piles driven in IGMs

1.4 Report Focus and Organization

This report focuses on developing LRFD recommendations for driven piles in IGMs. This report is designed to enable designers and engineers to use the LRFD recommendations in the design and construction of driven piles in IGMs. Chapter 1 presents the background, objectives, and tasks of this research. A description of the electronic dataset is presented in Chapter 2. Chapter 3 focuses on piles driven in fine-grained soil-based IGMs. Chapter 4 describes the analysis, results, and recommendations for piles driven in rock-based shale. Chapter 5 presents the improved WEAP methods. Chapter 6 presents the development of LRFD resistance factors. Finally, summary, recommendations, and conclusions are presented in Chapter 7, which is followed by the Reference section.

2. PILE DATA COLLECTION AND ELECTRONIC DATABASE

2.1 Introduction

Pile data are collected for developing foundation design. The accuracy and cost-effectiveness of a design are dependent on sample size and data reliability. However, data collection for geotechnical and structural analyses can be expensive and time-consuming (Machairas et al. 2018). Another challenge is to have the collected data in available databases in an organized and easily accessible format to be used as an information source for design, research, and development. Other desirable features of an electronic database include high quality and complete data, system flexibility, user-friendly interface, maintenance, and online accessibility (Abu-Hejleh et al. 2015). There have been attempts to organize pile load test data using electronic database systems. An example is the WyoPile briefly discussed below.

2.1.1 WyoPile

A database, namely WyoPile (Ng et al. 2019), is developed using the dynamic load tests of 45 test piles provided by the Wyoming Department of Transportation (WYDOT) from 17 bridge projects and one building project. This database collected information on site location, subsurface conditions, pile type and location, hammer information, pile driving information, and pile resistance from a dynamic load test. The database is created as a part of a research study to develop static analysis methods for piles driven in intermediate geomaterials (IGMs), and regional-specific LRFD resistance factor calibration.

2.1.2 Historical Pile Load Test Data

Like the WyoPile database developed for dynamic load test of driven H-piles from Wyoming, a comprehensive database is developed in this study for other transportation agencies: Colorado Department of Transportation (CDOT), Montana Department of Transportation (MDT), North Dakota Department of Transportation (NDDOT), Idaho Transportation Department (ITD), Iowa Department of Transportation (IADOT), and Kansas Department of Transportation (KDOT). Additional test piles from WYDOT are added to the WyoPile database. Information on the driven test piles from the corresponding states are also collected. In general, the collected information consists of hard copy reports as PDFs as well as digital reports as EXCEL spreadsheets. The complete information for a pile load test usually includes the project plan, pile information and driving records, hammer information, load test results (end of initial driving [EOD] and beginning of restrike [BOR]), and subsurface information (geotechnical reports or boring logs). Test piles with complete information are considered usable, whereas those with incomplete information are rendered as non-usable. The pile penetration depths in the load test reports are matched with the subsurface information using the pile bottom elevation and cutoff elevation from the design plan of the construction project.

A total of 393 test piles are collected from the seven state DOTs. A total of 223 test piles are usable. The breakdown of these usable piles by DOT is shown in Figure 2.2. Of the 223 usable test piles, 207 are drilled in IGMs and the breakdown is shown in Figure 2.3. The most common IGM is shale. In addition, a few test piles are driven into granite, breccia, granodiorite, and quartzite.

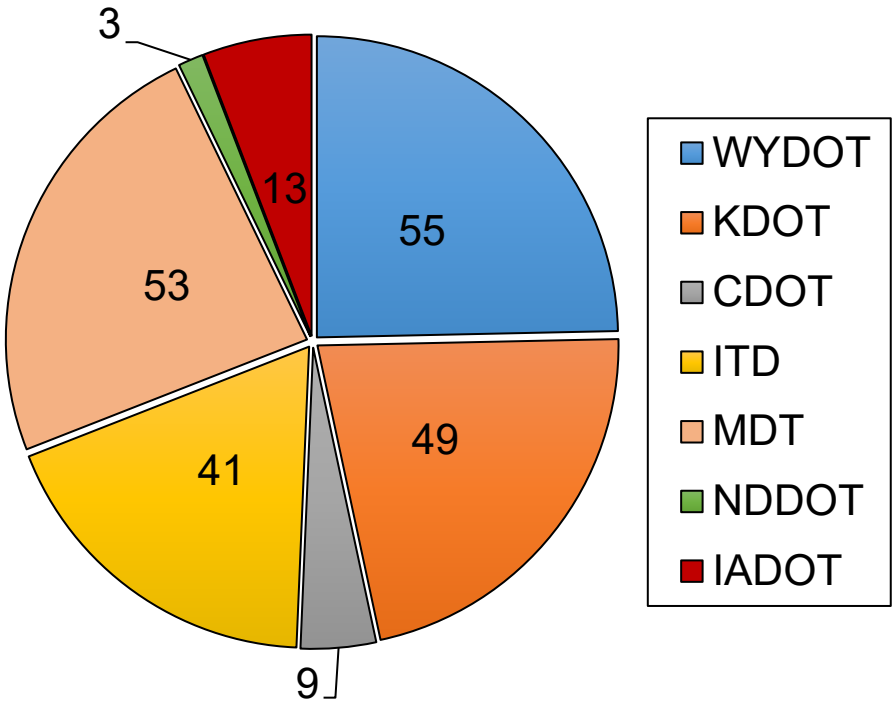

Figure 2.1 Breakdown of the 223 usable test piles collected from the seven states

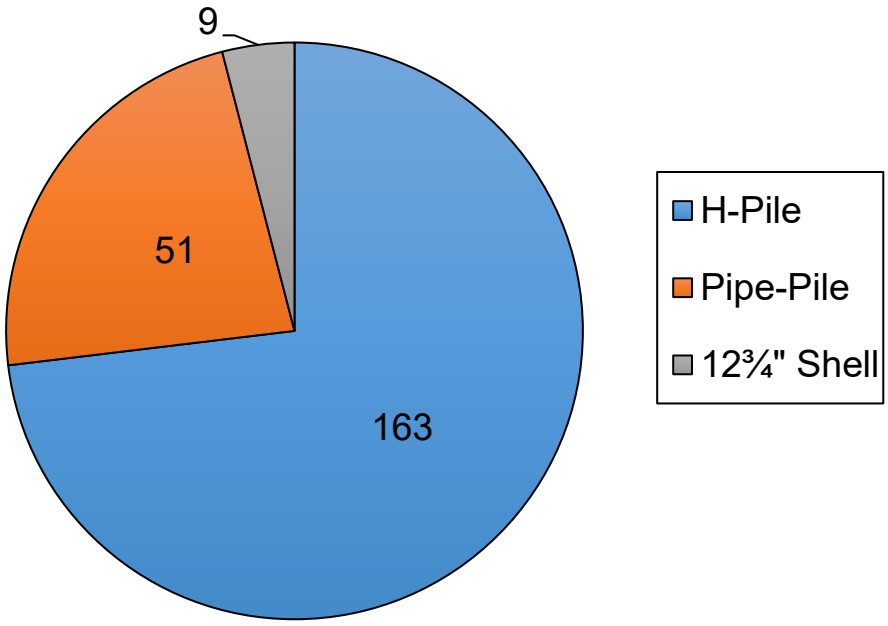

Figure 2.2 Breakdown of the 223 usable test piles collected according to pile type

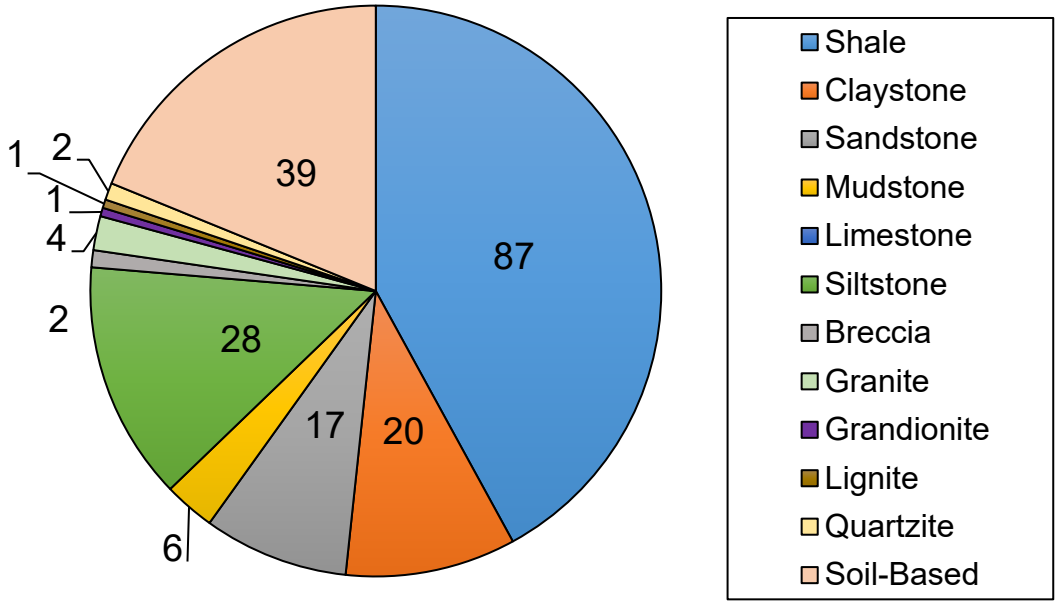

Figure 2.3 Breakdown of the 207 usable test piles collected according to known IGMs

2.2 Database Overview

Microsoft Access provides a user-friendly and easy-to-use tool for creating the database. The access database and the user manual are described in this chapter using the database created for the MDT, which is known as MontanaPile. The organization and the use of the database are propagated similarly across the database created for other state transportation agencies. The database consists of four major sections to describe the test pile records: pile test records, average subsurface profile, nominal unit shaft resistance, and nominal unit end bearing. Figure 2.4 shows a partial screenshot of the MontanaPile to represent the layout of the "Pile Load Test Records." The Pile Load Test Records consist of the general information regarding the driven test piles, such as pile ID, project number, state, county, project name or bridge/structure, pile location, LRFD factored design load, pile type, date of driving, pile elevations, and driving information such as hammer type, stroke height, blow count, CAPWAP measured capacity at each EOD, and subsequent restrikes. The test pile reports and subsurface information reports are attached to this section for detailed inspection.

Average Subsurface Profile | Nominal Unit Shaft Resistance | Nominal Unit End Bearing | **Pile Load Test Records**

ID	Project Number	State	County	Bridge/Structure	Pile Location	LRFD Factored load (	Pile Type	Date Driv
1	STPB 44303(2)	MT	Rosebud	Bridge Over Butte Creek	Bent 1, Pile 4	457	conical point	8/6/20
2	STPB 9003(50)	MT	Blaine	Milk River - 4 KM West Of Zurich	Bent 1, Pile 1	560	P with 0.5" w	6/19/2(
3	STPB 9003(50)	MT	Blaine	Milk River - 4 KM West Of Zurich	Bent 2, Pile 6	500	le fit cut shoe	5/22/2(
4	STPB 9003(50)	MT	Blaine	Milk River - 4 KM West Of Zurich	Bent 3, Pile 1	560	le fit cut shoe	4/17/2(
5	BR 81-1(11)34	MT	Fergus	Bridge Over Warm Spring Creek	Bent 1	1057	P with 0.75" w	8/15/2(
6	BR 81-1(11)34	MT	Fergus	Bridge Over Warm Spring Creek	Bent 2	1057	P with 0.75" w	8/20/2(
7	BR 253-1(11)4	MT	Prairie	Bridge Over Cherry Creek	Bent 1, Pile 2	674	P with 0.5" w	

Figure 2.4 Partial screenshot of MontanaPile showing the "Pile Load Test Records" table

The next major section of the database consists of the average subsurface profile. Figure 2.5 shows a partial screenshot of the MontanaPile showing the "Average Subsurface Profile" table. In this section, the subsurface profile obtained from the respective boring logs are shown as individual layers. The section includes layer number, pile ID (record ID), geomaterial type, descriptions provided in the boring logs or geotechnical reports, the thickness of the individual geomaterial layers, and relevant geomaterial properties such as SPT N-value, q_u, s_u, cohesion, friction angle, and RQD for rock geomaterial. These subsurface layers are extracted from the nearest boring logs by matching the pile top and toe elevations from the driving information provided in the dynamic load test reports. The dynamic load test results are used to match the pile resistances measured to the individual geomaterial layers to determine the unit shaft resistance and unit end bearing of those layers. The measured CAPWAP resistances are then updated on the database in the "Nominal Unit Shaft Resistance" and "Nominal Unit End Bearing" sections of the database represented by the partial screenshots of MontanaPile in Figures 2.6 and 2.7, respectively.

Average Subsurface Profile

Record ID	State	Layer	Geomaterial	Description	Thickness (ft)	SPT N	qu (ksf)	Su (ksf)
1	MT	1	Sandy Lean CLAY (CL)	stiff, dry, brown, Ocassional Orange stain	1.74	7		2.473
1	MT	2	Porly Graded Gravel With Sand (GP)	n dense, dry, tan, fine to coarse grained, r	3.5	27		
1	MT	3	Poorly graded SAND with gravel (SP)	iedium dense, dry to wet, tan, fine to coar	13.899	13		
1	MT	4	CLAYSTONE	gray, very soft field hardness	5.8	79	10.656	
1	MT	5	CLAYSTONE	gray, very soft field hardness	3.4		15.84	
2	MT	1	SAND (SM)	y loose to loose dry to wet, tan, fine, grai	18.3	6		
2	MT	2	Fat CLAY (CH)	medium,stiff,moist, brown	5.5	7		2.473
2	MT	3	Silty, Clayey SAND (SC-SM)	Loose, moist to wet. Brown	10	6		
2	MT	4	Sandy SILT (ML)	se to medium dense, wet, gray to tan, fine	20.5	17		4.684
2	MT	5	Sandy Lean CLAY(CL)	Very stiff, moist, brown	15	21		5.453
2	MT	6	Sandy CLAYSTONE	ed, medium bedded, soft field hardness, o	7	100	56.34	
2	MT	7	SANDSTONE	ie grained, thickly bedded, medium field h	4	167		
2	MT	8	Sandy CLAYSTONE	ed, medium bedded, soft field hardness, C	1.9		163.1	
3	MT	1	Sandy Lean CLAY(CL)	Medium stiff to stiff, wet, gray	14.099	13		3.861
3	MT	2	Poorly graded SAND (SC)	medium , dense, wet, brown	10.5	12		
3	MT	3	Silty SAND with Gravel (SM)	medium dense to dense, wet ,gray	22	25		
3	MT	4	Sandy CLAYSTONE	l, medium bedded, very soft to medium fi	3.7		56.304	

Figure 2.5 Partial screenshot of the MontanaPile showing the "Average Subsurface Profile" table

Average Subsurface Profile | Nominal Unit Shaft Resistance

Pile Rec ID	Layer	State	Geomaterial	Thickness (ft)	CAPWAP(ksf)	Remarks
1	1	MT	Sandy Lean CLAY (CL)	1.74	0.28	
1	2	MT	Porly Graded Gravel With Sand (GP)	3.5	0.28	
1	3	MT	Poorly graded SAND with gravel (SP)	13.9	0.64	
1	4	MT	CLAYSTONE	5.8	1.15	
1	5	MT	CLAYSTONE	3.4	1.27	
2	1	MT	SAND (SM)	18.3	0.12	
2	2	MT	Fat CLAY (CH)	5.5	0.25	
2	3	MT	Silty, Clayey SAND (SC-SM)	10	0.1	
2	4	MT	Sandy SILT (ML)	20.5	0.1	
2	5	MT	Sandy Lean CLAY(CL)	15	0.59	
2	6	MT	Sandy CLAYSTONE	7	2.28	
2	7	MT	SANDSTONE	4	3.6	
2	8	MT	Sandy CLAYSTONE	1.9	3.6	

Figure 2.6 Partial screenshot of the MontanaPile showing the "Nominal Unit Shaft Resistance" table

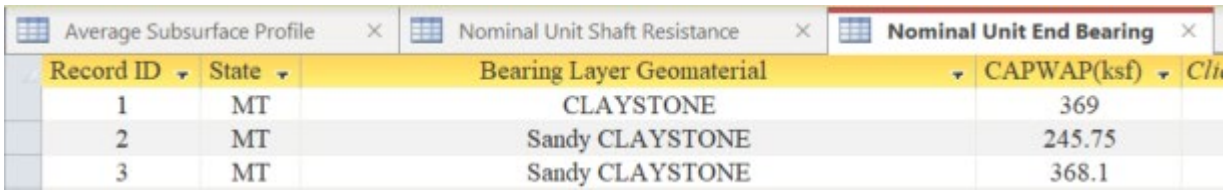

Record ID	State	Bearing Layer Geomaterial	CAPWAP(ksf)	Cli
1	MT	CLAYSTONE	369	
2	MT	Sandy CLAYSTONE	245.75	
3	MT	Sandy CLAYSTONE	368.1	

Figure 2.7 Partial screenshot of the MontanaPile showing the "Nominal Unit End Bearing" table

2.3 User Manual for the Electronic Database

The user manual provides detailed step-by-step information on how to access and use the electronic databases for each of the seven states, namely WyoPile for WYDOT, IowaPile for IADOT, IdahoPile for IDT, NorthDakotaPile for NDDOT, ColoradoPile for CDOT, and KanasPile for KDOT. Microsoft Access must be installed on a computer to use one of these databases. The database can be accessed by opening the database files from any location on the computer, such as the desktop, hard drive, USB flash drives, or network drive. As an example, the database files are shown in the partial screenshot in Figure 2.8. The database is designed such that the home screen of the database always shows the "Pile Load Test List" form and navigation pane window, which act as the access point of all other tables and forms. Figure 2.9 shows the home screen for the database along with different tables, forms, and queries attached to the database. Each table, form, or query can be accessed individually by double clicking the respective "object" in the navigation pane. All the general information is stored and can be accessed from the "Pile Load Test List" form. Additional information is stored in specific tables and forms. To view the detailed information of the individual test pile, "ID" can be clicked to open the "Pile Load Test Records" form. The "Pile Load Test Records" form for "ID 1" is shown in Figure 2.10. All the information such as "Subsurface Profile," "Nominal Shaft Resistance," "Nominal Unit End bearing," "Driving Information," "Dynamic Test Analysis Result," and" Static Load Test Result" can be accessed as individual tabs as shown in Figure 2.11.

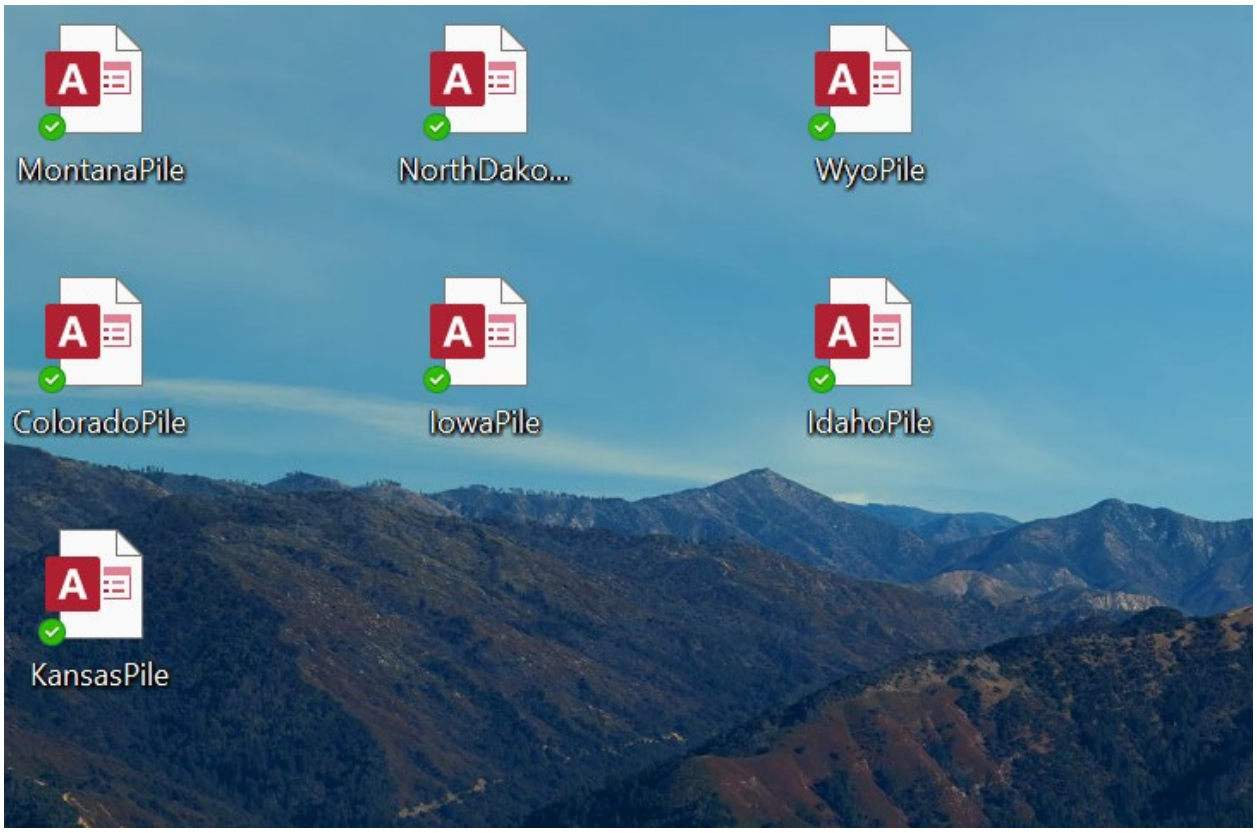

Figure 2.8 Partial screenshot of the desktop showing all database files stored on the hard drive of the computer

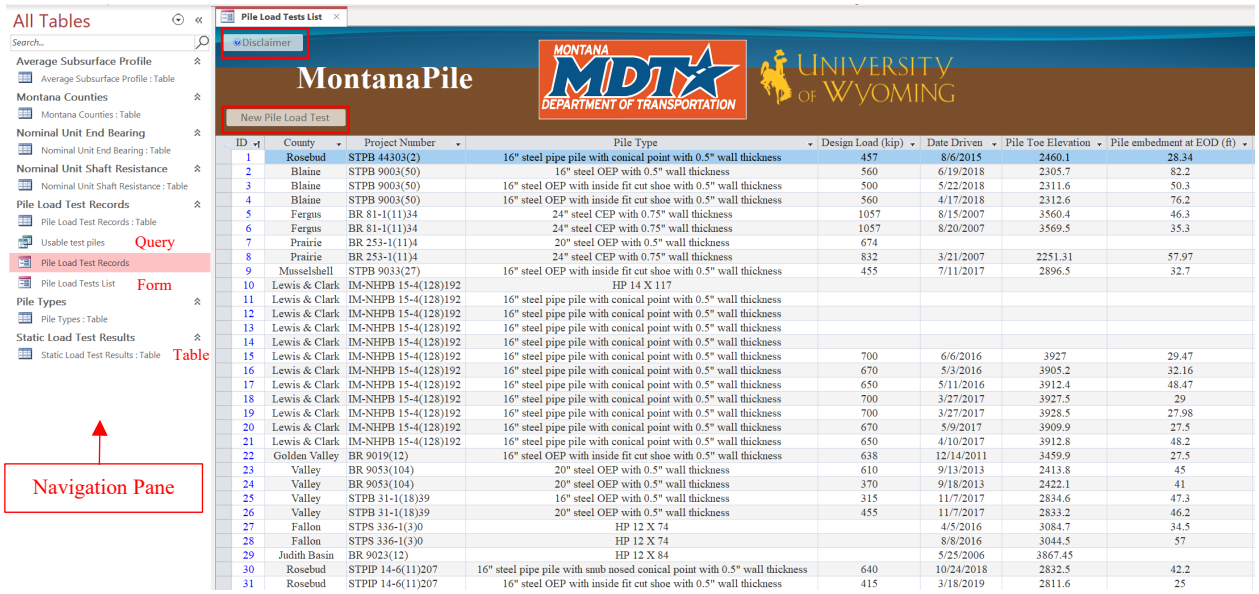

ID	County	Project Number	Pile Type	Design Load (kip)	Date Driven	Pile Toe Elevation	Pile embedment at EOD (ft)
1	Rosebud	STPB 44303(2)	16" steel pipe pile with conical point with 0.5" wall thickness	457	8/6/2015	2460.1	28.34
2	Blaine	STPB 9003(50)	16" steel OEP with 0.5" wall thickness	560	6/19/2018	2305.7	82.2
3	Blaine	STPB 9003(50)	16" steel OEP with inside fit cut shoe with 0.5" wall thickness	500	5/22/2018	2311.6	50.3
4	Blaine	STPB 9003(50)	16" steel OEP with inside fit cut shoe with 0.5" wall thickness	560	4/17/2018	2312.6	76.2
5	Fergus	BR 81-1(11)34	24" steel CEP with 0.75" wall thickness	1057	8/15/2007	3560.4	46.3
6	Fergus	BR 81-1(11)34	24" steel CEP with 0.75" wall thickness	1057	8/20/2007	3569.5	35.3
7	Prairie	BR 253-1(11)4	20" steel OEP with 0.5" wall thickness	674			
8	Prairie	BR 253-1(11)4	24" steel CEP with 0.75" wall thickness	832	3/21/2007	2251.31	57.97
9	Musselshell	STPB 9033(27)	16" steel OEP with inside fit cut shoe with 0.5" wall thickness	455	7/11/2017	2896.5	32.7
10	Lewis & Clark	IM-NHPB 15-4(128)192	HP 14 X 117				
11	Lewis & Clark	IM-NHPB 15-4(128)192	16" steel pipe pile with conical point with 0.5" wall thickness				
12	Lewis & Clark	IM-NHPB 15-4(128)192	16" steel pipe pile with conical point with 0.5" wall thickness				
13	Lewis & Clark	IM-NHPB 15-4(128)192	16" steel pipe pile with conical point with 0.5" wall thickness				
14	Lewis & Clark	IM-NHPB 15-4(128)192	16" steel pipe pile with conical point with 0.5" wall thickness				
15	Lewis & Clark	IM-NHPB 15-4(128)192	16" steel pipe pile with conical point with 0.5" wall thickness	700	6/6/2016	3927	29.47
16	Lewis & Clark	IM-NHPB 15-4(128)192	16" steel pipe pile with conical point with 0.5" wall thickness	670	5/3/2016	3905.2	32.16
17	Lewis & Clark	IM-NHPB 15-4(128)192	16" steel pipe pile with conical point with 0.5" wall thickness	650	5/11/2016	3912.4	48.47
18	Lewis & Clark	IM-NHPB 15-4(128)192	16" steel pipe pile with conical point with 0.5" wall thickness	700	3/27/2017	3927.5	29
19	Lewis & Clark	IM-NHPB 15-4(128)192	16" steel pipe pile with conical point with 0.5" wall thickness	700	3/27/2017	3928.5	27.98
20	Lewis & Clark	IM-NHPB 15-4(128)192	16" steel pipe pile with conical point with 0.5" wall thickness	670	5/9/2017	3909.9	27.5
21	Lewis & Clark	IM-NHPB 15-4(128)192	16" steel pipe pile with conical point with 0.5" wall thickness	650	4/10/2017	3912.8	48.2
22	Golden Valley	BR 9019(12)	16" steel OEP with inside fit cut shoe with 0.5" wall thickness	638	12/14/2011	3459.9	27.5
23	Valley	BR 9053(104)	20" steel OEP with 0.5" wall thickness	610	9/13/2013	2413.8	45
24	Valley	BR 9053(104)	20" steel OEP with 0.5" wall thickness	370	9/18/2013	2422.1	41
25	Valley	STPB 31-1(18)39	16" steel OEP with 0.5" wall thickness	315	11/7/2017	2834.6	47.3
26	Valley	STPB 31-1(18)39	20" steel OEP with 0.5" wall thickness	455	11/7/2017	2833.2	46.2
27	Fallon	STPS 336-1(3)0	HP 12 X 74		4/5/2016	3084.7	34.5
28	Fallon	STPS 336-1(3)0	HP 12 X 74		8/8/2016	3044.5	57
29	Judith Basin	BR 9023(12)	HP 12 X 84		5/25/2006	3867.45	
30	Rosebud	STPIP 14-6(11)207	16" steel pipe pile with snub nosed conical point with 0.5" wall thickness	640	10/24/2018	2832.5	42.2
31	Rosebud	STPIP 14-6(11)207	16" steel OEP with inside fit cut shoe with 0.5" wall thickness	415	3/18/2019	2811.6	25

Figure 2.9 Partial screenshot of MontanaPile representing the home screen and navigation pane

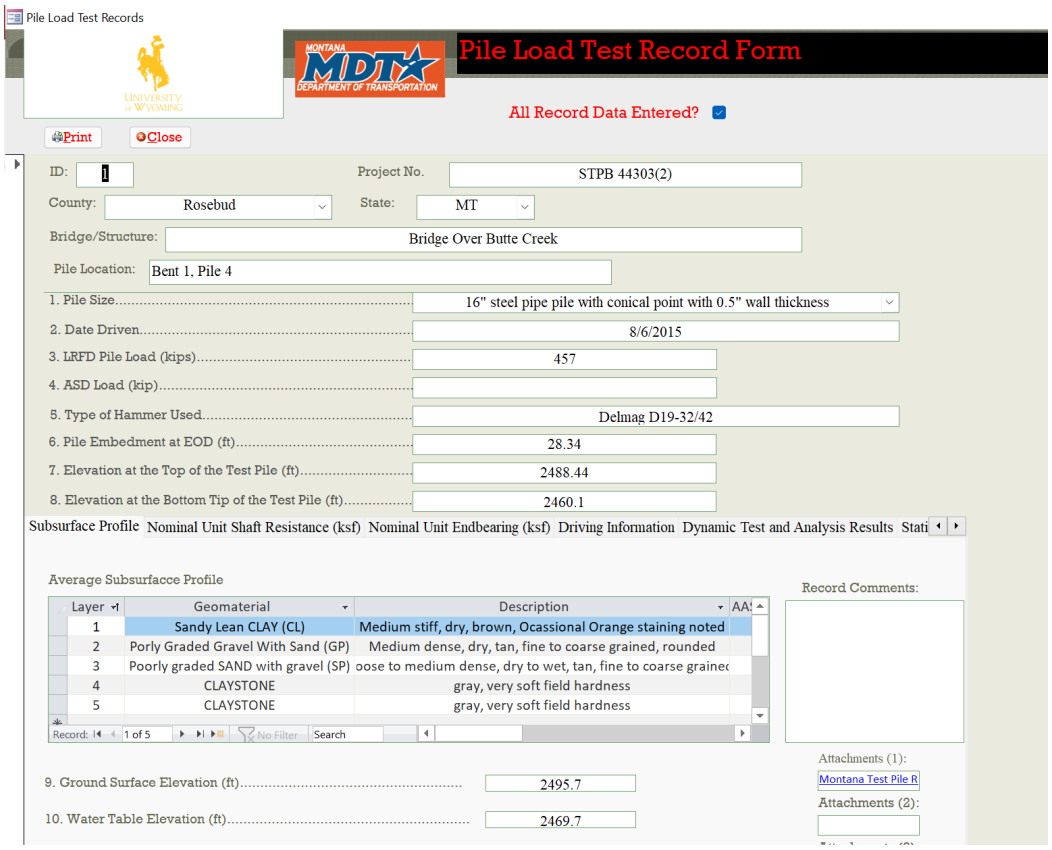

Figure 2.10 Partial screenshot of MontanaPile representing the "Pile Load Test Records" form for ID 1

The main form also includes a "New Pile Load Test" tab, shown in Figure 2.9, that can be clicked to access an input form for future pile load tests. All information input on that form automatically spreads over the tables and forms across the database. A sample of this form is presented as a partial screenshot in Figure 2.10. There is an option to print the pile test record using a "Print" tab in each "Pile Load Test Record" form as shown in Figure 2.11. It is recommended to print the data in a landscape paper layout. Also, disclaimers for all the databases are present in the "Disclaimer" tab at the right-hand top of the "Pile Load Test List" form, which is shown in Figure 2.9.

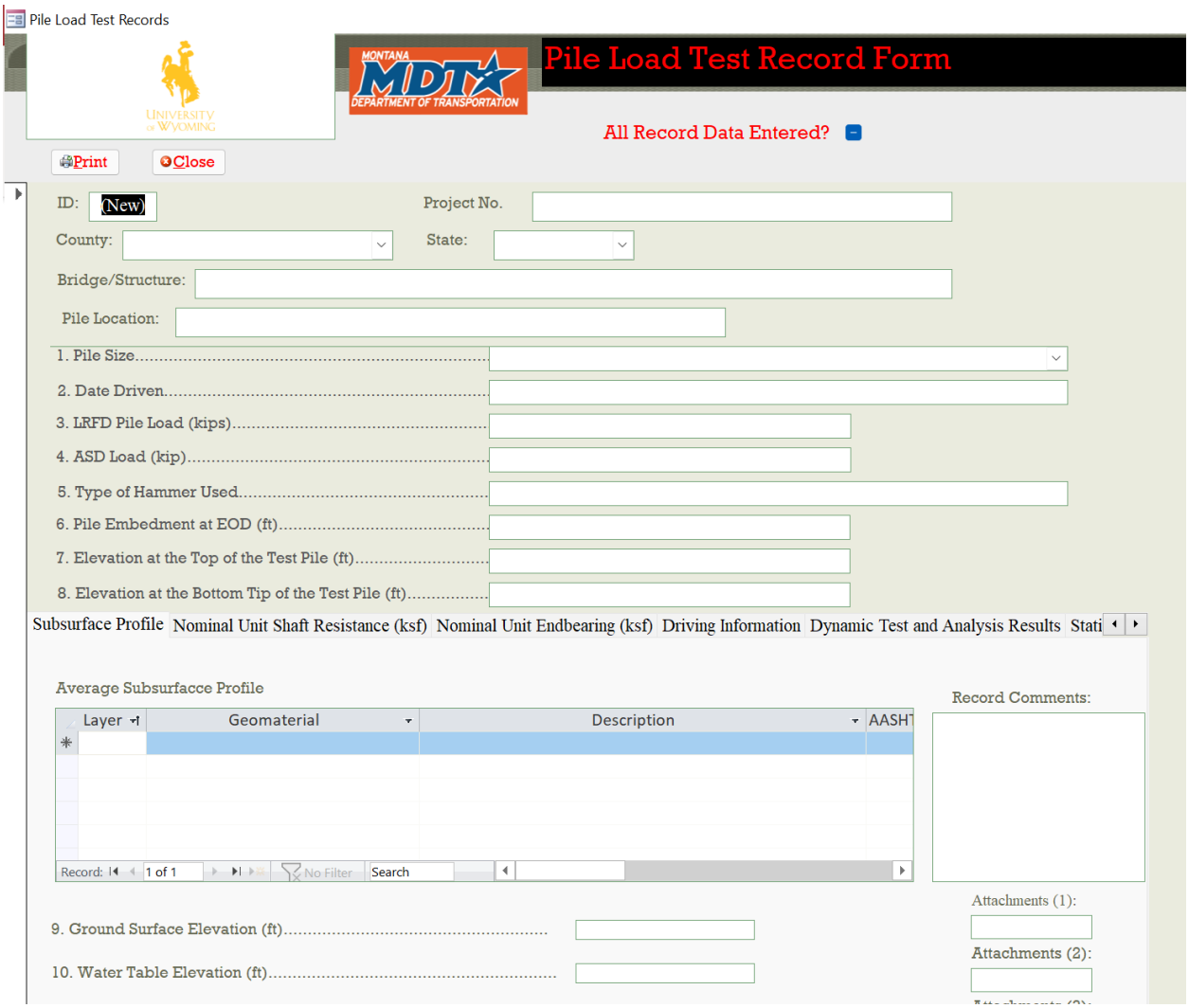

Figure 2.11 Partial screenshot of MontanaPile representing the "Pile Load Test Records" form for future pile load test input

The "Pile Load Test Records" form asks for information on the test pile. Some of the fields to be filled out for a new test pile record are listed and explained below.

- **All Record Data Entered:** This field allows an input of "Yes" or "No" corresponding to whether all the information has been entered or not. If all the fields in the form are completed, then the tick mark will appear automatically.
- **ID:** This is a unique number assigned automatically to the test pile record by Microsoft Office Access within each database. The "ID" could be the same for different test pile records in separate databases. This field does not need to be entered in the "Pile Load Test Record" form as inputting other fields will automatically assign a value.
- **Project No.:** This field identifies the project number assigned by the respective DOT.
- **County:** This field identifies the county where the project is located. This field can be filled using a drop-down menu consisting of all the counties in the respective state. The respective counties are assigned in a table titled "State Counties." For example, the Montana counties are shown in the partial screenshot in Figure 2.12.

Montana Counties

ID	County	State	Click to Add
1	Big Horn	MT	
2	Blaine	MT	
3	Broadwater	MT	
4	Carbon	MT	
5	Carter	MT	
6	Cascade	MT	
7	Chouteau	MT	
8	Custer	MT	
9	Daniels	MT	
10	Dawson	MT	
11	Deer Lodge	MT	
12	Beaverhead	MT	
13	Fallon	MT	
14	Fergus	MT	
15	Flathead	MT	
16	Gallatin	MT	

Figure 2.12 Partial screenshot of MontanaPile representing the "Montana Counties" table

- **State:** This field asks to enter the state where the project is implemented using a drop-down menu.
- **Bridge/Structure:** This field allows manual input of the name assigned to the bridge or any other structure.
- **Pile Location:** This field allows input of the pile location. The pile location is the identification of the test pile using the pile number in the bent/abutment/pier of the bridge, such as Bent 1, Pile 4.
- **Pile Size:** This field utilizes a drop-down menu for the selection of the test pile size. Most of the test piles types and sizes are already stored in a table titled "Pile Types" in each database. If the user wants to add pile type and size, then the table "Pile Types" can be accessed by double clicking the title in the navigation pane and manually inputting the information on the table. A partial screenshot of the table is shown in Figure 2.13

Pile Types

ID	Pile Type	Click to Add
1	16" steel pipe pile with conical point with 0.5" wall thickness	
2	16" steel OEP with 0.5" wall thickness	
3	16" steel OEP with inside fit cut shoe with 0.5" wall thickness	
4	16" steel OEP with inside fit cut shoe with 0.5" wall thickness	
5	24" steel CEP with 0.75" wall thickness	
6	24" steel CEP with 0.75" wall thickness	
7	20" steel OEP with 0.5" wall thickness	
8	24" steel CEP with 0.75" wall thickness	
9	16" steel OEP with inside fit cut shoe with 0.5" wall thickness	
10	HP 14 X 117	
11	16" steel pipe pile with conical point with 0.5" wall thickness	
12	16" steel pipe pile with conical point with 0.5" wall thickness	
13	16" steel pipe pile with conical point with 0.5" wall thickness	
14	16" steel pipe pile with conical point with 0.5" wall thickness	
15	16" steel pipe pile with conical point with 0.5" wall thickness	
16	16" steel pipe pile with conical point with 0.5" wall thickness	
17	16" steel pipe pile with conical point with 0.5" wall thickness	
18	16" steel pipe pile with conical point with 0.5" wall thickness	

Figure 2.13 Partial screenshot of MontanaPile representing the "Pile Type" table

- **Date Driven:** The date when the pile is driven on the site.
- **LRFD Pile Load (kips):** This database field specifies the factored LRFD load needed to be supported by an individual pile. This load is the sum of all design loads for which any given pile in the structure is anticipated to support based on the superstructure loading evaluation.
- **ASD Load (kips):** This database field specifies the allowable stress design (ASD) load needed to be supported by an individual pile if the ASD criteria are implemented during the design process.
- **Type of Hammer Used:** This database field contains information about the type of hammer used for driving the test pile, such as MVE M-19, Delmag D36, and Delmag D16-32.
- **Pile Embedment at EOD (ft):** This field identifies the pile embedment at the end of driving (EOD).
- **Elevation at the Top of the Test Pile (ft):** The elevation of the top of the driven test pile to the mean sea level datum.
- **Record Comments:** Any additional comments on the pile test record can be entered in this field.
- **Attachments:** Six attachment fields are used to attach relevant reports and files. The attachment is created as a hyperlink that is stored in these fields.
- **Subsurface Profile Tab:** The information from the boring logs matched with the test pile records can be entered in this tab.
- **Layer:** This database field stores the number of layers from the top of the test pile.
- **Geomaterial:** This database field identifies the geomaterial type described by the boring logs.
- **Description:** This database field stores additional descriptions of the geomaterial, including its composition, state, and coloring.
- **AASHTO Classification:** This field can be used to input the AASHTO classification of the geomaterial if provided in the geotechnical reports.

- **Thickness (ft):** A layer thickness can be identified based on different geomaterials or varying geomaterial properties of similar geomaterials.
- **SPT N:** Standard penetration test (SPT) value for the respective geomaterial in blows/ft.
- **$(N_1)_{60}$:** Corrected SPT N-value for hammer efficiency, rod length, borehole diameter, and effective overburden pressure.
- **Unit Weight (pcf):** The unit weight of the geomaterial from field tests or predictions (correlation from another geomaterial property).
- **q_u (ksf):** The unconfined compressive strength of the geomaterial from lab tests.
- **s_u (ksf):** Undrained shear strength of the geomaterial from the lab tests or predictions.
- **Friction Angle:** The friction angle of the coarse-grained geomaterials from lab tests or predictions.
- **RQD (%):** The rock quality designation value of the rock-based geomaterials from the boring logs and geotechnical reports.
- **Ground Surface Elevation (ft):** The elevation of the ground at the location of the driven pile to mean sea level obtained from the boring logs.
- **Water Table Elevation (ft):** The elevation of the groundwater level at the location of the driven pile to mean sea level obtained from the boring logs recorded during boring.
- **CAPWAP (ksf):** CAPWAP measured unit shaft resistance or unit end bearing for the respective geomaterial layer.
- **Usable-Dynamic Test?:** Database field with an input of "Yes" or "No" corresponding to whether dynamic test results are available or not. This database field receives a checkmark when the pile driving analyzer (PDA) device is used to monitor the installation of the test pile, which must be instrumented with accelerometers and strain transducers near the pile head, and assess bearing capacity at either the EOID or BOR conditions; otherwise, this database field is left unchecked.
- **Driven Pile Length (ft):** The total length of the driven pile in feet.
- **Pile Cross-Sectional Area (in^2):** The cross-sectional area of the pile from the specifications.
- **Pile Weight Per Linear ft (p/f):** Weight of the pile per unit length from the specifications.
- **Hammer Stroke (ft):** Maximum stroke height of the hammer is entered in this field. This value can be found in the specification of the hammer provided by the manufacturer.
- **Transferred Hammer Energy (ft-kip):** This database field is used to enter the maximum transferred hammer energy specified by the manufacturer.
- **Dynamic Test and Analysis Results:** This is located on the fifth tab of the "Pile Load Test Record Form" and holds information such as blow counts per foot, and pile capacity from WEAP, PDA, and CAPWAP for EOD as well as restrikes as shown in Figure 2.14.

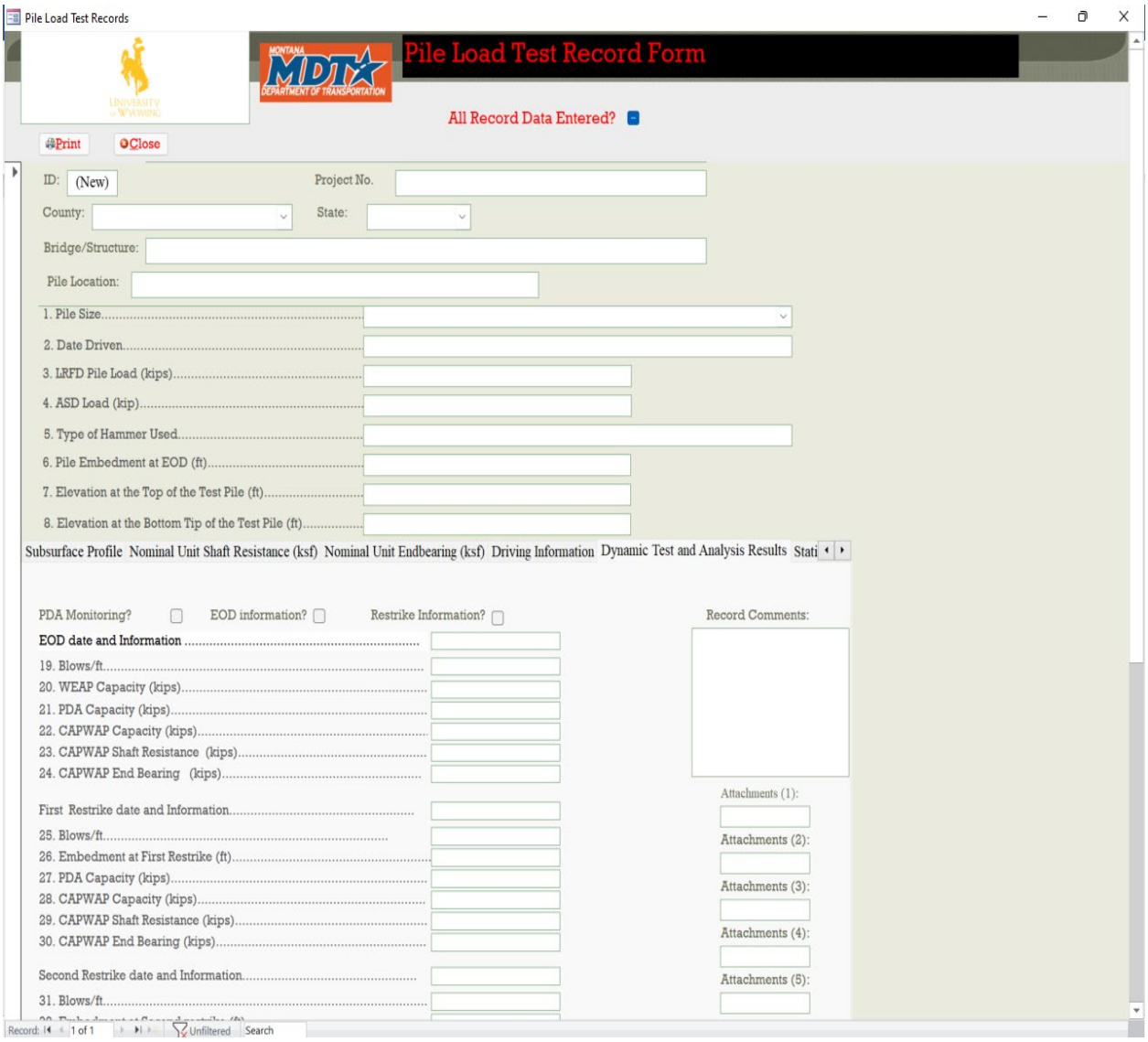

Figure 2.14 Partial screenshot of MontanaPile representing the "Dynamic Test and Analysis Results" tab in a new "Pile Load Test Records" form

- **Transferred Hammer Energy (ft-kip):** This database field is used to enter the maximum transferred hammer energy specified by the manufacturer.
- **Dynamic Test and Analysis Results:** This is located on the fifth tab of the "Pile Load Test Record Form" and holds information, such as blow counts per foot, and pile capacity from WEAP, PDA, and CAPWAP for EOD as well as restrikes as shown in Figure 2.14.
- **Blows/ft:** This database field is used to input the hammer blow count at EOD or BOR.
- **WEAP Capacity (kips):** The pile capacity, in kips, as predicted by the Wave Equation Analysis Program (WEAP), is input in this field.
- **PDA Capacity (kips):** The pile capacity, in kips, as predicted by pile driving analyzer (PDA) at EOD, or BOR is placed in this field.
- **CAPWAP Capacity (kips):** The total pile capacity, in kips, as predicted by the CAPWAP at EOR or BOR, is used as the input in this database field.

- **CAPWAP Shaft Resistance (kips):** The shaft resistance of the driven pile, in kips, as predicted by the CAPWAP at EOD or BOR, is used as the input in this database field.
- **CAPWAP End Bearing (kips):** The end bearing capacity of the driven pile, in kips, as predicted by the CAPWAP, is used as the input in this database field.
- **Static Load Test Results:** This is located on the sixth tab of the "Pile Load Test Records" form, as shown in Figure 2.16, and contains information on static load testing such as the load, displacement, and Davison pile capacity.

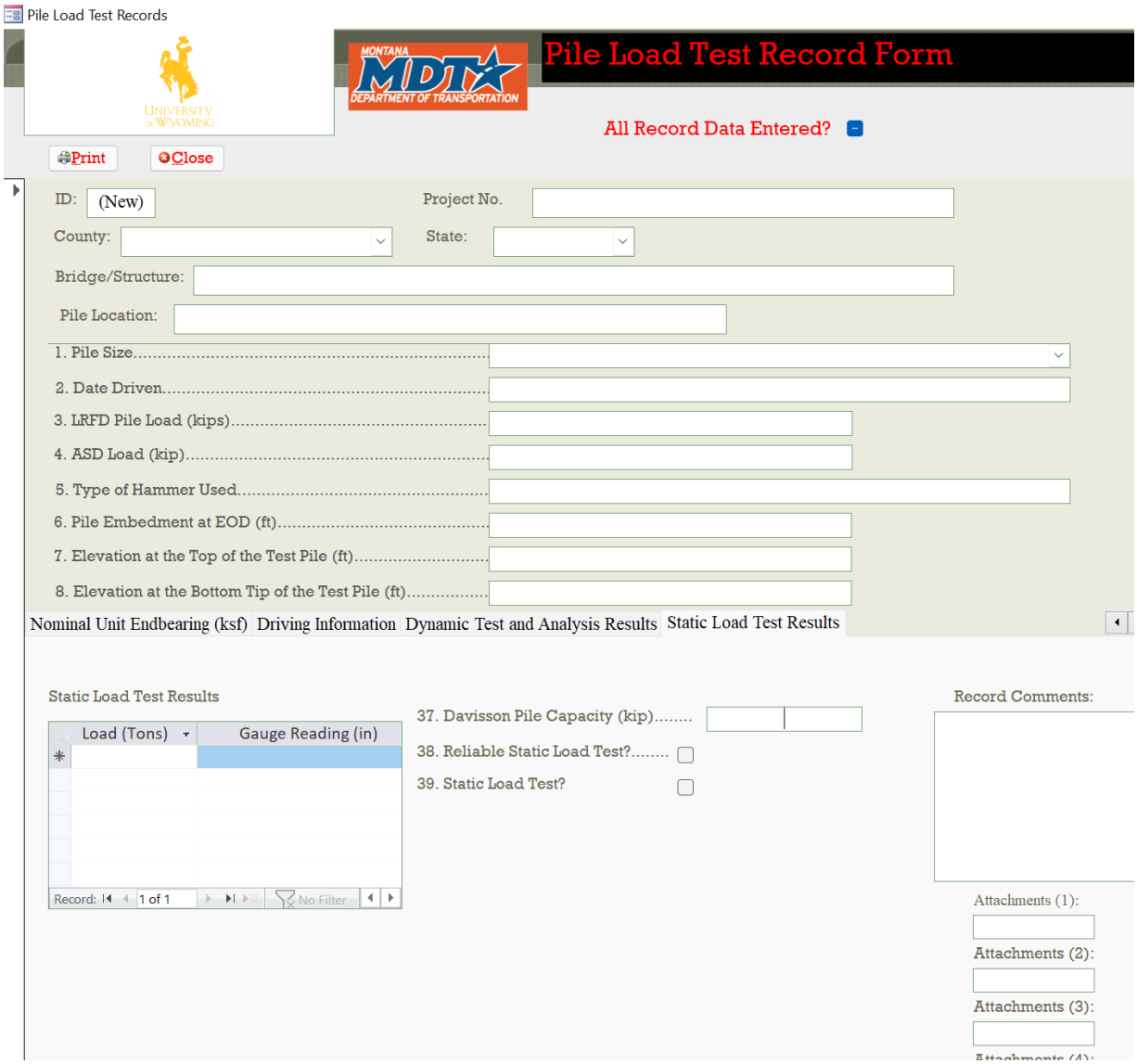

Figure 2.15 Partial screenshot of MontanaPile representing the "Static Load Test Results" tab in a new "Pile Load Test Records" form

- **Load (Tons):** This database field is used to input the load applied on the test pile during testing.
- **Gauge Reading (in):** This database field is used to enter the displacement recorded at the corresponding load (tons).

- **Davisson Pile Capacity (kip):** This database field is used to enter the pile capacity obtained from the static load test using the Davisson criterion.

In addition to the tables described previously, a built-in filter is set on the "Usable Test Piles" table that filters all the usable test pile records and provides a summary similar to the "Pile load Test Records" table. A partial screenshot of the "Usable Test Piles" is shown in Figure 2.16. This table facilitates easy access to the usable test piles without filtering the contents on the main "Pile Load Test Records" table or the "Pile Load Tests List" form.

Usable test piles

ID	State	County	Bridge/Structure	Pile Location	Pile Type	LRFD Factored load (
1	MT	Rosebud	Bridge Over Butte Creek	Bent 1, Pile 4	16" steel pipe pile with conical point with 0.5" wall thickness	457
2	MT	Blaine	Milk River - 4 KM West Of Zurich	Bent 1, Pile 1	16" steel OEP with 0.5" wall thickness	560
3	MT	Blaine	Milk River - 4 KM West Of Zurich	Bent 2, Pile 6	16" steel OEP with inside fit cut shoe with 0.5" wall thickness	500
4	MT	Blaine	Milk River - 4 KM West Of Zurich	Bent 3, Pile 1	16" steel OEP with inside fit cut shoe with 0.5" wall thickness	560
5	MT	Fergus	Bridge Over Warm Spring Creek	Bent 1	24" steel CEP with 0.75" wall thickness	1057
6	MT	Fergus	Bridge Over Warm Spring Creek	Bent 2	24" steel CEP with 0.75" wall thickness	1057
8	MT	Prairie	Bridge Over Cherry Creek	Bent 3, Pile 4	24" steel CEP with 0.75" wall thickness	832
9	MT	Musselshell	Bridge Over Mussehshell River	Bent 3, Pile 4	16" steel OEP with inside fit cut shoe with 0.5" wall thickness	455
15	MT	Lewis & Cla	Capitol Interchange/Cedar Interchange	Bent 1, Pile 1	16" steel pipe pile with conical point with 0.5" wall thickness	700
16	MT	Lewis & Cla	Capitol Interchange/Cedar Interchange	Bent 4, Pile 47	16" steel pipe pile with conical point with 0.5" wall thickness	670
17	MT	Lewis & Cla	Capitol Interchange/Cedar Interchange	Bent 5, Pile 8	16" steel pipe pile with conical point with 0.5" wall thickness	650
18	MT	Lewis & Cla	Capitol Interchange/Cedar Interchange	Bent 1, Pile 8	16" steel pipe pile with conical point with 0.5" wall thickness	700
19	MT	Lewis & Cla	Capitol Interchange/Cedar Interchange	Bent 1, Pile 2	16" steel pipe pile with conical point with 0.5" wall thickness	700
20	MT	Lewis & Cla	Capitol Interchange/Cedar Interchange	Bent 4, Pile 38	16" steel pipe pile with conical point with 0.5" wall thickness	670
21	MT	Lewis & Cla	Capitol Interchange/Cedar Interchange	Bent 5, Pile 11	16" steel pipe pile with conical point with 0.5" wall thickness	650
22	MT	Golden Valle	Bridge Over MusselShell River, Cushman	Bent 1, Pile 1	16" steel OEP with inside fit cut shoe with 0.5" wall thickness	638
23	MT	Valley	Bridge over Rock Creek	Bent 2, Pile 1	20" steel OEP with 0.5" wall thickness	610
24	MT	Valley	Bridge over Rock Creek	Bent 3, Pile 1	20" steel OEP with 0.5" wall thickness	370

Figure 2.16 Partial screenshot of MontanaPile representing the "Usable Test Piles" table

3. DRIVEN PILES IN FINE-GRAINED SOIL-BASED INTERMEDIATE GEOMATERIALS

3.1 Introduction

Driven piles are widely used for bridge foundations in the United States due to their availability, constructability, and economic benefits. Design and construction challenges are often encountered when piles are driven into intermediate geomaterial (IGM), which is a transitional material between soil and hard rock. IGMs have been defined as cohesive materials, such as clay shales or mudstones, with undrained shear strength (s_u) varying from 5 ksf to 50 ksf or non-cohesive materials with corrected standard penetration test (SPT) N-values falling between 50 and 100 blows per feet (Martin and Stacey 2018; O'Neill and Reese 1999). Most literature defines IGM based on unconfined compressive strength (q_u) (Clarke and Smith 1992; Akai 1997; Marinos 1997; De Freitas 1993). Definitions of IGM vary as they are developed for different applications, such as drilled shafts and tunneling (Santi et al. 1997), and most transportation agencies do not have criteria to define IGM for driven pile foundations. A study of driven piles in IGM has been recently completed to differentiate IGM based on corrected SPT N-value $(N_1)_{60}$, rock mass rating (RMR), and q_u (Adhikari et al. 2020c). The authors categorized the IGM into soil-based IGM and rock-based IGM. They recommended that if a soil-based geomaterial has $(N_1)_{60}$ greater than 50, it should be classified as a soil-based IGM. However, this recommendation is established from data limited to one state involving steel H-piles and coarse-grained geomaterials. Hence, classification criteria should be expanded to include fine-grained soil-based geomaterials and further reduce the uncertainty associated with the prediction of driven pile resistances. With relatively high geological variability of IGM and different IGM definitions, higher uncertainties in deep foundation designs are expected, which could lead to many construction challenges (Mokwa and Brooks 2008).

Static analysis (SA) methods have been well developed for the prediction of driven pile resistances in soil. The American Association of State Highway and Transportation Officials (AASHTO) Load and Resistance Factor Design (LRFD) Bridge Design Specifications (2020) recommended treating IGM in the same manner as soil for driven pile design. However, these existing SA methods cannot achieve the same target reliability for the prediction of pile resistances in IGM (Ng et al. 2015; Ng and Sullivan 2017a; Ng and Sullivan 2017b). Using 35 load test data of steel H-piles driven into IGM in Wyoming, a lower value for the resistance factor (φ) of 0.09 is calibrated for the α-method in IGM (Tomlinson 1980) compared with the AASHTO recommended value of 0.35 for soil to ensure the same target reliability index of 2.33 (Adhikari et al. 2020b). The economic study conducted by the authors revealed that the existing α-method overpredicted the pile resistances in IGM, and a direct cost overrun is predicted with an additional 0.085 kg of steel, on average, per kN of applied load (Adhikari et al. 2020a). A different study was conducted by Long (2016) in Wisconsin to predict the resistances of only steel H-piles in fine-grained IGMs described as clay and silt based on an equivalent hammer blow count (N_{MSPT}) obtained from a modified standard penetration test (MSPT) that was originally developed for drilled shafts in shale and weak rocks (Stark et al. 2017). The authors recommended predicting unit shaft resistance (q_s) as 0.021 N_{MSPT} for a narrow range of q_s less than 2 ksf and unit end bearing (q_b) as 0.935 N_{MSPT} and for smaller q_b less than 200 ksf. These prediction equations are neither evaluated nor validated using independent testing pile dataset, and hence, LRFD recommendations are not developed. Furthermore, most studies are conducted on piles driven in rock-based IGMs (Mokwa and Brooks 2008; Ng and Sullivan 2017a; Adhikari et al. 2018; Adhikari et al. 2020a; Adhikari et al. 2020b), and limited research has been conducted to specifically develop LRFD recommendations for piles in fine-grained soil-based IGMs (FG-IGM).

Piles driven in fine-grained soils have exhibited an increase in pile resistance after the end of driving (EOD) as a function of time known as pile setup (Ng et al. 2013a; Haque et al. 2017). The extensive study by Ng et al. (2013b) concluded that the amount of pile setup decreases in a denser fine-grained soil with a high SPT N-value, and the rate of pile setup decreases in the fine-grained soil with higher s_u. Past studies found that pile setup mostly occurred in the shaft resistance, but minimally in the end bearing (e.g., Ng and Sritharan 2016). However, similar studies have not been conducted to investigate the change in pile resistances in FG-IGM. It is not known if pile setup will occur in FG-IGM that have higher N-value and s_u, whether q_s and q_b will exhibit different pile setups, and how pile setup is affected by the s_u of FG-IGM.

To alleviate current limitations and to improve the understanding of pile responses in FG-IGM, 51 historical pile load test data from 25 bridge projects completed in four states are used to 1) develop a method to classify FG-IGM, 2) propose new SA methods to predict q_s and q_b of piles in FG-IGM, and 3) investigate the change in pile resistances after the EOD. The proposed SA methods are validated using 33 independent test piles from three different states**.** Changes in q_s and q_b from dynamic load tests at the EOD and beginning of restrikes (BOR) are determined and compared as a function of time and s_u of IGM. The SI version of this chapter can be found in the article published by Masud et al. (2022).

3.2 Overview of Pile Load Test Data

A total of 51 driven piles from 25 bridge projects in four states, Idaho, Montana, North Dakota, and Wyoming, are compiled and analyzed. Table 3.1 summarizes the 51 test pile data that include pile type and size, general subsurface profile, total pile penetration (D_B), driving hammer, type of FG-IGM, s_u of FG-IGM, q_s and q_b determined from the Pile Driving Analyzer (PDA) with subsequent signal matching using the Case Pile Wave Analysis Program (CAPWAP), and pile hammer blow count taken at the EOD. Among the 51 test piles, 22 test piles are steel H-piles and 29 are steel pipe piles (5 close-ended and 24 open-ended). Among 22 steel H piles, 19 test piles are in soil-based geomaterials and three test piles are in both soil and rock-based geomaterials. Among the 29 steel pipe piles, five test piles are in soil-based geomaterials and 24 test piles are in both soil and rock-based geomaterials. For the evaluation of q_b, only 14 test piles with pile tip embedding in the FG-IGM are included in the analysis. The classification for FG-IGM and the development of SA methods are conducted using the unit resistances determined from CAPWAP at the EOD as static load tests (SLT) are not conducted. Past studies have shown that CAPWAP results agree well with those measured from SLT (Likins and Rausche 2004; Sakr 2013). In particular, a recent study comparing 25 pile resistances in IGM from SLT and CAPWAP shows that the mean resistance bias of 1.077 is closer to unity and the coefficient of variation (COV) of the resistance bias of 0.121 for CAPWAP is relatively small (Adhikari et al. 2020a). Hence, in the absence of SLT measurements, it is reasonable to consider the pile resistance determined from CAPWAP as the measured resistance in this study.

Table 3.1 Summary of 51 driven piles in fine grained soil-based IGM

State	Project	Pile location	Pile	D_B (ft)	Subsurface	FG-IGM	s_u (ksf)	q_s (ksf)	q_b (ksf)	Hammer	BC
ID	US-95 WR bridge	Pi-10 at P-1	HP 14×117	41.6	SBM	CH	8.44-15.94[#]	3.61-4.68[*]	NA	Del. D19-42	590
ID	SH-51 SR bridge	Pi-1 at A-1	HP 14×117	68.9	SBM	ML	3.23-15.19[#]	0.28-3.05[*]	200.37	ICE I-30v2	73
ID	SH-51 SR bridge	Pi at A-2	HP 14×117	68.9	SBM	ML & CL	8.43-13.63[#]	1.31-3.36[*]	232.58	ICE I-30v2	52
ID	I-84B UPRR bridge	Pi-5 at A-2	HP 14×117	39.9	SBM	ML	9.07-12.00[#]	1.23-3.85[*]	NA	ICE I-30v2	64
ID	I-84B UPRR bridge	Pi-5 at P-1	HP 14×117	23.8	SBM	ML	12.96	4.3	NA	ICE I-30v2	77
ID	I-84B UPRR bridge	Pi-12 at P-2	HP 14×117	35.9	SBM	ML	11.86	3.49	NA	ICE I-30v2	69
ID	RP road bridge	Pi-1 at A-1	18-in OEP	48	SBM & RB	ML	4.52	0.16	NA	ICE I-30v2	23
ID	RP road bridge	Pi-8 at A-2	18-in OEP	42.9	SBM & RB	ML	5.50	0.27	NA	ICE I-30v2	52
ID	SH-55 SR bridge	Pi-3 at P-1	HP 14×117	56.2	SBM	CH & CL	6.06-8.43[#]	1.13-3.96[*]	119.42	Del. D19-42	1158
ID	SH-55 SR bridge	Pi-4 at A-1	HP 14×117	56.4	SBM	CH & CL	3.89-9.98[#]	0.88-3.85[*]	137.67	Del. D19-42	420
ID	SH-55 SR bridge	Pi-2 at P-3	HP 14×117	35	SBM	ML & CL	14.16-16.07[#]	2.61-4.35[*]	NA	Del. D19-42	72
ID	SH-55 SR bridge	Pi-1 at P-4	HP 14×117	20	SBM	CL	12.69-15.31[#]	2.87-4.24[*]	397.14	Del. D19-42	333
ID	SH-55 SR bridge	Pi-1 at P-2	HP 14×117	48	SBM	CH & CL	7.79-12.41[#]	3.11-3.96[*]	200.17	Del. D19-42	71
ID	SH-55 SR bridge	Pi-1 at P-5	HP 14×117	34	SBM	CL	7.78-9.83[#]	1.35-3.31[*]	199.69	Del. D19-42	144
ID	SH-55 SR bridge	Pi-10 at A-2	HP 14×117	33.2	SBM	ML	10.72-14.68[#]	1.83-3.87[*]	353.50	Del. D19-42	105
ND	Memorial bridge	Pi-1 at P-10	HP 14×102	90	SBM	CH & CL	3.45-4.72[#]	0.17-2.05[*]	NA	Del. D36	40
ND	Memorial bridge	Pi-2 at P-10	HP 14×102	97	SBM	CH & CL	3.22-4.22[#]	0.67-1.62[*]	NA	Del. D36	49
WY	PB-Parson street	Pi-5 at A-1	HP 12×53	87.9	SBM & RB	ML	4.24	0.31	NA	Del. D16-32	164
WY	PB-Muddy creek	Pi-1 at B-2	HP 12×53	35.3	SBM	ML & MH	2.7-4.72[#]	0.57-1.40[*]	142.10	Del. D16-32	108
WY	PB-Beech street	Pi-3 at A-2	HP 12×53	46.4	SBM	ML	4.5	0.90	147.35	Del. D16-32	82
WY	PB-Muddy creek	Pi-1 at A-2	HP 12×53	53.6	SBM	ML	4.68	1.09	101.50	Del. D16-32	109
WY	PB-Beech street	Pi-1 at A-2	HP 12×53	44.7	SBM	ML	4.5	1.15	147.45	Del. D16-32	62
MT	MR-west of Zurich	Pi-1 at B-1	16-in OEP	81.1	SBM & RB	ML	4.73-12.27[#]	1.60-3.07	NA	ICE I-30	74
MT	MR-west of Zurich	Pi-6 at B-2	16-in OEP	50.3	SBM & RB	CL	3.89	0.47	NA	ICE I-30	87
MT	MR-west of Zurich	Pi-1 at B-3	16-in OEP	76.2	SBM & RB	CL	4.92	0.89	NA	ICE I-30	106
MT	Bridge over CC	Pi-4 at B-3	24-in OEP	58	SBM & RB	CH	2.75	0.35	NA	ICE I-36	135
MT	Capitol interchange	Pi-1 at B-1	16-in CEP	29.5	SBM & RB	CH	3.45	0.73	NA	ICE I-30	30
MT	Capitol interchange	Pi-8 at B-1	16-in CEP	29	SBM	CH	7.45	1.57	NA	ICE I-36	48
MT	Capitol interchange	Pi-2 at B-1	16-in CEP	28	SBM & RB	CH	3.67	1.20	NA	ICE I-30	60
MT	Capitol interchange	Pi-38 at B-4	16-in CEP	27.5	SBM	CH	4.73	1.87	NA	ICE I-30	44
MT	Bridge over RC	Pi-1 at B-3	20-in OEP	41	SBM & RB	CL	5.50	0.59	NA	ICE I-30	42
MT	Bridge over RC	Pi-1 at B-2	20-in OEP	45	SBM & RB	MH	6.59	2.02	NA	ICE I-30	73
MT	M FK porcupine	Pi-4 at B-1	16-in OEP	47.5	SBM	MH	4.73	0.85	27.71	ICE I-30	23
MT	M FK porcupine	Pi-2 at B-3	20-in OEP	46.2	SBM & RB	MH	4.32	1.65	NA	ICE I-30	35
MT	Bridge over HC	Pi-1 at B-1	16-in OEP	42.2	SBM & RB	CL	3.68	0.52	NA	APE D30-42	120
MT	Bridge over BNSF	Pi-5 at A-1	HP 14×117	68	SBM & RB	CH	4.52	1.74	NA	ICE I-30v2	96
MT	Bridge over BNSF	Pi-1 at A-4	HP 14×117	69.4	SBM & RB	CL	6.06	1.13	NA	ICE I-30v2	96
MT	Bridge over MR	Pi-1 at B-1	20-in OEP	91.5	SBM & RB	CL	4.11	0.27	NA	ICE I-36	172

MT	PC overflow	Pi at B-1	20-in OEP	82	SBM & RB	CL	4.72	0.45	NA	Del. D46-42	30
MT	Bridge over PC	Pi at B-3	20-in OEP	93.8	SBM & RB	CH	3.67	0.77	NA	Del. D46-42	31
MT	Bridge over PC	Pi at B-1	20-in OEP	91.8	SBM & RB	CH	3.22	0.28	NA	Del. D46-42	29
MT	Bridge over LCC	Pi-3 at B-1	20-in OEP	136.5	SBM	CH	6.94	2.02	57.43	ICE I-36	313
MT	Bridge over SC	Pi-4 at B-2	16-in CEP	32.5	SBM & RB	CH	3.90	0.47	NA	Del. D19-32	109
MT	Bridge over LMC	Pi-1 at B-1	16-in OEP	95	SBM & RB	CH	4.32	1.65	NA	APE D36-26	74
MT	Bridge over LMC	Pi-3 at B-2	16-in OEP	97.9	SBM & RB	CH	5.50	0.59	NA	APE D36-26	192
MT	Bridge over LMC	Pi-4 at B-4	16-in OEP	81	SBM	CH	4.72	0.57	NA	APE D36-26	107
MT	I-94 bridge BI	Pi-2 at B-3	16-in OEP	45.8	SBM & RB	CL	3.67	0.34	NA	ICE I-36	87
MT	I-94 bridge BI	Pi-4 at B-1	16-in OEP	52	SBM & RB	CL	3.67	0.35	NA	ICE I-36	40
MT	Bridge over Cr.	Pi-16 at B-1	16-in OEP	20.7	SBM & RB	CL	4.72	1.60	NA	ICE I-36	74
MT	Bridge over Cr.	Pi-2 at B-4	16-in OEP	20	SBM & RB	CL	4.93	1.62	NA	ICE I-36	44
MT	Bridge over Co.	Pi-3 at B-2	16-in OEP	36.8	SBM & RB	CL	12.27	3.22	NA	ICE I-30v2	80

ID=Idaho; ND=North Dakota; WY=Wyoming; MT=Montana; WR=Weiser River; SR= Snake River; RP=Robinson Park; BC=Butte Creek; MR=Milk River; CC=Cherry Creek; RC=Rock Creek; HC=Home Creek; PC=Porcupine Creek; LCC=Little Cottonwood Creek; SC=Sharpy Creek; BI=Broadus interchange; Cr.=Crooked Creek; Co.=Coral Creek; LMC=Little Muddy Creek; A=Abutment; Pi=Pile; P=Pier; B=Bent; D_B=Total pile penetration; CEP=Close ended pipe pile; OEP=Open ended pipe pile; SBM=Soil based (both coarse and fine) geomaterials; SBM & RB=Soil- and rock-based geomaterials; CH-IGM=High plasticity clay IGM; CL-IGM=Low plasticity clay IGM; MH-IGM=High plasticity silt IGM; ML-IGM=Low plasticity silt IGM; s_u=Undrained shear strength; q_s=Unit shaft resistance; $^{\#}$=Range of s_u; *=Range of q_s; q_b=Unit end bearing; NA=Not applicable; Del.=Delmeg; ICE=International Construction Equipment; APE=American Pile Driving Equipment; BC=Hammer blow count at end of driving (bl/ft)

3.3 Proposed Classification for Fine Grained Soil-Based IGM

The soil-based geomaterials of 51 test piles are first classified according to the Unified Soil Classification System (USCS). The α-method (AASHTO 2020) is selected to distinguish FG-IGM from fine-grained soil as this method is currently and widely used in the estimation of driven pile resistances in fine-grained soil in terms of s_u. A total of 169 fine-grained layers of the 51 test piles that have s_u values ranging from 0.61 ksf to 16.07 ksf are identified for the q_s prediction using the α-method. The s_u values are determined from laboratory tests, and some are predicted using the prediction equation ($s_u/P_a = 0.29N^{0.72}$) that is chosen for a wider range of SPT N-values (Kulhawy and Mayne 1990). The uncertainty associated with this prediction equation for s_u will be accounted for in the LRFD calibration. The classification method is established by comparing the COV of q_s biases (ratio of q_s from CAPWAP to q_s from the α-method) to s_u.

Fine-grained layers with s_u values ranging from 0.61 ksf to 16.07 ksf are reduced by excluding the layer with the maximum s_u value from each analysis cycle to produce the next dataset for subsequent analyses. The COV values of resistance biases are then determined for different datasets and compared with their respective maximum s_u values in Figure 3.1. To clarify the analysis process, the first dataset consisting of 169 fine-grained layers yields a COV of 0.875, which is plotted against the maximum s_u of 16.07 ksf (Figure 3.1). In the next analysis cycle, the fine-grained layer with the s_u value of 16.07 ksf is eliminated from the dataset. Hence, the remaining 168 layers yields a COV of 0.88, which is plotted against the new maximum s_u of 15.94 ksf. The analysis is repeated until the maximum s_u of the dataset reached 1.01 ksf as the boundary between FG-IGM and fine-grained soil is less likely to occur below 1.01 ksf. This is justified by the suggested s_u value greater than 2.12 ksf for very stiff to hard fine-grained soil (Kulhawy and Mayne 1990), and the almost constant adhesion factor (α) of the α-method for s_u exceeding about 3 ksf (AASHTO 2020). Furthermore, the decreasing COV values for s_u less than about 2.7 ksf agrees with the efficiency of the α-method originally developed for fine-grained soil. Figure 3.1 shows two distinct groups of COV with the average lower COV of about 0.68 and the average upper COV of 0.95. The variation in COV values observed in the upper COV group for maximum s_u values ranging between 4 ksf and 5 ksf is attributed to the presence of both steel H-piles and steel pipe piles in the datasets used in the analysis. The transition from the lower COV to the upper COV group occurs at the maximum s_u of about 2.7 ksf. To facilitate the development of SA methods to improve the design efficiency of driven piles in FG-IGM, the s_u value of 2.7 ksf is recommended as the boundary separating FG-IGM from fine-grained soil. Figure 3.2 illustrates the proposed classification of fine-grained, soil-based geomaterials in a flow chart.

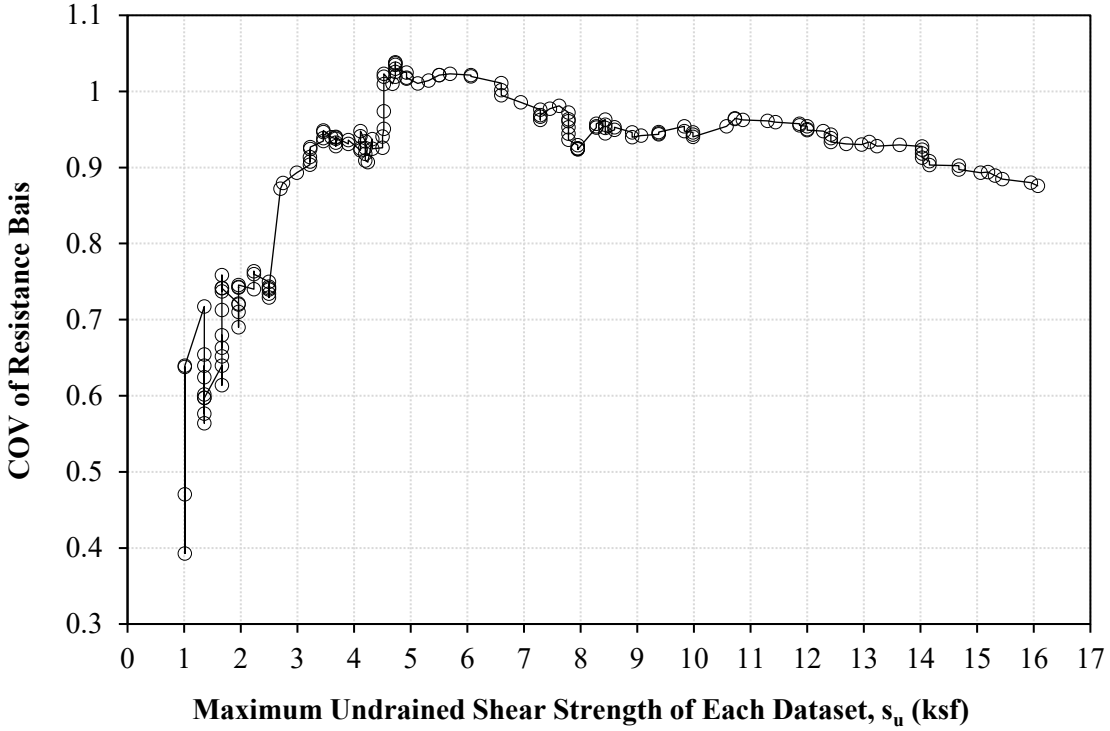

Figure 3.1 Comparison of COV and maximum s_u for the α-method

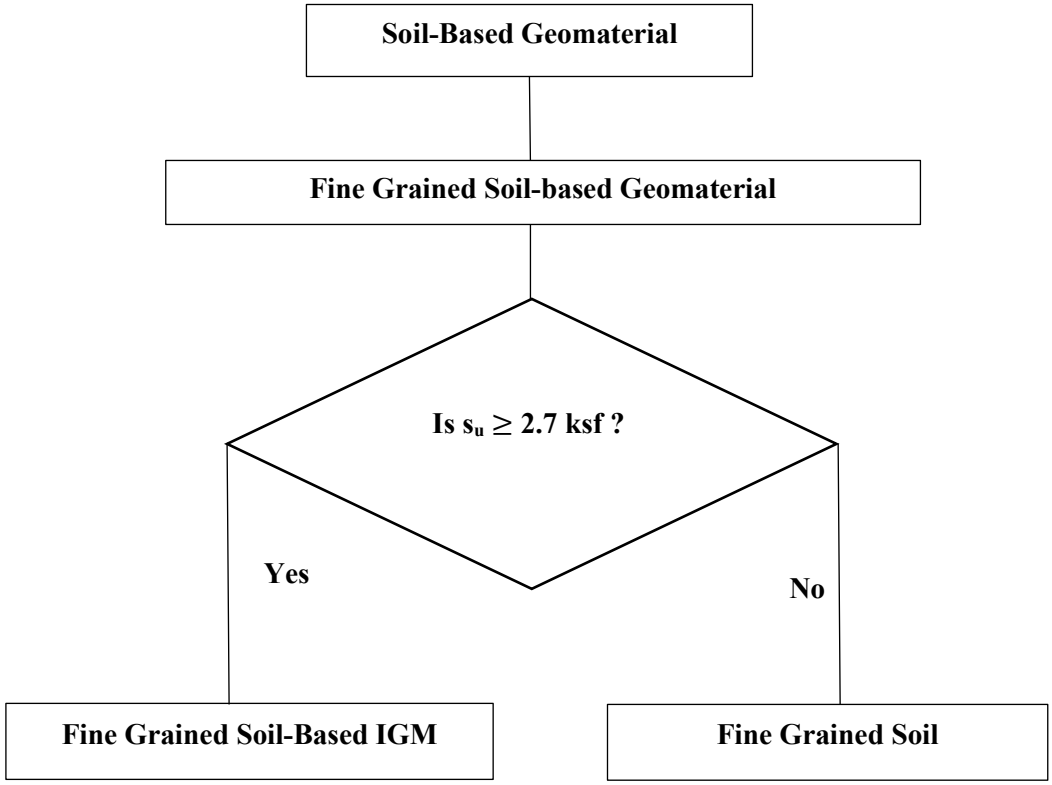

Figure 3.2 Proposed classification for fine grained soil-based geomaterial in a flowchart

3.4 Development of Static Analysis Methods

SA methods for the prediction of pile resistances in FG-IGM are developed for different subgroups of FG-IGM following the flow chart shown in Figure 3.3 to reduce uncertainties associated with different fine-grained geomaterials and to improve the accuracy of pile resistance prediction. To develop more efficient SA methods for the q_s prediction, FG-IGM is divided into clay-based IGM and silt-based IGM based on grain size. The clay-based IGM are further divided into high plasticity clay-based IGM (CH-IGM) and low plasticity clay-based IGM (CL-IGM). For the silt-based IGM, only low plasticity silt-based IGM (ML-IGM) is considered due to a small sample size of 4 in the high plasticity silt-based IGM (MH-IGM). The SA method for q_b is established using 14 piles with FG-IGM as the end-bearing layer. The q_b is calculated by dividing the end bearing from CAPWAP with a box area of H-piles or a close-ended area of pipe piles as soil plugging is assumed from the predicted soil plug weight in the CAPWAP reports.

The proposed SA methods for q_s are developed by comparing the q_s at the EOD from CAPWAP with s_u. Figures 3.4 shows the increasing nonlinear trend of q_s with respect to s_u for ML-IGM, CL-IGM, and CH-IGM, respectively. The proposed SA method for q_b prediction is developed by comparing q_b from CAPWAP with s_u and the ratio of pile dimension or diameter (D) to total pile penetration length (D_B) as shown in Figure 3.5.

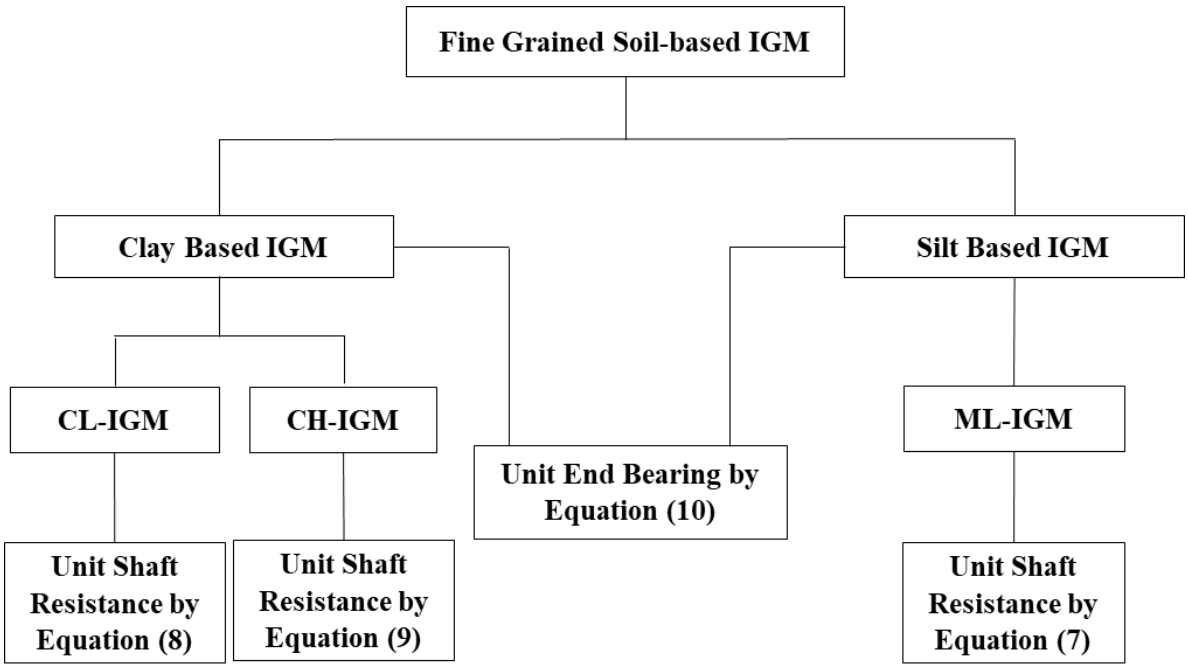

Figure 3.3 Proposed static analysis methods for fine grained soil-based IGM in a flowchart

3.4.1 Nonlinear Model Selection Criteria

The proposed nonlinear SA equations for q_s and q_b are developed using the statistical software RStudio (R Core Team 2016). Model selection criteria play an important role in choosing among different nonlinear models (Gu et al. 2018). The Akaike information criterion (AIC) (Akaike 1974) and the Bayesian information criterion (BIC) (Schwarz 1978) are the two popular selection criteria. The residual standard error (RSE), mean squared error (MSE), and leave-one-out cross-validation

mean standard error (CV) are also included to assess the nonlinear models. In selecting the best nonlinear model among the candidate models, lower RSE, MSE, CV, AIC, and BIC values are considered.

Both AIC and BIC have penalties involving the number of predictors. AIC and BIC can be calculated using Equations 3.1 to 3.3 in terms of the nonlinear function (f), vector of estimated coefficient values ($\underline{\hat{\beta}}$), estimated variance ($\hat{\sigma}^2 = \text{RSE}^2$), observation ($i$), number of observations (n), and number of predictors (p)

$$L\left(\underline{\hat{\beta}}, \hat{\sigma}^2 | \underline{y}\right) = \prod_{i=1}^{n} \frac{1}{\sqrt{2\pi\hat{\sigma}^2}} exp\left(-\frac{1}{2\hat{\sigma}^2}\left(y_i - f\left(x_i, \underline{\hat{\beta}}\right)\right)^2\right) \tag{3.1}$$

$$\text{AIC} = -2\ln\left(L\left(\underline{\hat{\beta}}, \hat{\sigma}^2 | \underline{y}\right)\right) + 2(p+1) \tag{3.2}$$

$$\text{BIC} = -2\ln\left(L\left(\underline{\hat{\beta}}, \hat{\sigma}^2 | \underline{y}\right)\right) + \ln(n)(p+1) \tag{3.3}$$

The RSE given by Equation 3.4 is the square root of the residual sum of squares divided by the residual degrees of freedom, and the MSE given by Equation 3.5 is the mean of sum of squared residuals, where y_i is the observed response and $\hat{y}_i$is the predicted response.

$$\text{RSE} = \sqrt{\frac{\sum(y_i - \hat{y}_i)^2}{n-p-1}} \tag{3.4}$$

$$\text{MSE} = \frac{1}{n}\sum_{i=1}^{n}(y_i - \hat{y}_i)^2 \tag{3.5}$$

CV is used to define the predictive ability of a statistical model (James et al. 2013). For validation, the full dataset is divided into two comparable parts: a training dataset and a testing dataset. The model is fit on the training dataset, and then the fitted model is used to predict the responses of the testing dataset. The resulting test error rate is assessed using the MSE. When the dataset is small, it is better to use a single observation for the validation set, and the remaining data as the training set to fit the model. This process is repeated for all observations in the full dataset to obtain predicted values. The CV is the average of the total test errors given by Equation 3.6 in terms of response for observation i (y_i) and the predicted value obtained from model fit without observation i ($\hat{y}_{(i)}$)

$$\text{CV} = \frac{1}{n}\sum_{i=1}^{n}\left(y_i - \hat{y}_{(i)}\right)^2 \tag{3.6}$$

3.4.2 Unit Shaft Resistance for Fine-grained IGM

SA methods are developed for the prediction of q_s in FG-IGMs (ML-IGM, CL-IGM, CH-IGM) using q_s values from CAPWAP and their respective s_u values. Three nonlinear models, power, logistic, and natural logarithm, are compared based on the aforementioned criteria. Table 3.2 shows that the logistic model has the lowest statistical indices, and hence is recommended for the prediction of q_s in each of

ML-IGM, CL-IGM, and CH-IGM. The respective prediction equations in terms of s_u and atmospheric pressure (P_a) for ML-IGM, CL-IGM, and CH-IGM are given by Equation 3.7, Equation 3.8, and Equation 3.9, respectively

$$\hat{q}_s(\mathrm{ML-IGM}) = \left[\frac{1.80}{1+44e^{-0.89\frac{s_u}{P_a}}}\right] P_a \tag{3.7}$$

$$\hat{q}_s(\mathrm{CL-IGM}) = \left[\frac{1.58}{1+47.6e^{-1.34\frac{s_u}{P_a}}}\right] P_a \tag{3.8}$$

$$\hat{q}_s(\mathrm{CH-IGM}) = \left[\frac{2}{1+50.4e^{-1.4\frac{s_u}{P_a}}}\right] P_a \tag{3.9}$$

It is important to note that the proposed prediction equations are applicable for q_s values ranging from 0.17 ksf to 4.68 ksf and s_u values ranging from 2.75 ksf to 16.07 ksf. Figure 3.4 shows the relationships between the s_u values and the q_s values from CAPWAP along with the prediction equations for ML-IGM in Figure 3.4a, CL-IGM in Figure 3.4b, and CH-IGM in Figure 3.4c. Figure 3.4a shows that q_s increases rapidly with the increase in s_u, and the increase in q_s reduces when the s_u is greater than about 10 ksf. Figures 3.4b and 3.4c show that the predicted q_s based on the proposed models will become almost constant when s_u exceeds about 10 ksf. The reducing rate on q_s at a higher s_u in all FG-IGM could be attributed to the plastic behavior of FG-IGM when an ultimate pile adhesion is reached.

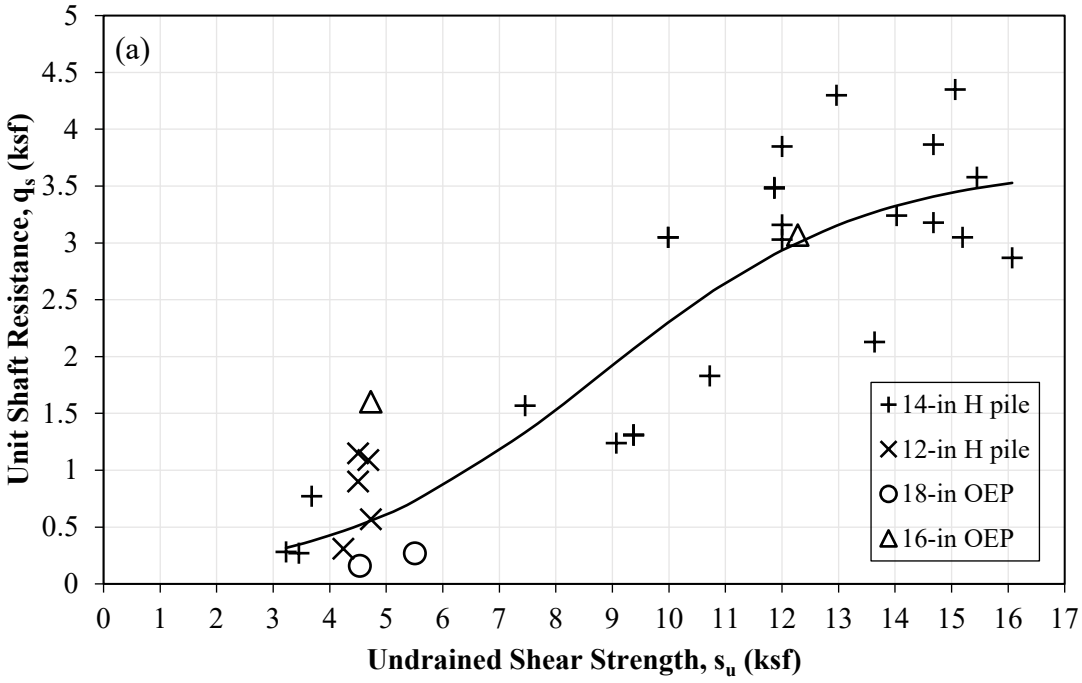

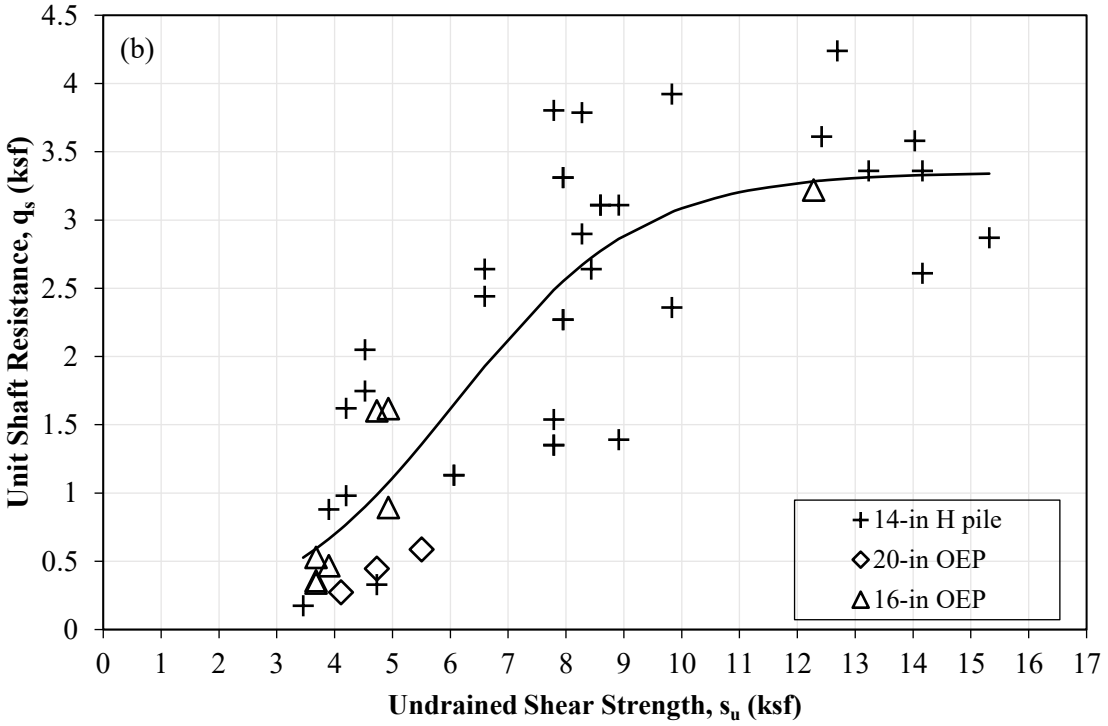

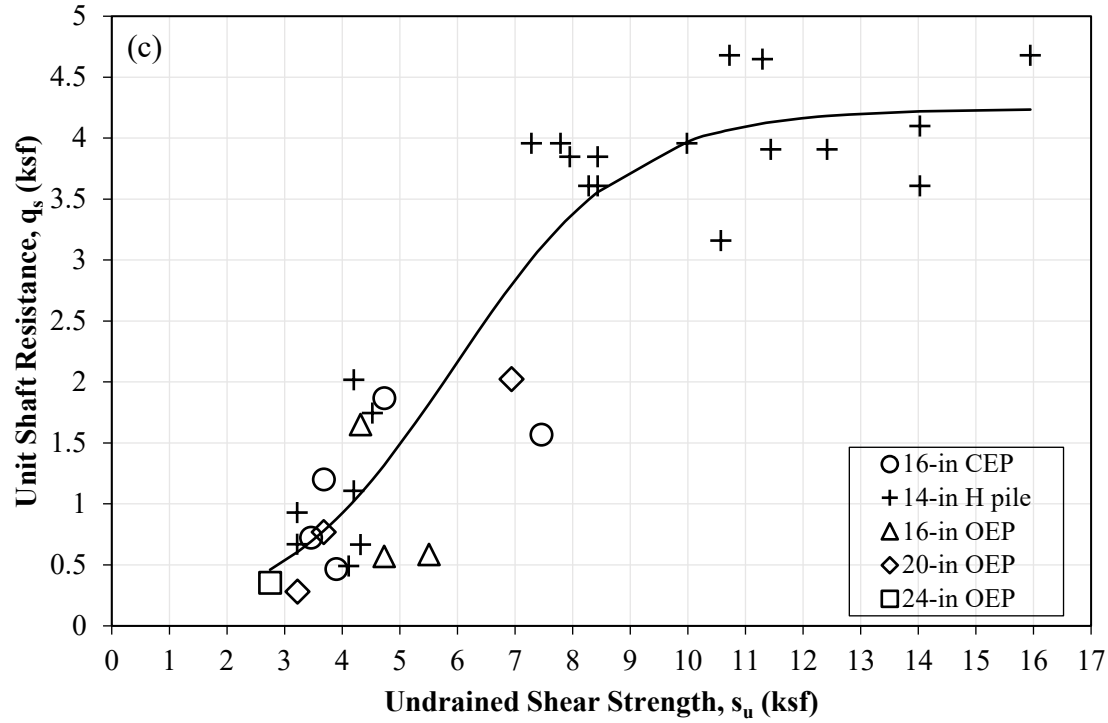

Figure 3.4 Plot of unit shaft resistance from CAPWAP versus s_u for (a) ML-IGM, (b) CL-IGM, and (c) CH-IGM.

3.4.3 Unit End Bearing for Fine-grained, Soil-based IGM

An SA method is developed to predict q_b of steel H- and pipe piles in FG-IGM. Three nonlinear models, power, reciprocal yield density (YD), and natural logarithm, are evaluated as the potential prediction equation. The reciprocal YD model had the lowest statistical indices (Table 3.2). The resulting prediction equation is given in Equation (3.10). The atmospheric pressure (P_a) is included to account for the unit used in the q_b prediction. It is important to note that the proposed Equation (3.10) is applicable for q_b values ranging from 27.71 ksf to 397.14 ksf and the combined term of $s_u \times D/D_B$ for values ranging from 0.08 to 0.89. Equation 3.10 should be used with caution for q_b and $s_u \times D/D_B$ values exceeding these ranges. Figure 3.5 shows a positive relationship between q_b from CAPWAP, s_u and D/D_B.

$$\hat{q}_b(\mathrm{FG-IGM}) = \left[\frac{\frac{s_u}{P_a}\times\frac{D}{D_B}}{0.001+0.0027\frac{s_u}{P_a}\times\frac{D}{D_B}}\right]P_a \tag{3.10}$$

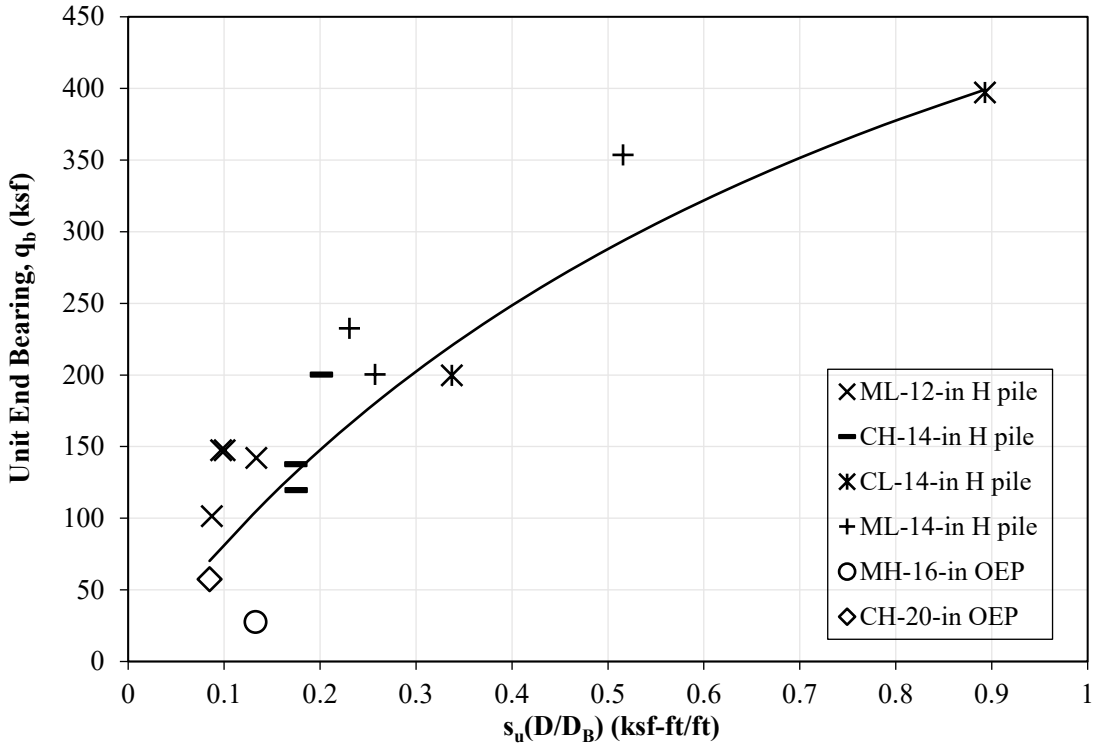

Figure 3.5 Plot of unit end bearing from CAPWAP versus undrained shear strength and a ratio of pile diameter to pile penetration $\left(\mathbf{s_u}\frac{\mathbf{D}}{\mathbf{D_B}}\right)$ for fine grained soil-based IGM

3.5 Validation of Static Analysis Methods

3.5.1 Unit shaft resistance

The validation is conducted by comparing predicted q_s from the proposed SA methods given by Equations (3.7), (3.8), and (3.9) with the q_s determined at the EOD from CAPWAP of 25 independent test piles from Kansas (8 test piles) and Illinois (17 test piles) (Long and Anderson 2012) summarized in Table 3.3. The 25 test piles are four HP 10 piles, seven HP 12 piles, two HP 14 piles, and twelve 14-in diameter close-ended pipe (CEP) piles. From the 25 test piles, a total 67 FG-IGM layers with q_s values from CAPWAP ranging from 0.15 ksf to 2.41 ksf are used in this study. To evaluate the performance of the proposed SA methods, comparisons are also conducted against the existing α-method. Figure 3.6a and Figure 3.6b show that the proposed SA methods improve the q_s predictions that are closer along the line of equality (solid line). The statistical summaries (mean resistance bias and COV) inserted in Figure 3.6 asserts that the proposed SA methods with the mean resistance bias of 0.91, on average, provide a more accurate q_s prediction than the α-method with a lower mean bias of 0.74. The proposed SA methods, on average, overpredict the q_s by about 10% while the α-method overpredicts the q_s by about 35%. The lower COV of 0.31 for the proposed SA methods compared with the 0.56 for the α-method suggests that the proposed SA methods will provide more consistent q_s prediction of piles driven into FG-IGM.

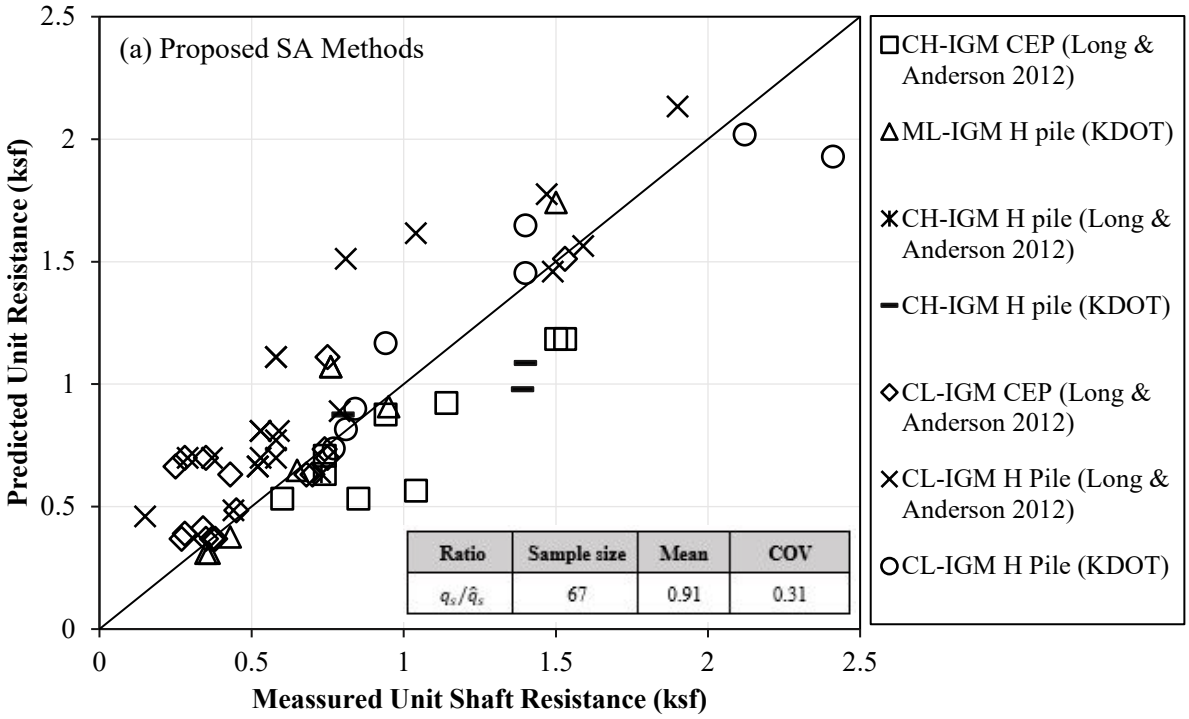

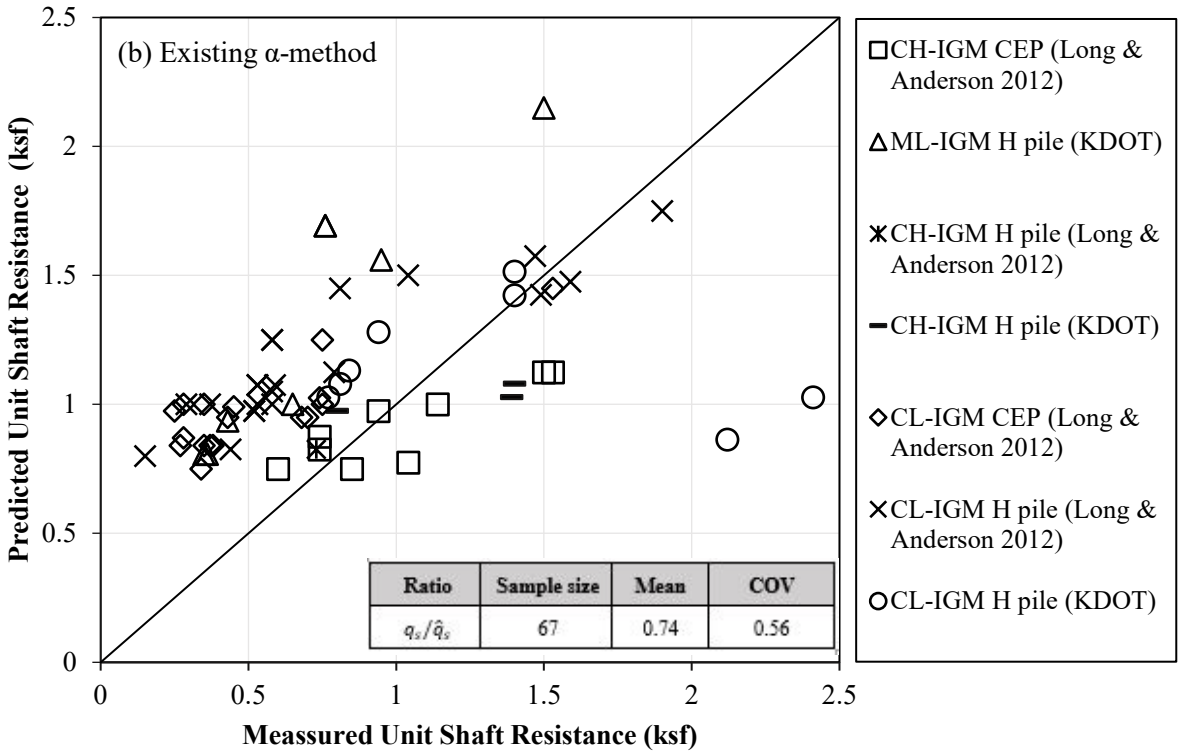

Figure 3.6 Comparison between unit shaft resistances from CAPWAP and predicted unit shaft resistances using (a) proposed SA methods, (b) the existing α-method. The inserts include the mean and coefficient of variation of the resistance bias

3.5.2 Unit End Bearing

The performance of the proposed SA method for q_b is similarly conducted using independent dynamic pile load test from the Kansas DOT, eight pile load tests in Wisconsin from Long (2016), and four pile load tests in Illinois from Long and Anderson (2012) as summarized in Table 3.3. The total 13 test piles are one HP 10 pile, one HP 12 pile, eight HP 14 piles, and three 14-in diameter CEP piles. The q_b values determined from CAPWAP range from 17.77 ksf to 305.8 ksf. The comparisons of q_b values for the proposed SA method given by Equation 3.10 and the α-method are shown in Figure 3.7a and Figure 3.7b, respectively. Figure 3.7 reveals that the proposed SA method improves the q_b prediction as most data points lie closer along the line of equality. The mean bias of 1.15 suggests that the proposed SA method, on average, underpredicts the q_b by about 13%. On the other hand, the relatively high mean bias of 2.1 reveals that the existing α-method underpredicts the q_b, on average, by about 52%. Furthermore, the lower COV of 0.37 for the proposed Equation 3.10 compared with the 0.48 for the α-method suggests that the proposed Equation 3.10 will provide a more consistent q_b prediction of piles driven in FG-IGM.

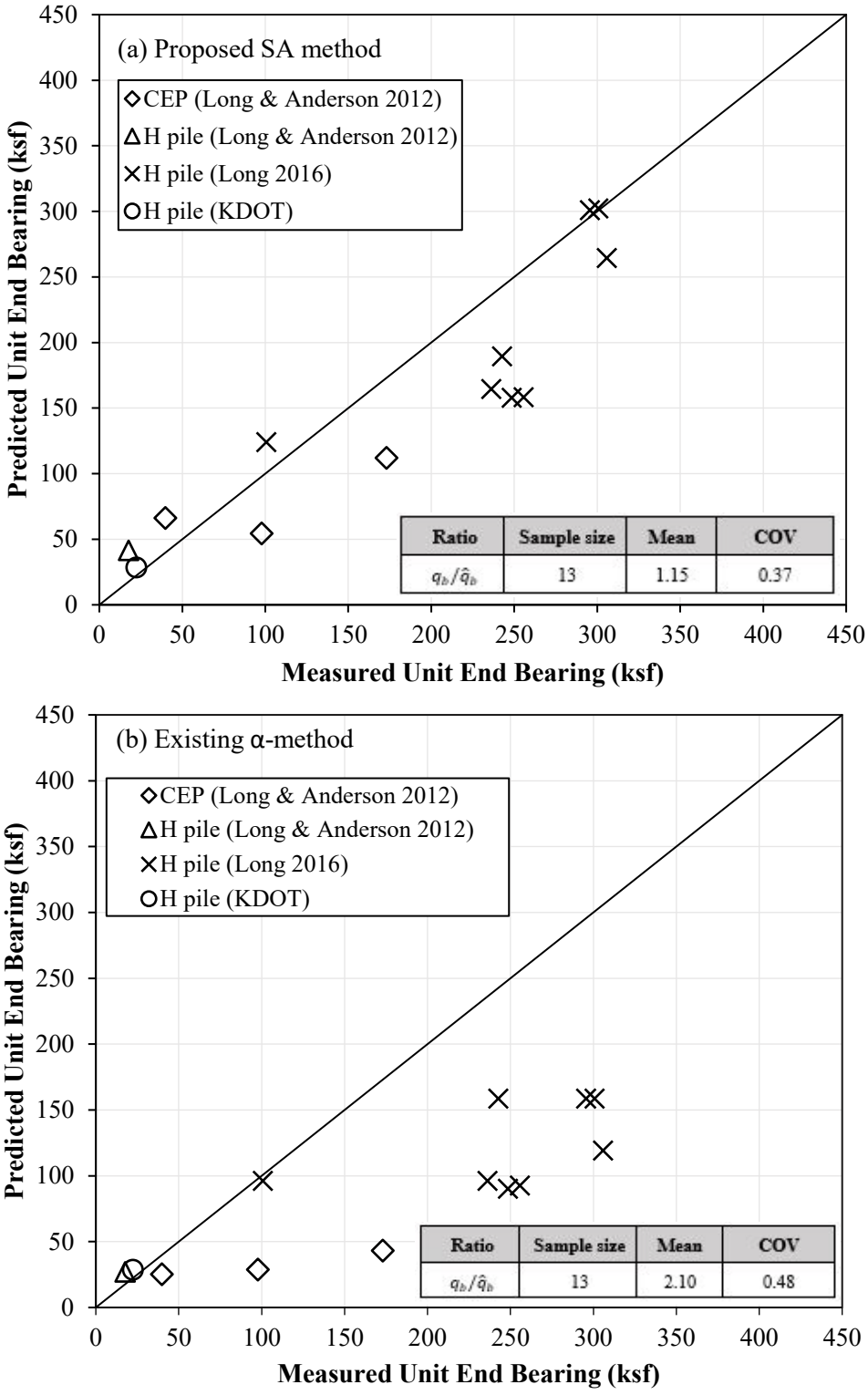

Figure 3.7 Comparison between unit end bearing from CAPWAP and predicted unit end bearing using (a) proposed SA method, (b) the existing α-method. The inserts include the mean and coefficient of variation of the resistance bias.

Table 3.2 Model comparison of the proposed SA methods for fine grained soil-based IGM

GM	Functional forms for the nonlinear models; Prediction **equation**s from nonlinear model fits	Selection criterion				
		RSE	MSE	CV	AIC	BIC
Unit shaft resistance						
ML-IGM	$f(x_i) = \beta_1 (x_i)^{\beta_2}$; $\hat{q}_s = 0.27 P_a \left[\frac{s_u}{P_a}\right]^{1.02}$ (Power)	0.3174	0.098	0.107	22.93	27.60
	$\mathbf{f(x_i) = \frac{\beta_1}{1+\beta_2(e^{\beta_3 x_i})}}$; $\mathbf{\hat{q}_s = \left[\frac{1.80}{1+44e^{-0.89\frac{s_u}{P_a}}}\right] P_a}$ **(Logistic)**	**0.2950**	**0.082**	**0.095**	**18.74**	**24.96**
	$f(x_i) = \beta_1 + \beta_2 \ln(x_i)$; $\hat{q}_s = \left[-0.5 + 1.1 \ln \frac{s_u}{P_a}\right] p_a$ (NL)	0.3175	0.097	0.104	22.94	27.61
CL-IGM	$f(x_i) = \beta_1 (x_i)^{\beta_2}$; $\hat{q}_s = 0.29 P_a \left[\frac{s_u}{P_a}\right]^{0.96}$ (Power)	0.37	0.126	0.143	43.86	49.42
	$\mathbf{f(x_i) = \frac{\beta_1}{1+\beta_2(e^{\beta_3 x_i})}}$; $\mathbf{\hat{q}_s = \left[\frac{1.58}{1+47.6e^{-1.34\frac{s_u}{P_a}}}\right] P_a}$ **(Logistic)**	**0.3213**	**0.097**	**0.109**	**31.54**	**38.94**
	$f(x_i) = \beta_1 + \beta_2 \ln(x_i)$; $\hat{q}_s = \left[-0.32 + 1.08 \ln \frac{s_u}{P_a}\right] P_a$ (NL)	0.3343	0.104	0.116	34.34	39.89
CH-IGM	$f(x_i) = \beta_1 (x_i)^{\beta_2}$; $\hat{q}_s = 0.33 P_a \left[\frac{s_u}{P_a}\right]^{1.01}$ (Power)	0.3745	0.134	0.149	33.64	38.22
	$\mathbf{f(x_i) = \frac{\beta_1}{1+\beta_2(e^{\beta_3 x_i})}}$; $\mathbf{\hat{q}_s = \left[\frac{2}{1+50.4e^{-1.4\frac{s_u}{P_a}}}\right] P_a}$ **(Logistic)**	**0.2875**	**0.078**	**0.092**	**16.58**	**22.68**
	$f(x_i) = \beta_1 + \beta_2 \ln(x_i)$; $\hat{q}_s = \left[-0.3 + 1.3 \ln \frac{s_u}{P_a}\right] P_a$ (NL)	0.3168	0.097	0.104	22.27	26.85
Unit end bearing						
FG-IGM	$f(x_i) = \beta_1 (x_i)^{\beta_2}$; $\hat{q}_b = 342.26 P_a \left[\frac{s_u}{p_a}\frac{D}{D_B}\right]^{0.67}$ (Power)	54.8	2606.04	3810.65	155.67	157.59
	$\mathbf{f(x_i) = \frac{x_i}{\beta_1+\beta_2 x_i}}$; $\mathbf{\hat{q}_b = \left[\frac{\frac{s_u}{P_a}\times\frac{D}{D_B}}{0.0011+0.0027\frac{s_u}{P_a}\times\frac{D}{D_B}}\right] P_a}$ **(Reciprocal YD)**	**54.11**	**2602.11**	**3234.68**	**155.32**	**157.24**
	$f(x_i) = \beta_1 + \beta_2 \ln(x_i)$; $\hat{q}_b = \left[236 + 69 \ln\left(\frac{s_u}{p_a}\frac{D}{D_B}\right)\right] p_a$ (NL)	55.01	2765.54	3453.15	155.78	157.7

GM=GeoMaterials; NL=Natural Logarithm; YD=Yield density; RSE=Residual standard error; MSE=Mean squared error; CV=Leave one out cross validation; AIC=Akaike information criterion; BIC= Bayesian information criterion

Table 3.3 Summary of 33 independent test piles driven into fine grained soil-based IGM

State	Project	Pile location	Pile	D_B (ft)	Subsurface	No of layers-FG-IGM	s_u (ksf)	q_s (ksf)	q_b (ksf)	Hammer	BC
IL	Oquawka	Pi at EA	14-in CEP	57	SBM	2-Clay	3.0-3.2[#]	0.6-0.85[*]	97.8	MKT DE-42	37
IL	Oquawka	Pi at WA	14-in CEP	62	SBM	2-Clay	4.5	1.5-1.53[*]	NA	MKT DE-42	172
IL	Oquawka	Pi at P	14-in CEP	51	SBM	2-Clay	2.8-3.3[#]	0.38-0.45[*]	NA	MKT DE-42	68
IL	Godfrey	Pi at P-2	14-in CEP	39	SBM	4-Clay	2.8-4.8[#]	0.27-0.74[*]	173.06	Del. D12-43	64
IL	Godfrey	Pi at WA	14-in CEP	66	SBM	3-Clay	2.8-4.0[#]	0.4-1.04[*]	39.25	Del. D12-43	60
IL	Jacksonville	Pi at P-1	HP 12×53	39	SBM	6-Clay	4.0-7.0[#]	0.58-1.90[*]	NA	Del. D12-43	194
IL	Jacksonville	Pi at P-2	HP 12×53	62	SBM	10-Clay	3.0-5.9[#]	0.53-1.59[*]	17.77	Del. D12-43	172
IL	Greenville	Pi-3 at P-1	14-in CEP	28	SBM	1-Clay	3.8	0.43	NA	Del. D25-32	41
IL	Greenville	Pi-13 at P-1	14-in CEP	50	SBM	1-Clay	3.8	0.68	NA	Del. D25-32	37
IL	Greenville	Pi-12 at P-1	14-in CEP	23	SBM	1-Clay	3.8	0.7	NA	Del. D25-32	19
IL	Mahomet	Pi at P-2	HP 12×53	31.2	SBM	1-Clay	3.3	0.44-0.73	NA	Del. D30-32	49
IL	Plymouth	Pi at P-2	HP 14×102	43.2	SBM & RB	1-Clay	3.2	0.15	NA	Del. D19-32	403
IL	Plymouth	Pi at SA	HP 14×102	46	SBM & RB	4-Clay	4.0-4.3[#]	0.29-0.59[*]	NA	Del. D19-32	85
IL	RCS Godfrey	TPi at SA	14-in CEP	40	SBM	3-Clay	3.9-5.8[#]	0.94-1.54[*]	NA	Del. D19-32	80
IL	RCS Godfrey	Pi at NA	14-in CEP	38	SBM	3-Clay	2.8-3.0[#]	0.34-0.37[*]	NA	Del. D19-32	128
IL	RCS Godfrey	PPi at SA	14-in CEP	40	SBM	3-Clay	3.9-5.0[#]	0.25-0.75[*]	NA	Del. D19-32	65
IL	Stronghurst	Pi-1 at P-1	14-in CEP	69	SBM & RB	Clay	2.9	0.28	NA	Del. D19-42	38
KS	K-23 over PR	Pi at P-1	HP 12×63	50	SBM & RB	1-ML, 1-CL	3.23-4.11[#]	0.36-0.77[*]	NA	Del. D19-32	160
KS	K-4 over CCD	Pi at A-1	HP 10×42	79	SBM & RB	2-CL, 1-CH	3.89-4.52[#]	0.8-0.84[*]	NA	Del. D19-32	46
KS	MS over I-135	Pi at P-1	HP 10×42	84	SBM & RB	1-ML	4.0	0.65	NA	Del. D30-32	51
KS	K-14 over CC	Pi at P-2	HP 10×42	85	SBM	2-CL, 1-CH, 3-ML	4.32-6.77	0.76-1.5	22.33	Del. D19-42	25
KS	Int. of I-235 & 13 st.	Pi at P-2	HP 12×63	59	SBM & RB	CL	4.1	2.41	NA	Pil. D30-32	23
KS	Int. of I-235 & 13 st.	Pi at P-9	HP 12×63	59	SBM & RB	CL	3.46	2.12	NA	Pil. D30-32	25
KS	Int. of I-235 & 13 st.	Pi at P-5	HP 12×74	55	SBM & RB	CH	4.11	1.39	NA	Pil. D30-32	23
KS	K-14 over CC	Pi at P-6	HP 10×42	91	SBM & RB	3-ML, 1-CL	3.2-6.24[#]	0.35-0.95[*]	NA	Del. D19-42	13
WI	Int. of US41 & IH43	TPi-1 at P-5	HP 14×73	38	SBM	Clay	17.62	NA	300.72	Del. D25-32	NA
WI	Int. of US41 & IH43	Pi-1 at P-5	HP 14×73	35	SBM	Silt	13.25	NA	305.80	Del. D25-32	NA
WI	Int. of US41 & IH43	Pi-2 at P-5	HP 14×73	38.3	SBM	Clay	17.60	NA	295.65	Del. D25-32	NA
WI	Int. of US41 & IH43	Pi-1 at P-10	HP 14×73	53.8	SBM	Clay	10.02	NA	248.55	Del. D25-32	NA
WI	Int. of US41 & IH43	Pi-2 at P-10	HP 14×73	55	SBM	Clay	10.28	NA	255.80	Del. D25-32	NA
WI	Int. of US41 & IH43	TPi-1 at P-10	HP 14×73	54.5	SBM	Clay	10.69	NA	236.23	Del. D25-32	NA
WI	Int. of US41 & IH43	Pi-1 at P-1	HP 14×73	77	SBM	Clay	10.70	NA	100.72	Del. D25-32	NA
WI	Int. of US41 & IH43	TPi-1 at P-1	HP 14×73	74.8	SBM	Clay	17.62	NA	242.75	Del. D25-32	NA

IL=Illinois; KS=Kansas; WI=Wisconsin; PR=Pawnee River; CCD=Cow Creek drainage; MS=Maple Street; Int.=Interchange; St.=Street; CC=Cow creek; A=Abutment; Pi=Pile; P=Pier; B=Bent; TPi=Test pile; PPi=Production pile; EA=East abutment; WA=West abutment; NA=North abutment; SA=South abutment; D_B=Total pile penetration; CEP=Close ended pipe pile; SBM=Soil based (both coarse and fine) geomaterials; SBM & RB=Soil- and rock-based geomaterials; CH-IGM=High plasticity clay IGM; CL-IGM=Low plasticity clay IGM; ML-IGM=Low plasticity silt IGM; s_u=Undrained shear strength; q_s=Unit shaft resistance; [#]=Range of s_u; [*]=Range of q_s; q_b=Unit end bearing; NA=Not applicable; Del.=Delmeg; Pil.=Pileco; BC=Hammer blow count at end of driving (bl/ft).

3.6 Change in Pile Resistances

3.6.1 Change in Unit Shaft Resistance

A total 69 FG-IGM layers from 25 test piles and four states (Wyoming, North Dakota, Kansas, and Illinois) are included in this study to investigate the change in q_s over time. Among these 25 test piles, 15 are steel H-piles and 10 are 14-in CEP. The elapsed times (t) from the EOD to BOR range from 15 minutes (0.0104 day) to 156 days. Figure 3.8 shows the percent change in $q_{s\text{-}t}$ with respect to the $q_{s\text{-}to}$ is determined at the EOD from CAPWAP for clay-IGM and silt-IGM. The q_s generally increases with a logarithmic time (Figure 3.8a) as similarly observed in fine-grained soils (Ng et al. 2013b). A setup factor (A) given by Equation 3.11 (Skov and Denver 1988) is determined by assuming the initial time (t_o) at 0.0104 days to compare the rate of change in q_s. The insert in Figure 3.8a indicates that steel H-piles driven in clay-IGM, with an average A=0.28, have a higher pile setup than in silt-IGM with an average A=0.20. Higher pile setup in clay-IGM could be attributed to the higher fine-grained particles in clay-IGM that delay the dissipation of excess pore water pressure and consolidation of FG-IGM induced during pile installation as is similarly observed in fine-grained soils (Ng et al. 2013a; Haque et al. 2017). For clay-IGM, CEP piles with a larger cross-sectional area exhibit a higher pile setup with an average A=0.53 compared with H-piles. Higher pile setup is expected from a larger pile size that creates greater radial displacement, disturbance, and remolding in the FG-IGM during pile installation. If a one-day pile restrike would be performed, the q_s of H-piles and CEP piles in clay-IGM will increase, on average, by 56% and 105%, respectively (Figure 3.8a). A lower average of 39% increase in q_s would be expected on H-piles in silt-IGM at one day after the EOD. Figure 3.8b shows that the pile setup factor generally decreases with the increase in s_u of FG-IGM. This agrees with the higher pile setup experienced in soft clays than in stiff clays (Long et al. 1999).

$$A = \frac{{}^{q_{s-t}}/_{q_{s-t_o}} - 1}{\log(t/t_o)} \tag{3.11}$$

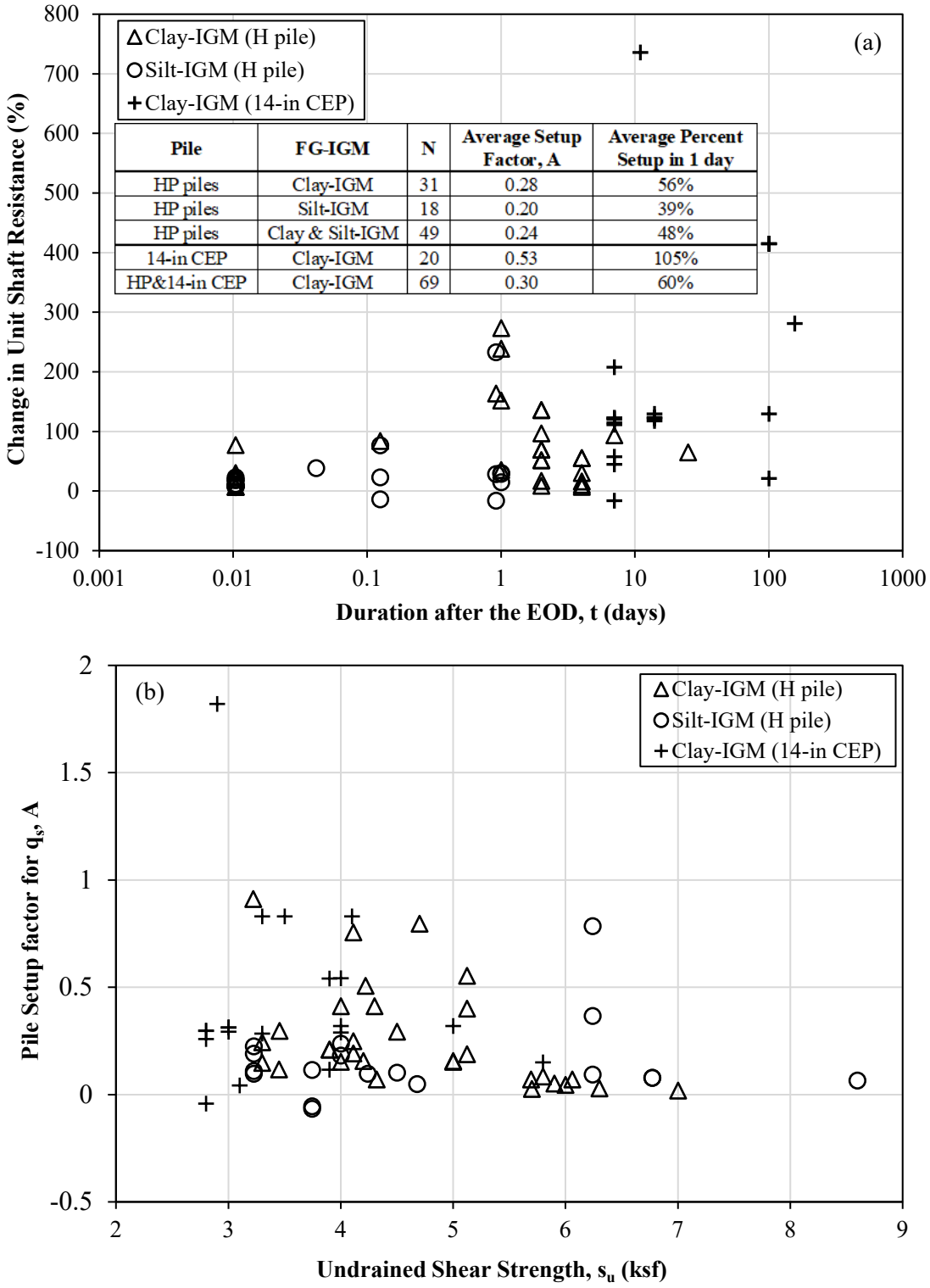

Pile	FG-IGM	N	Average Setup Factor, A	Average Percent Setup in 1 day
HP piles	Clay-IGM	31	0.28	56%
HP piles	Silt-IGM	18	0.20	39%
HP piles	Clay & Silt-IGM	49	0.24	48%
14-in CEP	Clay-IGM	20	0.53	105%
HP&14-in CEP	Clay-IGM	69	0.30	60%

Figure 3.8 (a) A plot of percent change in unit shaft resistance against a duration after the EOD in a logarithmic scale, (b) the comparison of pile setup factor for q_s and undrained shear strength of FG-IGM.

3.6.2 Change in Unit End Bearing

A total of 17 test piles from Wyoming, Wisconsin, Kansas, and Illinois, with both q_b determined at the EOD and BOR from CAPWAP, are used to investigate the change in q_b over time. Among these 17 test piles, 14 are steel H-piles, and three are 14-in CEP. Thirteen test piles (10 H-piles and three 14-in CEP) are bearing on clay-IGM, and the remaining four H-piles are on silt-IGM. The elapsed times between the EOD and BOR range from 15 minutes (0.0104 day) to 156 days. Figure 3.9a shows that four H-piles in clay-IGM experience pile setup with percent increase in q_b varying from 5.3% to 345%, while six H-piles experience a decrease in q_b (known as pile relaxation) with the percent change in q_b varying from -0.6% to -23%. The percent change in q_b of H-piles in silt IGM varies from -33% to 22%. For 14-in CEP in clay-IGM, two piles exhibit pile relaxation of -17% and -51%, while one experiences pile setup of 202%. A logarithmic relationship between percent change in q_b and time is not observed, and in fact, q_b in silt-IGM decreases with time. Furthermore, the effect of pile type and size on the percent change in q_b is not apparent. Figure 3.9b shows that the pile setup factor decreases from positive to negative values as the s_u of FG-IGM increases from 2.8 ksf to 17.6 ksf. In particular, piles driven into FG-IGM with a s_u value greater than about 4 ksf will unlikely exhibit pile setup, and pile relaxation could occur in these cases. It is believed that pile relaxation could be attributed to the creation of a gap beneath a pile tip due to hard driving on stiffer FG-IGM and the development of negative excess pore water pressure due to the fracturing of stiff FG-IGM at the EOD.

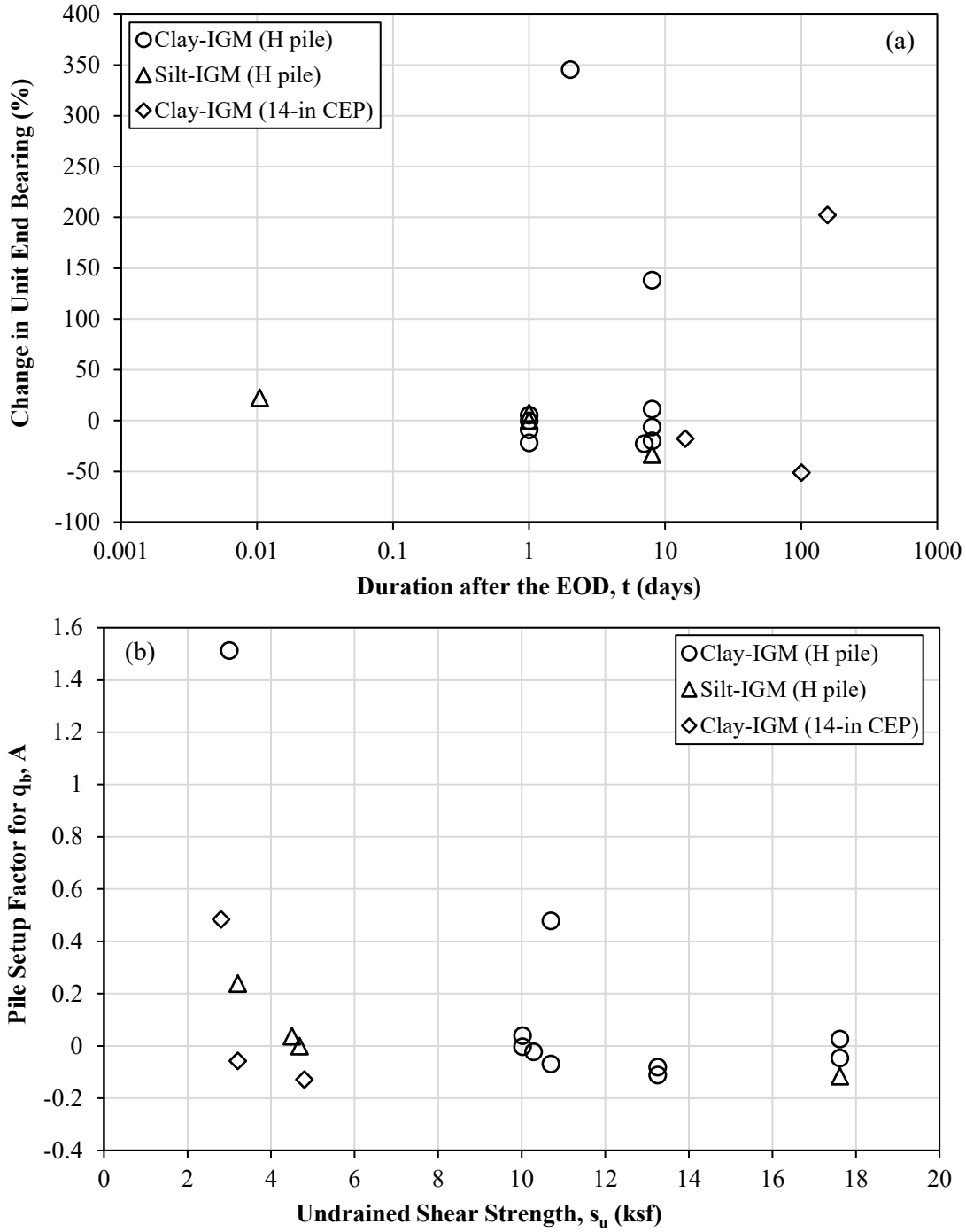

Figure 3.9 (a) A plot of percent change in unit end bearing against a duration after the EOD in a logarithmic scale, (b) the comparison of pile setup factor for q_b and undrained shear strength of FG-IGM

4. DRIVEN PILES IN ROCK-BASED SHALES

4.1 Introduction

Driven steel piles are a foundation system for shallow bedrock stratigraphy due to economy and durability. Many states in North America have an extensive distribution of soft rocks such as shales, sandstone, siltstone, and mudstone. For pile design in these materials, various foundation design manuals provided different guidelines. For example, the Canadian Foundation Design Manual defined rocks as a soil mass if they are weakly cemented with q_u less than 20 ksf, have closely spaced discontinuities, and have heavy fragmentation (Becker and Moore 2006). However, the American Association of State Highway and Transportation Officials (AASHTO 2020) suggested treating these materials as soil during pile design while the limiting structural capacity of a pile governs the axial pile resistance in hard rock. Among the soft rocks, shale has been considered a problematic material due to its degradation of shear strength and shrink-swell potential (Yagiz 2001). Shale is a fine-grained, clastic sedimentary rock formed by the deposition and compaction of silt and clay-size mineral particles over time. Shale is considered a transitional material due to having wide range of strength properties. Lacking pile load test data has delayed the understanding of driven piles in shales, particularly pile resistances. Currently, there are no specific guidelines and design methods in existing foundation design manuals to predict unit shaft resistance (q_s) and unit end bearing (q_b) of piles driven in shale. Instead, the existing empirical static analysis (SA) methods developed for soils are being used to design the driven piles in shale.

Several empirical design methodologies described in the literature focused on steel H-piles on soft rock types other than shale. Experimental data suggested that q_b of steel piles in granite, limestone, and sandstone is about $4q_u$ to $6q_u$ (Rehnman and Broms 1971). Morton (2012) proposed $q_b = 7.5q_u$ for 112 ksf $\leq q_u \leq$ 375 ksf and driven H-piles primarily in sandstone and mudstone, and discrepancies are observed in this linear relationship between q_b and q_u. Belbas (2014) proposed lower q_b values ranging from $2q_u$ to $5.7q_u$ for 480 ksf $\leq q_u \leq$ 1750 ksf based on 22 dynamic tests conducted on various steel H-piles in siltstones and mudstone from six bridge sites in Winnipeg, Canada. In addition, Tomlinson and Woodward (2014) reported a lower $q_b = 1.2q_u$ to $1.75q_u$ for 52 ksf $\leq q_u \leq$ 226 ksf from two static load tests (SLTs) and one dynamic test on 80- to 11-inch diameter pipe piles in mudstone, siltstone, and sandstone. Alternatively, using 19 dynamic tests of HP 14×88 on clay shale, sandstone, and siltstone from six bridge sites in Edmonton, Canada, Soliman et al. (2018) calibrated α and β-methods for pile resistance predictions. The calibration yielded the following: 0.35 ≤ adhesion factor (α) ≤ 0.62 and 21 ≤ end bearing capacity factor (N_c) ≤ 30 for the α-method, and 0.1 ≤ shaft resistance factor (β) ≤ 1 and 8 ≤ end bearing capacity factor (N_t) ≤ 50 for the β-method. A recent study using 17 dynamic load test data on H-piles from Wyoming resulted in a calibrated α-method in terms of q_u for predicting pile resistances in sandstone, claystone, and siltstone (Adhikari et al. 2020a).

For q_s prediction, Beake and Sutcliffe (1980) limited q_s = 3.5 to 6.2 ksf from two SLTs of 36- and 42-inch diameter open-ended pipe (OEP) piles in carbonate siltstones and sandstones with q_u = 66 and 98 ksf, respectively. From pile load tests of small-displacement OEP piles in low- to high-density chalk, q_s values ranging from 0.2 to 25 ksf are suggested (CIRIA 2002). Barrett and Prendergast (2020) recently developed an empirical relationship to predict q_s in terms of q_u for 24- to 50-inch OEP piles using five SLTs: one in mudstone, two in siltstone, one in sandstone, one in breccia, and two dynamic load tests in conglomerate rock. Neither of these studies recommended design methods for predicting q_s and q_b in shale.

The challenge with the pile design and construction in shale is further exacerbated by the change in pile resistance with time, particularly the decrease in pile resistance known as pile relaxation reported in literature (Hannigan et al. 2020; Morgano and White 2004; Thompson and Thompson 1985). From a study of H-piles in shale from four project sites, Likins and Hussein (1984) reported pile relaxation of 10% to 50% on weathered shale within two weeks after pile driving. Thompson and Thompson (1985) suggested a range of 11% to 25% decrease in pile capacity determined from the dynamic measurement of close-ended pipe (CEP) piles in shale. An average 35% relaxation on end bearing is reported on piles driven into shales, and OEP piles experienced a greater average relaxation of 44% compared with 34% for H-piles (Hannigan et al. 2020). On the other hand, based on the 17 H-piles tested in shale, Long and Anderson (2014) found almost constant total pile capacity with time with a maximum total setup and relaxation of 19% and 14%, respectively. The aforementioned limited past studies indicate different setup and relaxation in shale materials. Hence, the time-dependent pile responses in shale due to shale weathering deserves further investigation. It is believed that pile relaxation in shale is caused by 1) the development of negative pore water pressure resulting from shale fracture and dilation, 2) change in rock mineralogy and fractures resulting from pile driving, 3) relaxation of stresses in the rock around the pile, 4) shale shattering beneath a pile toe caused by driving adjacent piles to a deeper depth, and 5) shale softening from water migration to the pile toe resulted from negative pore pressure development (Hannigan et al. 2020).

Due to the limited research on driven piles in shale and the absence of reliable design methods, the performance of piles in shale is currently determined based on driving observation, local experience, and load demand through construction control approaches. Considering these shortcomings and challenges, this paper presents a shale classification system, relationships for predicting engineering properties of shale, new SA methods for predicting q_s and q_b for four different shale types and weathering conditions, load and resistance factor design (LRFD) recommendations for the proposed SA methods, and time-dependent pile responses in different shales. The SI version of this chapter can be found in the article published by Islam et al. (2022).

4.2 Usable Pile Data

Seventy-one historical pile load test data from eight counties in Kansas are collected from the Kansas Department of Transportation (KDOT). These test pile data contained all relevant information, including Pile Driving Analyzer (PDA) with Case Pile Wave Analysis Program (CAPWAP) analysis from 16 bridges in nine projects constructed between 2010 to 2017. Among the 71 test piles, 49 test piles with complete information are considered usable in this study. The relevant information of 49 usable test piles with 40 steel H-piles and nine 12.75-inch steel shell driven piles are summarized in Table 4.1. The overburden soil layers included sand, clay, silt, and mixed soil, while the bearing layers are shale. These shale layers are categorized as soil-based shales and rock-based shales. The pile embedment lengths ranged from 22 to 105 ft, and the penetration lengths in shale varied from 33 to 30.1 ft. The q_s and q_b summarized in Table 4.1 are determined from CAPWAP at the end of driving (EOD). These piles are driven using diesel hammers with blow counts (bl) varying from 17 to 640 bl/ft.

Comparing pile resistances in IGMs determined from 19 SLTs and PDA/CAPWAP (Mokwa and Brooks 2008; Long 2016), a mean resistance bias (λ)=1.08 closer to unity and a relatively low coefficient of variation (COV) of resistance bias=0.121 suggested reliability in the CAPWAP results (Adhikari et al. 2020b). Furthermore, past research studies have concluded that pile resistances predicted from CAPWAP are comparable to the measured resistances from SLT (Likins and Rausche 2004). Due to the current design and construction practices as well as high cost, SLT is rarely conducted on driven piles in shale. Hence, to advance the current knowledge and to improve pile

resistance predictions, it is reasonable to use CAPWAP results in this study. However, it is recommended to use available SLT results in future studies.

4.3 Shale Classification and Properties

4.3.1 Shale Classification

A shale classification system based on texture, strength, grain size, plasticity, chemical, or mineralogical characteristics, and bonding has been proposed by several investigators (Coduto 1999; Eid 2006; Underwood 1967). In addition, a shale classification system has been established based on Atterberg limits, slake durability, and the jar slake test (Deo 1972; Erguler and Shakoor 2009; Gamble 1971; Hopkins and Deen 1984). These shale classification systems are developed over time for different applications. Considerable discrepancies in the shale categorization and properties suggested the need for a more comprehensive classification system. The classification system by Underwood (1967) has been widely used to distinguish problematic shales from stronger shales for engineering design purposes (Yagiz 2001). This study adopted recommendations from Underwood (1967) and classified the shales into two broad types: “soil-like or soil-based shale” and “rock-based shale” based on the field identification system. The soil-based shales are defined as compacted shale that contained soil particles without having intergranular cement such as calcareous, siliceous, and carbonaceous. The rock-based shales are defined as cemented or bonded shale having intergranular cement (Underwood 1967). Generally, soil-based shales are easily separated while rock-based shale is harder and more durable and cannot be easily separated into smaller pieces.

Depending on the presence of clay, silt, and sand-sized particles, KDOT classified soil-based shales into three subgroups: clayey shale, silty shale, and sandy shale. The proposed classification system is to first distinguish the soil-based shales from the rock-based shales using the field identification system. Furthermore, the “soil-based” (SS) shales included clayey shale and silty shale, with hardness defined as soft, moderately hard, and hard. The swell potential is used to distinguish clayey from silty shale as clayey shale swells in a barrel or core box. Five degrees of weathering (fresh, slightly weathered, moderately weathered, weathered, and highly weathered) are used by KDOT to describe the rock-based shale weathering. The fresh rock-based shale does not contain decomposition of the parent material and microcracks, and the slightly weathered rock-based shale showed a slight decomposition of parent material in joints with hairline cracks. On the other hand, moderately and weathered rock-based shale contained well-developed and decomposed joints with visible microcracks. The highly weathered rock-based shale is highly decomposed and extremely broken. Using those descriptions, the rock-based shale is classified into three different subgroups: soft & highly weathered shale (HW), moderately hard & moderately weathered to weathered shale (MW), and hard, fresh & slightly weathered shale (SW) as indicated in Table 4.1.

Table 4.1 Summary of usable driven piles in shales from Kansas

Pile ID	County of Kansas	Pile	L_{EMB} (ft)	L_{IGM} (ft)	Overburden Geomaterial	End bearing shale layer at pile toe	Shale	q_u[a] (ksf)	RQD[a] (%)	q_s[a] (ksf)	q_b (ksf)	Pile Hammer	BC
1	Clark	HP 14×73	94	19.26	sand	clayey, maroon shale	SS	9.6	73	1.4	59.9	Del. D19-42	87
2	Finney	HP 12×63	50	6.5	mixed	dark gray, calcareous, slightly w. shale	SW	124.1	100	3.8	302.0	Del. D19-42	120
3	Finney	HP 10×42	58	6.1	mixed	dark gray, calcareous, slightly w. shale	SW	124.1	100	2.9	326.4	Del. D19-42	59
4	Finney	HP 12×63	50	4.4	mixed	gray, calcareous, slightly w. shale	SW	125.9	84	2.8	332.1	Del. D19-42	160
5	Sedgwick	HP 12×63	81	12.1	sand	gray, calcareous, hard slightly w. shale	SW	39.3	76	3.4	305.1	Pil. D30-32	87
6	Sedgwick	HP 10×42	80	6.3	mixed	dark gray, clayey shale	SS	4.6	92	1.1	71.0	Del. D19-32	28
7	Sedgwick	HP 12×53	73	9.8	sand	shades of gray, silty shale	SS	4.8	91	1.0	96.3	Del. D30-02	18
8	Sedgwick	HP 12×74	68	8.5	sand	green gray, highly w. shale	HW	5.8	88	0.6	157.7	Del. D30-02	27
9	Sedgwick	HP 12×74	69	10.2	sand	dark gray to gray, clayey shale	SS	5.8	88	NA	102.1	Del. D30-02	20
10	Sedgwick	HP 12×53	87	20.8	mixed	gray to dark gray, silty shale	SS	10.2	75	2.3	134.9	Pil. D30-32	40
11	Sedgwick	HP 10×42	80	4.96	clayey sand	Moderately hard, silty shale	SS	8.1	86	1.5	138.7	Del. D16-32	53
12	Sedgwick	HP 12×84	33	11.1	sand	hard, silty, gray shale	SS	24.9	57	2.2	162.5	Pil. D30-32	25
13	Sedgwick	HP 12×63	68	6.4	mixed	dark gray, banded, w. shale	MW	5.0	86	1.3	175.6	Del. D30-02	36
14	Sedgwick	HP 10×42	105	18.2	sand	dark gray to gray, w. shale	MW	11.1	85	1.6	190.7	Del. D19-32	60
15	Sedgwick	HP 12×53	73	3.4	clayey sand	dark gray, w. shale	MW	6.9	86	1.8	200.7	Del. D30-02	30
16	Sedgwick	HP 10×42	105	10.2	mixed	gray, calcareous shale, slightly w.	SW	17.1	87	2.5	197.8	Del. D19-32	192
17	Sedgwick	HP 12×63	68	16.2	sand	gray, generally w. shale	MW	4.2	92	1.4	226.2	Del. D30-02	24
18	Sedgwick	HP 10×42	84	11	sand	gray to dark gray, w. shale	MW	17.1	87	1.2	292.0	Del. D19-32	51
19	Sedgwick	HP 12×74	70	11.8	sand	dark gray to gray, w. shale	MW	21.9	86	1.3	384.5	Del. D30-02	80
20	Sedgwick	HP 12×74	47	26.8	sand	gray, hard, slightly w. shale	SW	33.2	80	3.3	35.1	Pil. D30-32	34
21	Sedgwick	HP 12×63	59	12.03	sand	gray, soft, highly w. shale	HW	7.7	85	0.8	50.8	Pil. D30-32	17
22	Sedgwick	HP 12×63	58	16.5	mixed	dark gray, silty shale	SS	4.4	22	0.9	129.9	Pil. D30-32	25
23	Sedgwick	HP 12×74	46	18.9	sand	gray, soft, highly w. shale	HW	6.3	66	0.8	135.5	Pil. D30-32	27
24	Sedgwick	HP 12×74	45	16.7	sand	gray, soft, highly w. shake	HW	8.1	90	2.0	87.3	Pil. D30-32	23
25	Sedgwick	HP 12×74	53	8.66	mixed	gray, soft, highly w. to w. shale	HW	8.6	35	0.9	99.8	Pil. D30-32	27
26	Sedgwick	HP 12×74	61	19.76	sand	gray, soft, highly w. shale	HW	4.6	68	1.5	39.7	Pil. D30-32	26
27	Sedgwick	HP 12×63	47	15.8	sand	clayey shale, firm	SS	8.1	84	2.4	84.8	Pil. D19-42	28
28	Sedgwick	HP 12×74	50	16.6	mixed	gray, moderately hard, w. shale	MW	3.8	50	1.7	48.2	Pil. D19-42	32
29	Sedgwick	HP 12×74	35	14.9	sand	gray, soft, highly w. shale	HW	20.7	87	2.0	143.7	Pil. D30-32	52
30	Sedgwick	HP 12×63	50	11.5	mixed	gray, moderately hard, w., thin bedded shale	MW	4.0	89	2.1	163.1	Pil. D30-32	34
31	Sedgwick	HP 12×63	52	25.9	mixed	gray, hard, slightly w., gypsum shale	SW	8.8	95	1.5	195.9	Pil. D30-32	26
32	Sedgwick	HP 12×74	61	20.5	mixed	gray, moderately hard, highly w. shale	MW	7.5	NA	2.4	262.5	Pil. D30-32	34
33	Sedgwick	HP 12×74	61	19	sand	gray, hard, slightly w. shale	SW	2.9	82	1.6	262.5	Pil. D30-32	34
34	Sedgwick	HP 12×74	54	20.7	mixed	gray, soft, highly w. shale	HW	5.0	79	1.0	158.7	Pil. D30-32	28
35	Clay	HP 12×74	29.9	30.1	mixed	clayey, gray, stiff to moderately hard shale	SS	51.6	83	2.6	182.7	Del. D19-42	62
36	Sheridan	12.75"D shell	41	6.9	sand	very dark gray, w. shale	MW	5.2	65	1.4	171.7	Del. D16-32	60

37	Sheridan	12.75"D shell	24	3.4	sand	very dark gray, w. shale	MW	13.6	79	NA	206.6	Del. D16-32	28
38	Sheridan	12.75"D shell	24	3.5	sand	very dark gray, w. shale	MW	5.2	83	1.3	282.2	Del. D16-32	40
39	Sheridan	12.75"D shell	24	6.9	sand	very dark gray, w. shale	MW	22.6	89	2.1	326.9	Del. D16-32	60
40	Sheridan	12.75"D shell	22	4	sand	very dark gray, w. shale	MW	5.2	88	1.5	334.8	Del. D16-32	60
41	Sheridan	12.75"D shell	23	3.3	sand	very dark gray, w. shale	MW	10.0	80	1.4	260.6	Del. D16-32	40
42	Sheridan	12.75"D shell	55	14.5	sand	very dark gray, w. shale	MW	7.1	94	1.6	221.4	Del. D16-32	90
43	Sheridan	12.75"D shell	36	29.4	sand	very dark gray, w. shale	MW	2.5	80	1.1	218.7	Del. D16-32	34
44	Sheridan	12.75"D shell	38	6.7	sand	very dark gray, w. shale	MW	10.0	80	1.4	221.4	Del. D16-32	41
45	Barton	HP 12×63	72	25.24	silty clay	clayey, gray with maroon mottling shale	SS	12.3	96	1.4	87.3	Del. D19-42	102
46	Barton	HP 10×42	82	17.3	mixed	clayey, greenish-gray, maroon shale	SS	9.2	36	1.5	98.0	Del. D19-42	46
47	Franklin	HP 12×53	26	5.45	silty clay	firm, non-weathered shale	SW	30.3	72	2.9	293.6	Del. D19-42	48
48	Geary	HP 12×63	47	21.8	silty clay	gray to blue gray, very hard shale	SW	41.6	69	2.3	236.2	Del. 16-32	640
49	Geary	HP 12×63	60	16.37	silty clay	tan to light gray, vuggy, hard shale	SW	55.3	67	2.7	283.2	Del. 16-32	128

q_u–Unconfined compressive strength; q_s–Unit skin friction at EOD from CAPWAP; q_b–Unit end bearing at EOD from CAPWAP; RQD–Rock quality designation; L_{EMB}–Embedded pile length; L_{IGM}–Embedded pile length in IGM; soil based shale (SS); bl–Pile hammer blow; w.–Weathered; Del.–Delmag; Pil.–Pileco; HW–Soft & highly weathered shale; MW–Moderately hard & weathered shale; SW–Hard & slightly weathered shale; [a]–Average value of all shale layers; and BC–Hammer blow count at EOD per 0.3m of penetration.

Table 4.2 Range, mean, and standard deviation of mechanical properties of shales

Shale type	Qualitative description	N	q_u (ksf)	E (ksf)	γ (lb/ft^3)	ω (%)	RQD (%)	Recovery (%)	q_s (ksf)
Soil-Based Shale (SS)	Clayey shale, silty shale, soft to hard	80	2.1-60 12.7±12.1	77.2-7660.8 877±1368	88.5-140.7 110.8±10.2	7.6-27.9 18.8±5.2	8-100 77±22	27-100 96±12	0.75-2.76 1.65 ± 0.65[a]
Highly Weathered Shale (HW)	Soft, highly weathered	42	2.1-3.47 9.2±7.7	48-3968 490.8±620	93.6-131.8 103.1±8.3	12.7-35.3 24.7±4.4	10-92 70±21	33-100 91±17	0.19-1.1 0.58 ± 0.27[b]
Moderately Hard & Weathered Shale (MW)	Moderately hard, weathered, and moderately weathered	43	2.1-155 24.6±37	52.2-11487 1754.4±2822	78.9-138.1 110.1±13.4	7.6-27.9 18.8±5.2	30-100 81±17	58-100 96±8	1.1-2.4 1.61 ± 0.33[c]
Hard & Slightly Weathered Shale (SW)	Hard, slightly weathered, and fresh	56	3.13-247 73.5±66	85.6-30699 5998±7107	96.8-143 122.9±12.1	7.2-21 14.5±3.3	45-100 86±18	55-100 95±11	2.4-3.78 2.97 ± 0.4[d]

N–Sample size; q_u–Unconfined compressive strength; E–Modulus of elasticity; γ–Dry unit weight; ω –Water content; RQD–Rock Quality Designation; q_s–Unit skin friction; [a]–Sample size 25; [b]–Sample size 16; [c]–Sample size 27 and [d]–Sample size 28.

4.3.2 Shale Properties

KDOT has conducted extensive laboratory tests to measure q_u, Young's modulus (E), unit weight (γ), and water content (ω) of shales following the ASTM standard methods (2005). Similarly, rock quality designation (RQD) of rock cores is determined according to the ASTM (2002). Table 4.2 shows that the mean and standard deviation of q_u, γ, and E of rock-based shales decreased from slightly to highly weathered conditions (i.e., Slightly Weathered, SW) shales exhibit higher mean q_u, γ, and E than that of Moderately Weathered (MW) and Highly Weathered (HW) shales. This trend of properties is expected because the degree of weathering defined the decomposition of parent material in joints and presence of cracks in shale materials. The higher degree of weathering meant the shale materials could be more porous and softer due to the weakening of grain-to-grain bonding. The growing microcracks led to rupture and produced local tensile stress in the shale material under compression. The mean shale properties decreased with the degree of weathering. The natural water content of rock-based shales increased from slightly to highly weathered conditions, and HW shales had the highest mean water content of 24.7%. Similarly, the mean RQD values of rock-based shales decreased from 86% of SW shales to 70% of HW shales, while the mean percent recovery did not show dependency on the weathering conditions. The upper and lower limits of q_s suggest that the q_s of HW shales should be less than 1.1 ksf, the q_s of MW shales should be between 1.1 ksf and 2.4 ksf, and the q_s of SW should be greater than 2.4 ksf. Hence, the rock-based shales can be objectively classified using the suggested q_s ranges, mean RQD, q_u, and E values (Table 4.2).

The mean q_u, γ, and E of SS shales are higher than that of HW, but lower than the MW and SW shales. The SS shale group contained soft to hard shales, which could be a possible reason for having higher q_u than the HW shales. Furthermore, the SS shales are heavily over-consolidated and hardened during their geologic history through overlaying sediments (Bjerrum 1967; Mohamadi 2015). From an extensive study of 121 samples of soil-based shales (geologic group Eagle Ford Shale), Hsu and Nelson (2002) reported that the q_u of shales ranged from 9 to 120 ksf with an average 43 ksf. Another study on slightly weathered clayey shale reported a wide range of q_u from 42 to 167 ksf (Agung et al. 2017). There are several factors, such as mineral constituents, formation, geologic history, which can influence the properties of SS shales.

4.3.3 Stress Strain Behaviors

The available stress-strain behaviors of SS, HW, MW, and SW shales under uniaxial compression are plotted in Figure 4.1. A total 31 samples of various shale groups are tested at a 0.5mm/min strain rate. The Young's modulus, drop modulus (M), and failure strain, along with the pre-failure and post-failure responses, are determined for each sample. The drop modulus described the post-failure behavior is estimated as the slope of a linear fit line in that region (Kivi et al. 2018; Tutluoğlu et al. 2015). In the pre-failure region, some stress-strain curves of both SS and HW shales exhibited a nonlinear response initially followed by a linear-elastic region (Figure 4.1a and 4.1b). In the post-failure region, these two shale groups behaved either almost elastic or perfectly plastic for small strain or more ductile failure with very low drop modulus. The drop modulus is compared with the Young's modulus with an M/E ratio for each sample to evaluate brittle to ductile behaviors. The M/E value greater than one indicates a more brittle failure behavior, equal to one means elastic-perfectly plastic failure, and less than one indicates a more ductile failure behavior. The M/E ratios are always less than one for both SS and HW shales, which indicates less brittle and more ductile behavior. The mean void ratio (e) of 0.6 for SS shales is comparable to the mean e of 0.64 for HW shales.

The stress-strain response of MW and SW shales are shown in Figures 4.1c and 4.1d, respectively. The stress-strain curves initially exhibited nonlinear responses followed by linear elastically at a higher stress level. Immediately after reaching the peak stress, instantaneous stress drop occurred, which indicates more brittle failure behavior. The M/E ratios for all MW and SW shales are more than one, with average ratios of 1.9 and 2.1, respectively. The comparison of stress-strain results concluded that MW and SW shales exhibited brittle failures while the SS and HW shales exhibited more ductile failure behavior. The average e values of MW and SW shales are 0.47 and 0.43, respectively. The lower e values indicated that the MW and SW shales are stiffer and could fracture more easily than the SS and HW shales that are more flexible, deformable, and cannot easily fracture.,

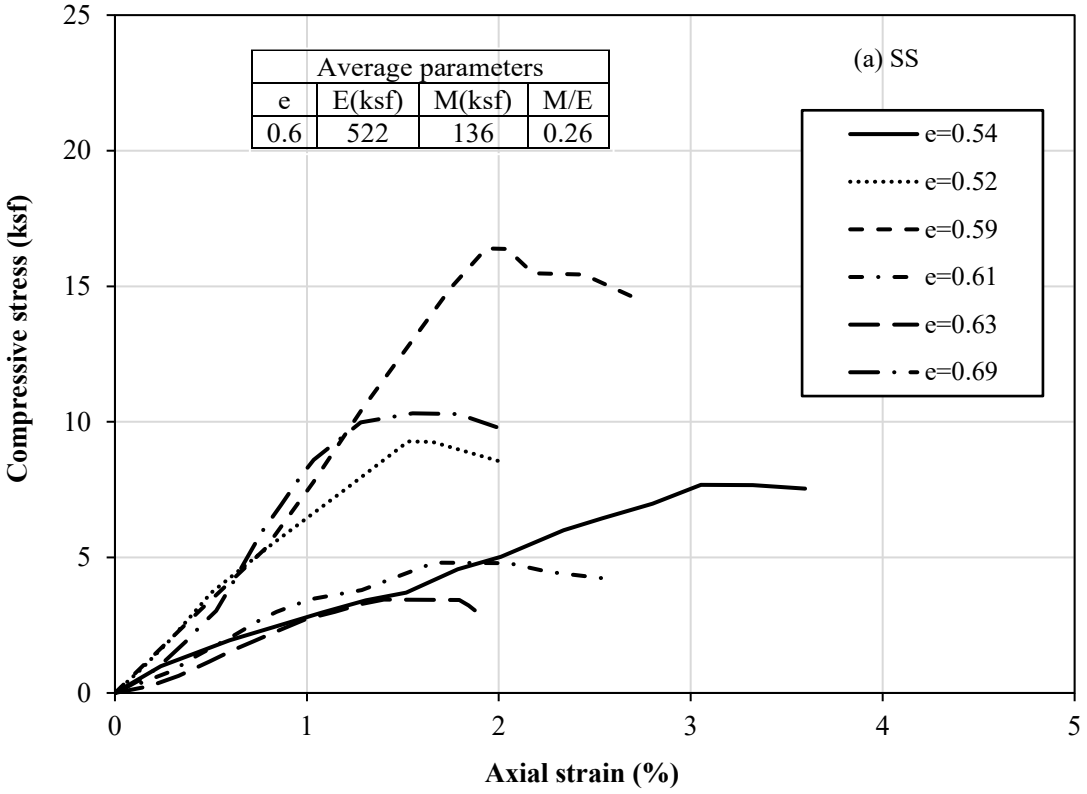

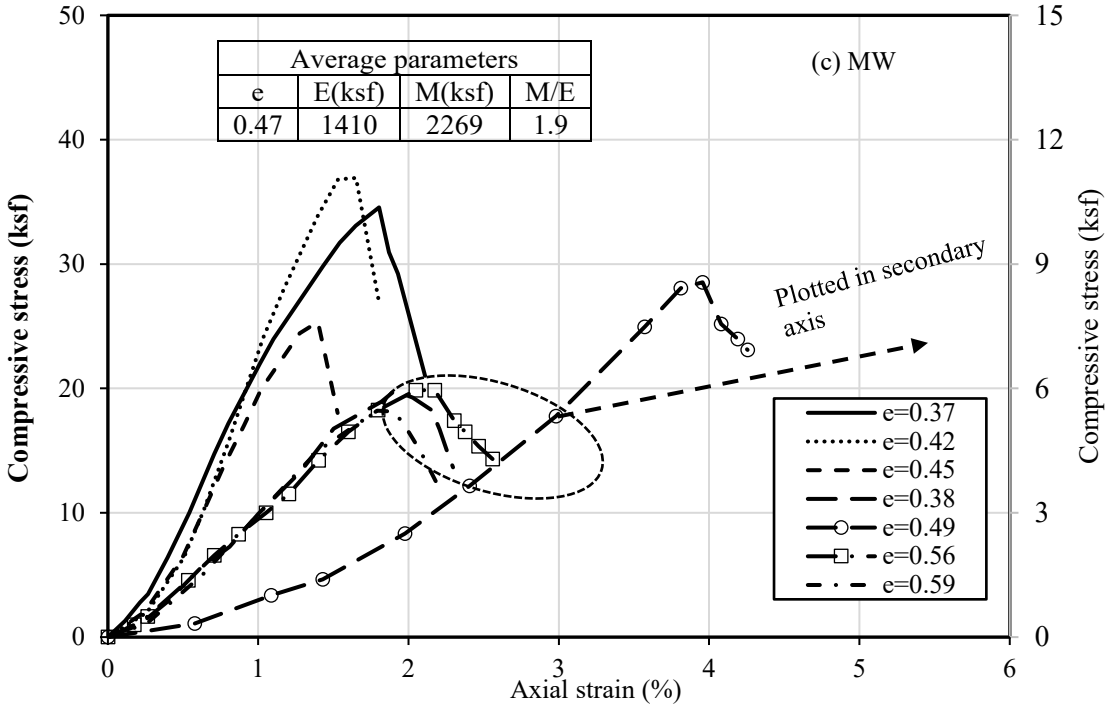
(c) MW
Average parameters
e | E(ksf) | M(ksf) | M/E
0.47 | 1410 | 2269 | 1.9
Plotted in secondary axis
e=0.37
e=0.42
e=0.45
e=0.38
e=0.49
e=0.56
e=0.59
Compressive stress (ksf)
Compressive stress (ksf)
Axial strain (%)

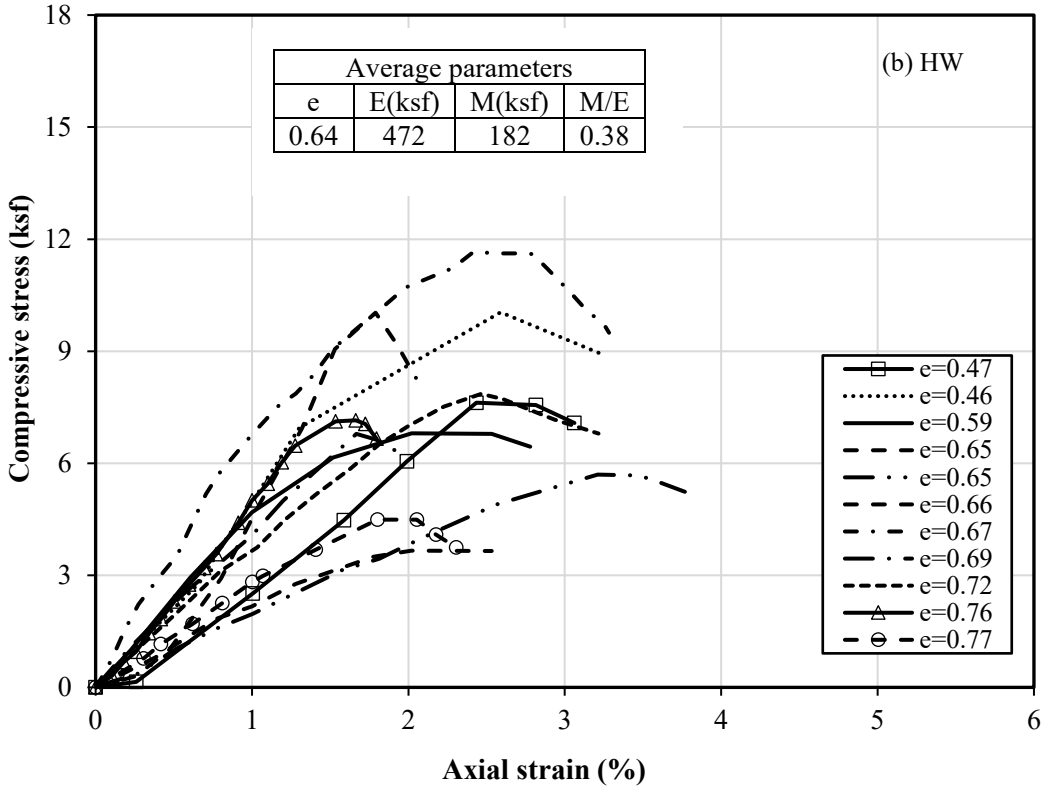
(b) HW
Average parameters
e | E(ksf) | M(ksf) | M/E
0.64 | 472 | 182 | 0.38
e=0.47
e=0.46
e=0.59
e=0.65
e=0.65
e=0.66
e=0.67
e=0.69
e=0.72
e=0.76
e=0.77
Compressive stress (ksf)
Axial strain (%)

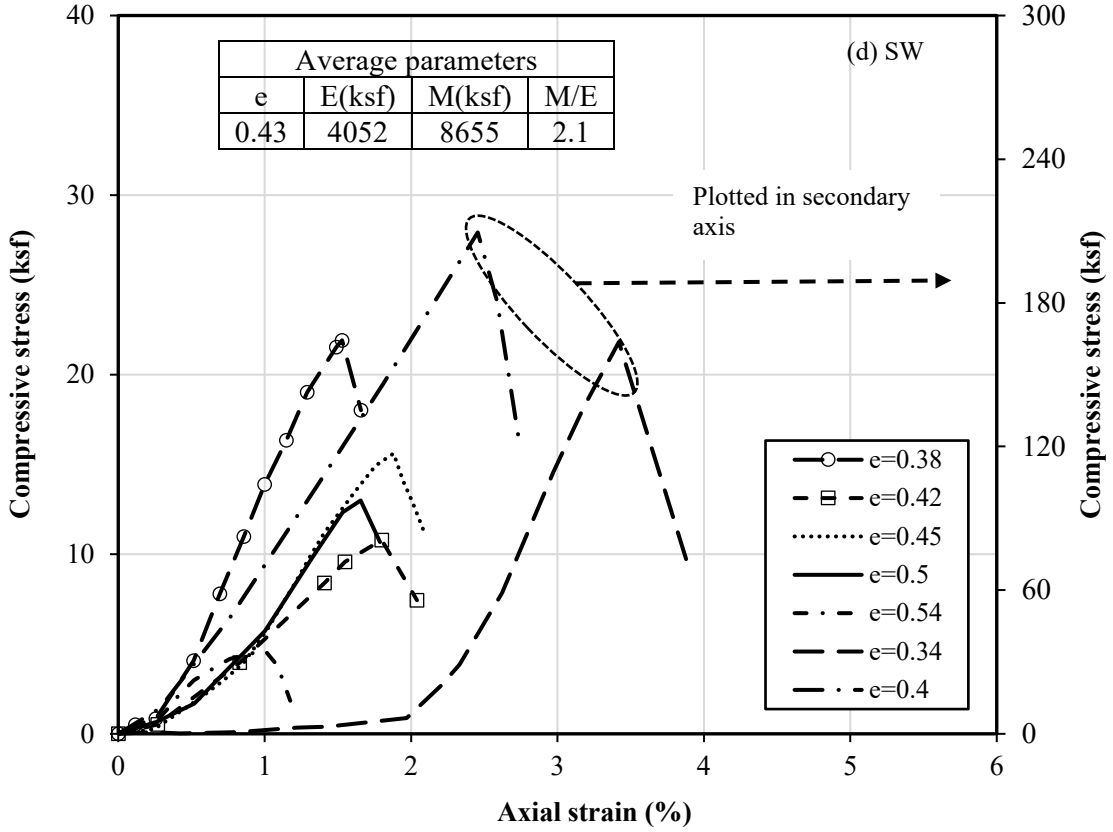

Figure 4.1 Stress–strain curves of (a) soil-based shale, (b) soft & highly weathered shale, (c) moderately hard & weathered shale, (d) hard & slightly weathered shale at their respective void ratios

4.3.4 Young's Modulus of Shale

The logarithmic relationship given by Equation 4.1 between E and a ratio of q_u to ω (%) is shown in Figure 4.2a for 1.7 ksf ≤ q_u ≤ 272 ksf and 7.5 ≤ ω ≤ 35.3%. Statistical indices based on Akaike Information Criteria (AIC) and relative standard error (RSE) are included for comparison. This relationship suggested that a shale with a higher q_u is stiffer and that the stiffness will be softened by the presence of water. The adverse effect of water content on the value of E for shale is attributed to weakening of intermolecular bonds, reduction of cemented quality, porosity, and grain size distribution (Cherblanc et al. 2016; Wang et al. 2017). The effect of q_u and ω on E is similarly observed on shales considered as the bearing layer for drilled shafts (Stark et al. 2013).

$$\widehat{E} = 1173\left(\frac{q_u}{\omega}\right)^{0.86} \tag{4.1}$$

4.3.5 Unconfined Compressive Strength of Shale

Figure 4.2b shows a logarithmic relationship between q_u and ω, whereby the q_u decreases with increase in ω. This relationship is expected because water changes the mineralogy and structure of shales, weakens cementing bonds, alters shale fabric, increases pore water pressure, and serves like a

lubricant during shearing that reduces both stiffness and strength (Talal 2013). Furthermore, softening and expansion of clay minerals in the presence of water contributed to the reduction in q_u (Hawkins and McConnell 1992). In the absence of laboratory strength tests, ω (%) can be used as an index property to predict q_u (ksf) by Equation 4.2. Figure 4.2b also shows the upper and lower bound of the 95% prediction band.

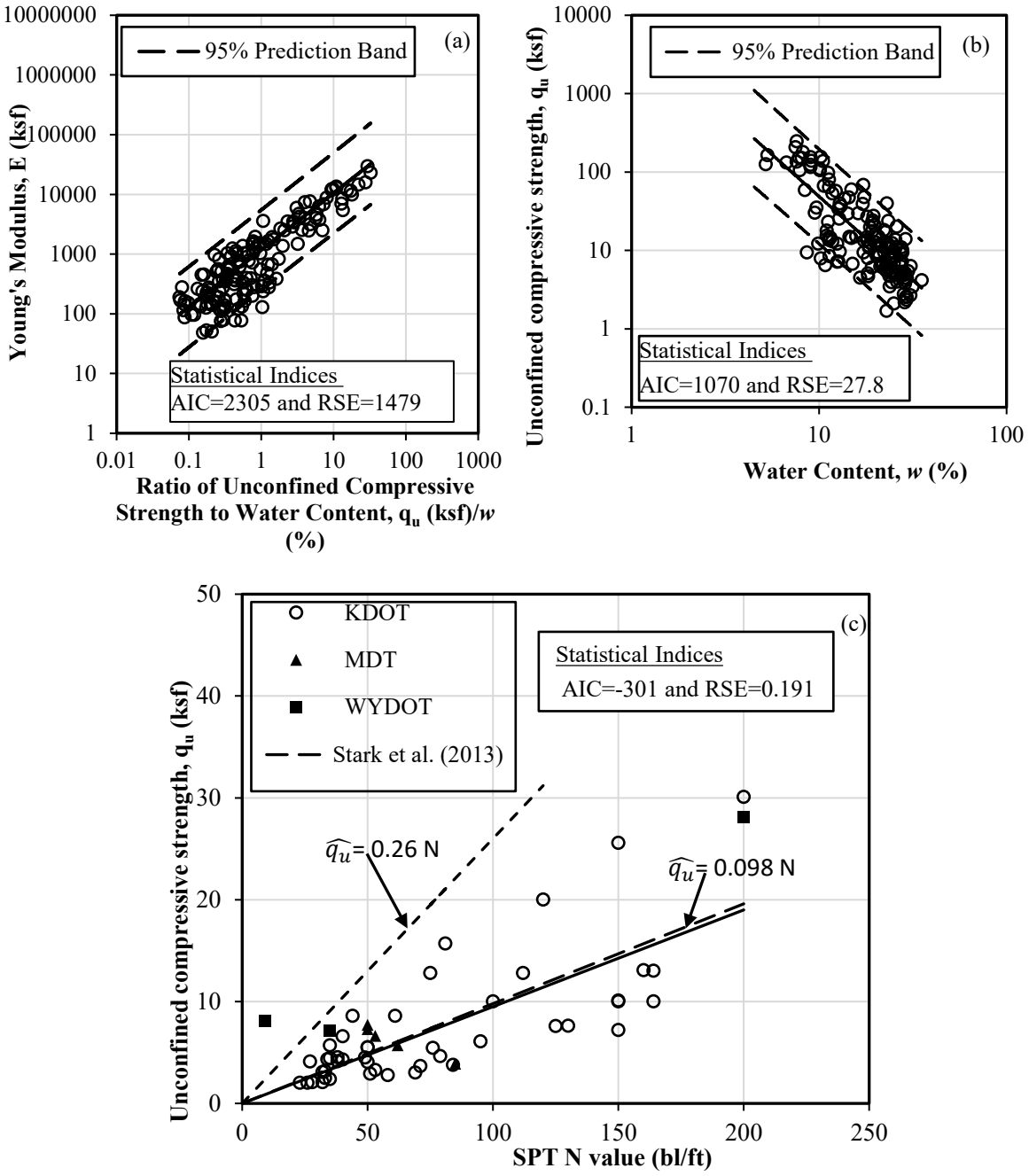

Figure 4.2 Relationships for (a) Young's modulus based on the ratio of unconfined compressive strength q_u to water content ω, (b) q_u based on ω, and (c) q_u based on SPT N-value

$$\hat{q}_u = 670\, e^{-w/4.56} \quad (4.2)$$

Figure 4.2c shows a positive relationship between q_u and SPT N-value of shales obtained from KDOT, Montana Department of Transportation (MDT), and Wyoming Department of Transportation (WYDOT). A linear relationship between q_u and N-value of IGMs had been suggested by researchers. Abu-Hejleh et al. (2005) proposed a linear equation (i.e., q_u=0.26 N) for claystone using four data points collected from two boreholes at two bridge projects on drilled shafts in Colorado. Using 20 load test data on drilled shafts in shales from five bridge projects in Illinois, Stark et al. (2013) developed a linear equation (q_u=0.078 N_{MSPT}) to predict q_u (ksf) using the N-value obtained from a modified standard penetration test (MSPT) that is explicitly described in Long (2016). Based upon our compiled shale data, Equation (4.3) is proposed for q_u, ranging from 2 to 30 ksf for N-values from 23 to 200. Equation 4.3 is comparable to that by Stark et al. (2013).

$$\hat{q}_u = 0.094\, N \quad (4.3)$$

Equation 4.3 can be applied to predict q_u when intact and high-quality shales are difficult to sample for laboratory strength testing. Sampling challenges are exacerbated during a site investigation when the shale is highly weathered, moist, and disturbed by sampling.

4.4 Development of Static Analysis Methods

4.4.1 Unit Shaft Resistance Prediction

The q_s of each shale layer determined from CAPWAP (Table 4.1) is compared with the measured q_u, which is the most widely measured shale property in current practice. Figure 4.3 shows the nonlinear and increasing relationship between q_s and q_u for four shale types based on the aforementioned classification criteria. The q_s for SS increased rapidly with q_u up to about 15 ksf and leveled off thereafter (Figure 4.3a). This behavior indicated the minimal effect of $q_u \geq 15$ ksf on q_s. Similar behavior is observed in SW shales where q_s increased rapidly with q_u up to about 37 ksf (Figure 4.3d). The value of q_s leveled off after a particular q_u value is due to the relative deformation between pile and shale along the pile-shale interface. A softer shale (SS and HW shales) is more ductile or deformable and will experience a higher deformation, which caused full shaft resistance mobilization. A harder shale will have a higher strength for shaft resistance, but less deformability and will dilate and fracture during the relative movement leading to pile-shale slippage. Additionally, localized shear failure may occur at the pile-shale interface at higher q_u. This behavior supported the findings of decreasing shear strength in steel-rock interface with increasing q_u and decreasing steel roughness from the direct shear test of sandstone samples (Ziogos 2020). These similar observations in all shales suggested that q_s will not increase indefinitely with q_u and plastic behavior of shale that eventually governs the ultimate q_s. Figure 4.3 also shows that the q_s of rock-based shales decreased with an increase in weathering conditions (i.e., from slightly to highly weathered). This behavior is attributed to the decrease in q_u and E of shales at higher weathering conditions (Table 4.2). A higher E reduced shale deformation, resulting in an increase in the lateral stress along the pile-shale interface. The maximum q_s values from CAPWAP are 1.1, 2.3, and 3.78 ksf for HW, MW, and SW shales, respectively. The scatter of the measured q_s values in all shale types (Figure 4.3) could be attributed to the heterogeneous nature and intrinsic variability of shale properties from weathering, joint conditions, and sampling disturbance. These heterogeneities are assessed using the power, reciprocal, logarithmic, and exponential models to develop predictions for q_s (ksf) based on q_u (ksf) for four shale types. The best model is selected based on the smallest RSE and AIC. It is important to note that these proposed SA equations (Equation 4.4 through 4.7) are applicable for 0.19 ksf $\leq q_s \leq$ 3.78 ksf and 2.18 ksf $\leq q_u \leq$ 126 ksf and developed for a homogenous shale with no interbedded rock layers along a pile.

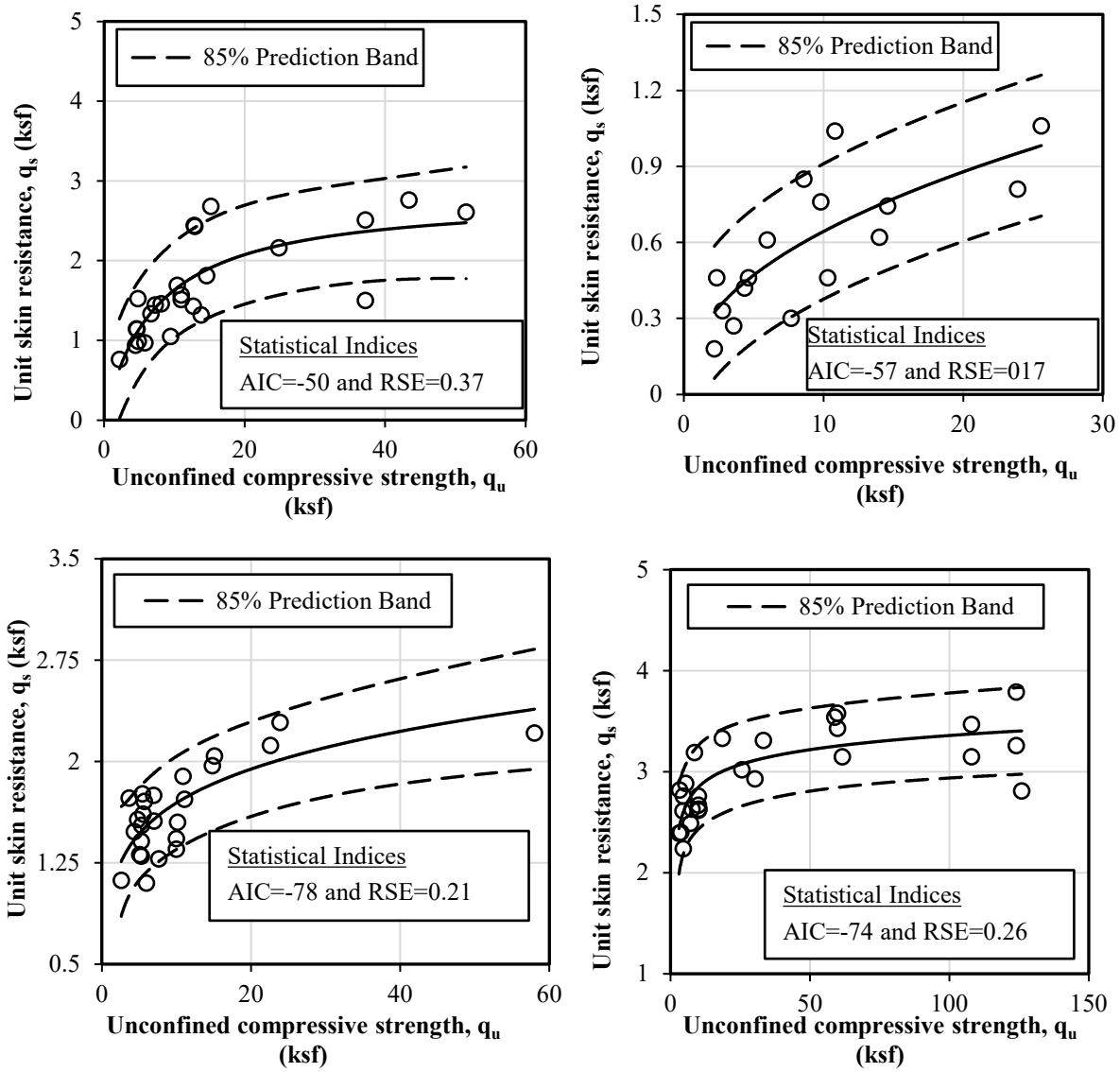

Figure 4.3 The unit shaft resistance of piles driven in: (a) soil-based shale, (b) soft & highly weathered shale, (c) moderately hard & weathered shale, (d) hard & slightly weathered shale

$$\hat{q}_s(\text{SS}) = \frac{3.523\, q_u}{(8.6 + q_u)^{1.05}} \tag{4.4}$$

$$\hat{q}_s(\text{HW}) = 0.23\, q_u^{0.45} \tag{4.5}$$

$$\hat{q}_s(\text{MW}) = \frac{1.196\, q_u}{(0.5 + q_u)^{0.83}} \tag{4.6}$$

$$\hat{q}_s(SW) = \frac{2.62\, q_u}{(0.467 + q_u)^{0.945}} \quad (4.7)$$

4.4.2 Unit End Bearing Prediction

The measured q_b used in this study is calculated by dividing CAPWAP end bearing with a box area of H-pile and a close-ended area of 12.75-in diameter shell pile using the CAPWAP estimated weight of test piles. The test piles data provided by KDOT suggested that MW and SW shales have higher q_b than that of SS and HW shales due to having higher q_u and E as shown in the Table 4.2. Moreover, the stress-strain behavior of MW and SW shales are similar in both the pre-failure and post-failure region (Figures 4.1c and 4.1d). Additionally, these two shale groups exhibited high drop modulus in the post-failure region, which is an indication of brittle failure of these materials. On the other hand, SS and HW shales showed more ductile response in the post-failure region (Figures 4.1a and 4.1b). Table 4.2 indicate that the SS and HW shales are softer than the MW and SW shales. It would be expected that a punching shear failure may occur in SS and HW shales due to lower stiffness. However, a general shear failure may be expected in MW and SW shales due to higher stiffness. Considering the strength and stress-strain response, shales are categorized into two types in the q_b predictions: soil-based, soft & highly weathered (SS-HW) shales with most $q_b \leq 150$ ksf, and moderately hard to hard & weathered to slightly weathered (MW-SW) shales with most q_b values greater than or equal to 150 ksf.

The relationships between q_b and q_u are shown in Figure 4.4 for 20 test piles in SS-HW shales and 29 test piles in MW-SW shales. Figure 4.4a shows a nonlinear and increasing relationship between q_b and q_u for SS-HW shales with 3 q_b values slightly larger than 150 ksf. These 3 q_b values are for harder and more-intact soil-based shale with q_u and RQD greater than 24 ksf and 83%, respectively. Figure 4.4b shows that the q_b of MW-SW shales increased rapidly with q_u up to 37 ksf, and then the increase in q_b reduced thereafter. These rapidly decreasing q_b-q_u trends suggested that either local failure or punching failure is more likely to occur in the shale beneath a pile tip. Table 4.1 shows that among 49 test piles, five rested on the SW shale reached to refusal (blow count greater than 120). This may cause partial mobilization of end bearing due to inadequate energy transferred during the dynamic tests. Consequently, the overall q_b-q_u trend showed a decreasing trend at higher q_u. The ratios of q_b to q_u of SS-HW and MW-SW shales ranged from 3.55 to 21.76 and 2.44 to 80, respectively. The relatively high q_b of MW-SW shales are due to the higher E and q_u against shale deformation. The following prediction equations are proposed to predict q_b (ksf) in terms of q_u (ksf) for the two shale types. Equation 4.8 is applicable for 39 ksf $\leq q_b \leq$ 182 ksf and 3.23 ksf $\leq q_u \leq$ 52 ksf, and Equation 4.9 is applicable for 35 ksf $\leq q_b \leq$ 384 ksf and 3.23 ksf $\leq q_u \leq$ 124 ksf. Similarly, these equations are developed for a homogenous shale layer without any other interbedded rock layers within a distance of 3 times of pile dimension below a pile tip.

$$\hat{q}_b(SS - HW) = 45.72\, {q_u}^{0.35} \quad (4.8)$$

$$\hat{q}_b(MW - SW) = \frac{190.64\, q_u}{(1 + q_u)^{0.88}} \quad (4.9)$$

Although q_b is influenced by q_u, other factors such as frequency and inclination of fissures and joints and the nature of discontinuity can influence the end bearing of the pile in shale. The q_b of a pile could be high if the shale is strong with closely spaced joints. However, shale with an open joint may fail by splitting due to the nonexistence of confining pressure, thus reducing q_b. Consequently, it is

recommended to perform a pile restrike to confirm the target resistance if a pile is driven into a heavily jointed or steeply dipping shale formation (Tomlinson and Woodward 2014).

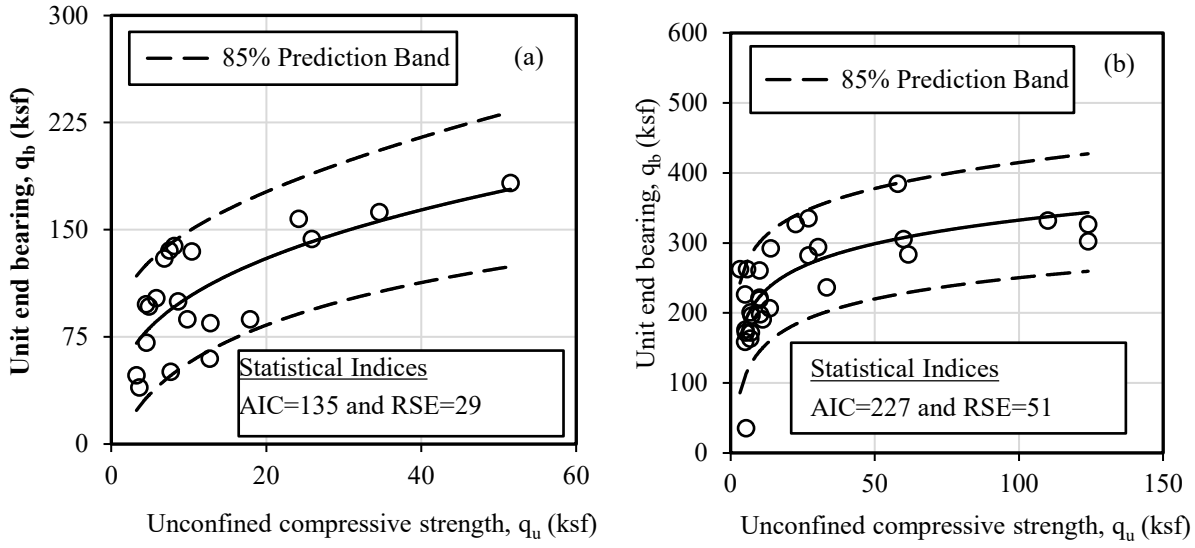

Figure 4.4 Relationship between unconfined compressive strength and unit end bearing of piles driven into: (a) soil based, soft & highly weathered shale, (b) moderately hard to hard & weathered to slightly weathered shale.

4.5 Validation of Proposed Static Analysis Methods

4.5.1 Unit Shaft Resistance Prediction

The performance of the proposed SA methods are evaluated by comparing the predicted resistances with the resistances determined from CAPWAP on 27 independent test piles and one static load test (pile ID 56) from four other DOTs and the literature (Long and Anderson 2012; Morton 2012). The pile, geomaterial, driving, hammer information, average shale properties, and average measured pile resistances of 28 independent test piles are summarized in Table 4.3. Among 28 piles, 27 are tested in 16 counties and five states, and one is tested in Canada. The bearing layers included soil-based and highly weathered to slightly weathered shale, while the overburden layers consisted of sand and mixed soil. The 28 test piles comprised 18 H-piles, 8 OEP, and 2 CEP piles.

Figure 4.5a compares the predicted q_s from Equations (4.4) to (4.7) and measured q_s from CAPWAP and SLT of 39 shale layers and highlights the applicable q_s range between 0.19 and 3.78 ksf used in the development of the proposed prediction equations. The comparison showed that the proposed SA methods underpredicted q_s for $q_s > 3.78$ ksf. Considering all 39 shale layers, the SA methods underpredicted q_s, on average, by about 26% (i.e., mean bias=1.36) and yielded a relatively high COV of 0.86, and the underprediction exacerbated at higher q_s. If the SA methods are applied to the applicable q_s range, the q_s prediction improved with only an average 3% underprediction (mean bias=1.03) and a much lower COV of 0.36. The SA methods provided better q_s predictions on H-piles than pipe piles with about an average 6% overprediction on H-piles and 19% underprediction on pipe piles. Figure 4.5a compares the predicted q_s=2.46 ksf with the measured q_s=2.53 ksf from the static load test on pile ID 56 of the Cerro Gordo 63 bridge in Adair County, Iowa. The subsurface profile consisted of silty clay, sand, glacial till, and a MW shale layer. The proposed method underpredicted the measured q_s value by about 2.5%.

4.5.2 Unit End Bearing Prediction

The performance of the proposed SA methods given by Equation 4.8 and Equation 4.9 for q_b prediction are evaluated by comparing the predicted q_b with the q_b from CAPWAP analysis on 25 independent test piles and one SLT on shale layers from three state DOTs and the literature (Long and Anderson 2012; Morton 2012). Figure 4.5b compares the predicted and measured q_b and highlighted the applicable q_b range between 35 and 384 ksf. The proposed SA methods overpredicted q_b by about 14%, on average, for all 26 data and 20% for 24 data within the applicable q_b range. The mean bias of 0.97 is closer to unity, and a smaller COV of 0.31 suggested that the SA methods provided better prediction of q_b for H-piles than pipe piles. In fact, the SA methods overpredicted q_b for pipe piles by about 69%. Comparing with q_b prediction on SS-HW and MW-SW shales, Equation 4.8 yields better prediction on SS-HW shales with a mean bias of 1.03 and a smaller COV of 0.33 compared with that for MW-SW shales with Equation 4.9. The predicted q_b=85 ksf from the proposed equation is close to the measured q_b=62 ksf from SLT. The difference is attributed to the full mobilization of q_b during the dynamic testing. The proposed SA method for steel H-pile provided a reasonable prediction for q_s and q_b compared with that from CAPWAP and SLT.

Table 4.3 Summary of independent test pile data used in the validation study

Pile ID	Source	County, State or Country	Pile	L_{EMB}	L_{IGM}	Over-burden	End bearing shale layer	Shale Group	qua	RQD[a]	q_s[a]	q_b	Pile	BC
50	IADOT	Franklin	HP 10×57	20.0	3.5	sand	light gray, hard, slightly w. shale	SW	491*	86	6.22	221.80	Del. D19-42	120
51	WYDOT	Franklin	HP 10×57	20.0	3.5	sand	light gray, hard, slightly w. shale	SW	11.5*	86	7.21	298.24	Del. D19-42	120
52		Cerro Gordo	HP 14×73	11.1	9.0	sand	gray, slightly w. shale	SW	4.39*	NA	2.15	135.76	Del. D19-42	84
53		Cerro Gordo	HP 10×42	28.5	6.7	sand	gray, slightly w. shale	SW	8.14*	NA	NA	342.10	Del. D19-42	74
54		Ottumwa	HP 10×42	36.0	2.0	mixed	gray, slightly w. shale	SW	34.3*	NA	2.28	526.10	Del. D19-42	151
55		Adair	HP 10×57	56.0	6.5	mixed	Moderately w. shale	MW	4.59	NA	3.11	54.72	Del. D22	156
56		Adair	HP 10×57	56.0	6.5	mixed	Moderately w. shale	MW	4.59	NA	NA	NA	NA	NA
57		Plymouth	HP 10×57	44.0	10.2	mixed	dark gray firm to hard shale	SW	14.2*	NA	1.96	284.88	APE D19-42	53
58		Warren	HP 10×42	49.0	6.9	mixed	Highly w. shale	HW	14.2*	NA	0.31	85.63	Del. D19-32	18
59		Davis	HP 14×88	21.7	3.4	mixed	soft, clayey shale	SS	1.04	NA	2.84	119.46	Del. D19-42	53
60		Davis	HP 14×117	26.0	5.0	mixed	soft, maroon clayey shale	SS	1.25	NA	1.82	148.91	Del. D19-42	160
61		Hot Springs	HP 14×73	27.0	13.5	sand	hard slightly w. shale	SW	170.63	72	3.59	293.02	ICE 42-S	263
62	ITD	Natrona	HP 14×117	20.0	0.5	mixed	soft, highly w. shale	HW	8.15	11	0.50	149.33	MVE D-19	120
63		Lemhi	HP 12×74	71.0	70.4	mixed	moderately hard, w. shale	MW	5.22*	NA	0.54	NA	ICE I-30-V2	61
64	MDT	Lemhi	HP 12×74	64.0	61.9	mixed	dark, very soft-soft shale	HW	7.31*	NA	0.92	NA	ICE I-30-V3	64
65		Carbon	HP 14×117	32.6	18.2	mixed	moderately w. shale	MW	8.56	NA	1.63	377.19	ICE 80S	156
66	Morton (2012)	Teton	16"×0.75" OEP	26.6	13.0	gravel	slightly w. shale	SW	195.28	90	4.89	444.23	ICE I-36	240
67		Roosevelt	16"×0.5" OEP	95.0	2.5	mixed	gray, laminated, hard shale	SW	6.06*	86	2.07	134.08	APE D36-26	74
68		Roosevelt	16"×0.5" OEP	97.9	10.7	mixed	gray, laminated, hard shale	SW	6.06*	86	4.59	138.26	APE D36-26	192
69		Roosevelt	16"×0.5" OEP	81.0	5.2	mixed	gray, laminated, hard shale	SW	7.31*	89	3.78	141.39	APE D36-26	109
70		Musselshell	16"×0.5" OEP	32.7	21.3	mixed	dark grey to grey, hard shale	SW	13.16	70	3.45	139.10	Del. D19-32	160
71		Valley	20"×0.5" OEP	93.8	8.9	mixed	slightly w. shale	SW	3.97	100	3.76	61.40	Del.D-46-42	31
72		Valley	20"×0.5" OEP	91.8	7.2	mixed	moderately w. shale	MW	5.64	100	1.92	113.20	Del.D-46-32	29
73		Phillips	20"×0.5" OEP	136.5	2.1	mixed	dark gray, very hard shale	SW	11.7*	NA	3.34	57.43	ICE I-36	47
74		Treasure	16" CEP	32.5	21.5	mixed	dark grey to grey shale	SW	6.26*	NA	2.84	160.82	Del. D19-32	109
75		Golden Valley	16" CEP	27.5	12.0	mixed	dark grey, hard shale	SW	13.78	55	2.51	238.72	ICE 42S	160
76		Canada	HP 14×117	NA	NA	NA	dark shale, severely fractured	HW	208.85	13	NA	279.86	NA	108
77	L&A (2012)	Illinois	HP 14×117	15.0	2.0	mixed	moderately w. shale	MW	6.27	NA	0.84	169.59	NA	NA
50	IADOT	Franklin	HP 10×57	20.0	3.5	sand	light gray, hard, slightly w. shale	SW	491*	86	6.22	221.80	Del. D19-42	120

q_u–Unconfined compressive strength; *– estimated using **Equation** (3); q_s–Unit skin friction; q_b–Unit end bearing; RQD–Rock quality designation; L_{EMB}–Embedded pile length; L_{IGM}–Embedded pile length in IGM; bl–Pile hammer blow; L&A–Long and Anderson; w.–Weathered; Del.–Delmag; Pil.–Pileco; SS–Soil based shale; HW–Soft & highly weathered shale; MW–Moderately hard & weathered shale; SW–Hard & slightly weathered shale; NA–not available; [a]–Average value of all shale layers; and BC–Hammer blow count at EOD.

4.6 Change in Pile Resistance in Shale

4.6.1 Change in Unit Shaft Resistance

CAPWAP results at EOD and beginning of restrike (BOR) of 39 test piles conducted in Kansas, Wyoming, and Iowa are used to investigate the change in pile resistances in shales. The 39 test piles consisted of 33 H-piles, and six 12.75-inch diameter shells driven into 76 shale layers. The percent change in $q_{s\text{-}t}$ at an elapsed time (t) after EOD with respect to $q_{s\text{-}to}$ at EOD is plotted against t ranging from 0.25 hours to 25 hours on a logarithmic scale (Figure 4.6). Logarithmic time is selected following the pile response in fine-grained soil determined from past studies (Abu-Farsakh and Haque 2020; Haque et al. 2017; Ng et al. 2013b). To compare the change in q_s, a rate of change in q_s with respect to t known as the A factor is determined using Equation 3.11 considering the initial time (t_o) at 0.01 hour (Skov and Denver 1988) as shown in Table 4.4. A positive A factor indicated an increase in pile resistance with time known as pile setup, while a negative A factor indicated a decrease in pile resistance with time known as pile relaxation. A ratio of maximum pile hammer energy (EMX) at BOR to EMX at EOD is calculated for each event to evaluate the effect of hammer performance on the pile resistances determined from PDA testing. The EMX ratios, ranging from 0.94 to 1.23 at one standard deviation with an average ratio of 1.07 (Table 4.4), suggested that the hammer performance had little to no effect on the time-dependent pile resistances, and apparent pile setup or relaxation is not a concern in this study.

Figure 4.6a indicated that the SS shale always exhibited a positive change in pile resistance or pile setup with an average A factor of 0.76. This is attributed to the presence of fine-grained soils in the SS shale, described as clayey shale and silty shale. Pile setup in SS shale is attributed to the dissipation of excess pore water pressure induced from pile installation that caused consolidation of SS shale along the pile and increased the effective stress with time. This phenomenon is similarly observed in fine-grained soils (Long et al. 1999; Ng et al. 2013a; b). The q_s in the SS shale increased, on average, by about 75% and 89% within 15 minutes and 24 hours, respectively after the EOD. The broad range of A factors summarized in Table 4.4, which changed in q_s (Figure 4.6a), could be attributed to the range of permeability of SS shales resulting from geological processes (Neuzil 1994) that influenced the rate of pore water pressure dissipation and consolidation.

Table 4.4 Summary of setup factors for driven piles in shales

Pile ID	Pile	End bearing layer	Shale Group	EOD		BOR		Setup factor, A	
				BC	E_{max} (kip-ft)	BC[a]	E_{max} (kip-ft)	Shaft[a]	End bearing
4	HP 12×63	gray, calcareous, slightly w. shale	SW	160	22.90	480	22.09	0.06	-0.04
6	HP 10×42	dark gray, clayey shale	SS	28	16.20	32	17.66	0.21	0.89
7	HP 12×53	shades of gray, silty shale	SS	18	31.90	24	30.55	0.07	0.58
8	HP 12×74	green gray, highly w. shale	HW	27	31.20	34	37.46	0.39	0.35
11	HP 10×42	Moderately hard, silty shale	SS	53	20.70	80	22.08	0.59	0.08
12	HP 12×84	hard, silty, gray shale	SS	25	22.30	48	21.01	0.11	0.95
13	HP 12×63	dark gray, banded, w. shale	MW	36	18.60	80	20.88	1.87	0.15
14	HP 10×42	dark gray to gray, w. shale	MW	60	21.10	69	19.82	1.32	-0.01
15	HP 12×53	dark gray, w. shale	MW	30	22.40	53	20.97	0.16	0.47
16	HP 10×42	gray, calcareous shale, slightly w.	SW	192	19.20	240	20.56	0.1	0
17	HP 12×63	gray, generally w. shale	MW	24	35.20	30	38.06	0.11	0.88
18	HP 10×42	gray to dark gray, w. shale	MW	51	19.20	63	19.69	0.63	-0.28
19	HP 12×74	dark gray to gray, w. shale	MW	80	35.90	60	36.49	0.83	-0.16
21	HP 12×63	gray, soft, highly w. shale	HW	17	30.50	32	37.05	0.32	0.57
22	HP 12×63	dark gray, silty, shale	SS	25	34.70	32	37.30	0.11	0.63
23	HP 12×74	gray, soft, highly w. shale	HW	27	31.50	37	35.11	0.1	0.07
24	HP 12×74	gray, soft, highly w. shake	HW	23	22.30	37	25.18	0.03	0.22
25	HP 12×74	gray, soft, highly w. to w. shale	HW	27	27.00	33	26.68	-0.06	0.53
26	HP 12×74	gray, soft, highly w. shale	HW	26	26.70	46	29.09	0.17	0.31
27	HP 12×63	clayey shale, firm	SS	28	21.70	38	22.24	0.45	0.32
29	HP 12×74	gray, soft, highly w. shale	HW	52	24.50	960	30.10	0.15	0.23
31	HP 12×63	gray, hard, slightly w., gypsum shale	SW	26	29.70	35	29.30	0.93	-0.28
34	HP 12×74	gray, soft, highly w. shale	HW	28	26.40	44	25.45	0.75	0.15
35	HP 12×74	clayey, gray, stiff to moderately hard shale	SS	62	15.90	68	18.09	0.14	0.48
36	12.75"D shell	very dark gray, w. shale	MW	60	14.30	96	17.07	0.34	0.11
38	12.75"D shell	very dark gray, w. shale	MW	40	19.50	40	21.92	1.28	-0.06
39	12.75"D shell	very dark gray, w. shale	MW	60	21.40	67	22.30	0.47	-0.15
40	12.75"D shell	very dark gray, w. shale	MW	60	19.40	69	20.66	-0.56	0.07
41	12.75"D shell	very dark gray, w. shale	MW	40	19.31	60	20.46	0.15	0.19
42	12.75"D shell	very dark gray, w. shale	MW	90	14.90	160	17.86	0.19	0.1
45	HP 12×63	clayey, gray with maroon mottling shale	SS	102	18.30	120	17.20	0.36	0.76
54	HP 10×42	gray, slightly w. shale	SW	151	23.03	160	22.06	0.01	-0.02
55	HP 10×57	Moderately w. shale	MW	156	12.50	173	13.96	0.08	0.22
56	HP 10×57	Moderately w. shale	MW	68	15.80	120	19.00	0.39	-0.1
57	HP 10×57	dark gray firm to hard shale	SW	53	18.40	60	20.20	0.04	-0.04
58	HP 10×42	Highly w. shale	HW	18	15.77	120	19.32	1.59	1.71
59	HP 14×117	soft, clayey shale	SS	53	16.10	40	18.00	1.42	0.57
60	HP 14×117	soft, maroon clayey shale	SS	160	15.80	156	15.63	1.35	0.08
61	HP 14×73	hard slightly w. shale	SW	263	23.10	240	23.01	-0.1	-0.07

SS–Soil based shale; HW–Soft & highly weathered shale; MW–Moderately hard & weathered shale; SW–Hard & slightly weathered shale; NA–not available; [a]–Average value of all shale layers; and BC–Hammer blow count and E_{max}– maximum hammer energy

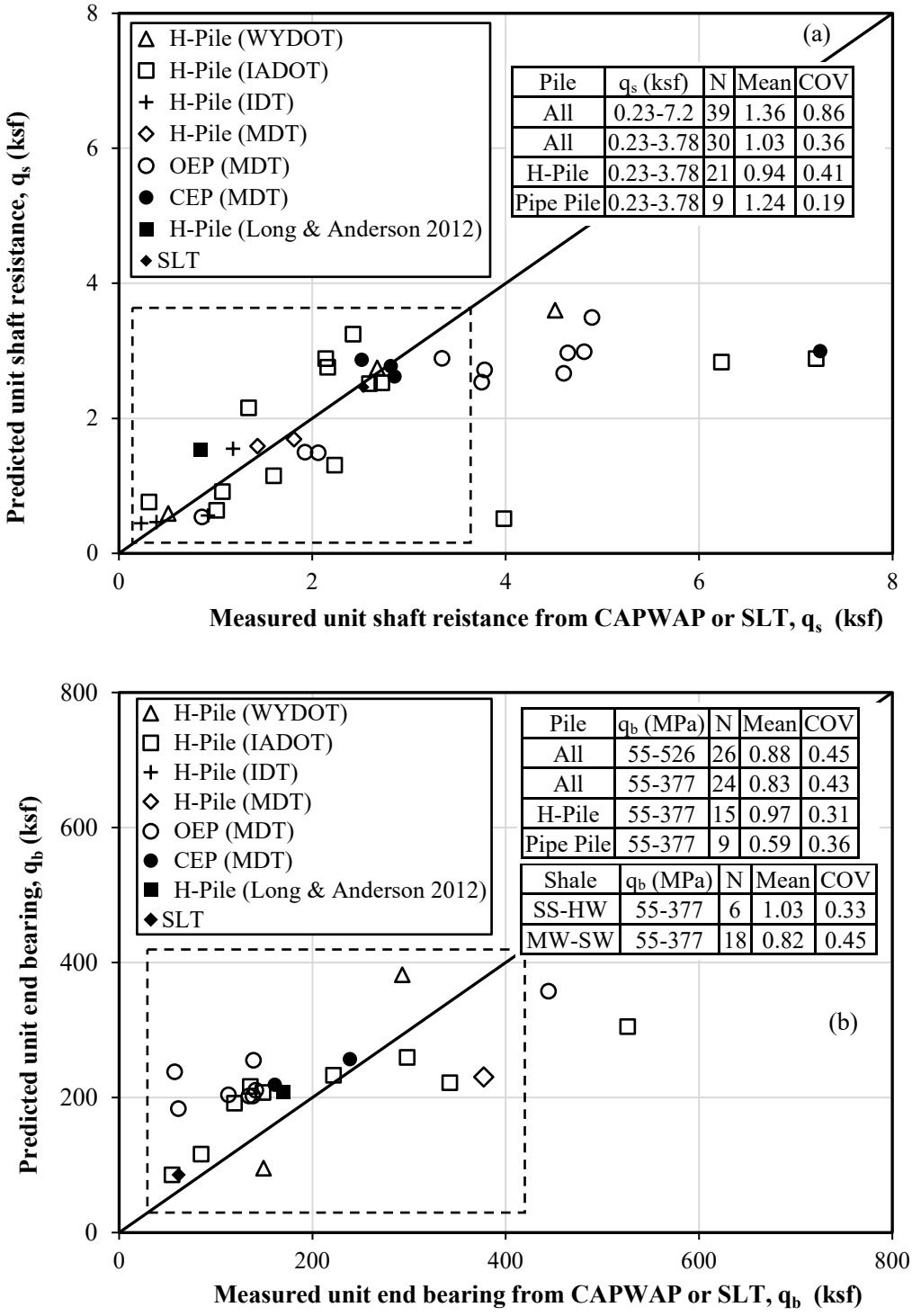

Figure 4.5 Comparison of unit pile resistances from CAPWAP with (a) predicted unit skin frictions from Equations 4.4 to 4.7, and (b) unit end bearings from Equations 4.8 and 4.9

On the other hand, rock-based shales exhibited both pile setup and relaxation. Among the three rock-based shales, piles in the HW shale exhibited the highest pile setup with an average A factor of 0.36 (Figure 4.6b). Additionally, the q_s in HW shale increased, on average, by 32% and 52% in 15 minutes and 24 hours, respectively. A slightly lower average A value of 0.22 (Figure 4.6c) is found on piles driven in MW shales due to more relaxation in MW shales. In contrast, piles driven in SW shales exhibited mostly relaxation with an average A factor of -0.004 and an average 6.5% decrease of q_s in 24 hours (Figure 4.6d). Figures 4.6b through 6d indicated that the average time-dependent q_s changed from setup to relaxation from high to low degree of weathering (i.e., from HW to SW shales). This is likely due to the excess pore pressure dissipation and consolidation of HW shales leading to pile setup and shattering of some softer HW shales from pile driving leading to pile relaxation. The dilation of less weathered and stiffer MW and SW shales resulted in negative pore water pressure generation. The negative water pressure collected water toward the pile and softened the shales leading to pile relaxation. Furthermore, the high lateral stress possibly relieved around the disturbed zone, which resulted from displacement and dilation of less weathered and stiffer shales along the pile shaft due to pile driving (Hannigan et al. 2020; Samson and Authier 1986). Higher dilation and relief of lateral stress in SW and MW shales are attributed to higher stiffness (Table 4.2 and Figure 4.1). Therefore, relaxation and setup should be cautiously considered during pile design in rock-based shales, and pile construction control should be performed to evaluate the time-dependent pile shaft resistances in rock-based shales.

4.6.2 Change in Unit End Bearing

The percent change in q_b *with* t in a logarithmic scale is shown in Figure 4.7. Piles driven in the SS and HW shales exhibited setup in all cases due to higher compressibility and lower stiffness that caused less pile rebound during driving. Additionally, the pile driving created instantaneous excess pore water pressure followed by dissipation that led to consolidation and an increase in effective shale strength. The SS shale exhibited more setup than HW shale for 15 minutes and 24 hours (Figure 4.7a and 4.7b), and the average A factor 0.53 of SS shales is slightly higher than the 0.46 of HW shales. However, according to the four steel H-piles driven in HW shales reported by Hannigan et al. (2020), q_b relaxation is reported with an average A factor of -0.08. Although the magnitude of this relaxation A factor is relatively small, considering that q_b setup in pile design should be accompanied with construction control to evaluate the time-dependent q_b during construction.

Piles driven in the MW and SW shale experience both setup and relaxation in q_b (Figure 4.7c and 4.7d). An average setup factor of 0.11 is determined for piles in MW shales with an average 34% increase in q_b at 24 hours after the EOD. However, an average relaxation factor of 0.07 is determined for piles in SW shales with an average 14% relaxation in q_b at 24 hours after the EOD. Figure 4.7c and 4.7d clearly indicated that SW shales exhibited more prominent relaxation than MW shales. This behavior is attributed to higher stiffness of SW shales that led to pile rebound during driving and created a gap between the pile toe and SW shale. From the case study of the pile in weak rock, Peiris et al. (2010) and Samson and Authier (1986) reported that piles driven through lower shaft resistance grounds into higher end bearing layer are more susceptible to relaxation, which could be a possible reason for relaxation in MW and SW shales. Furthermore, relaxation could result from shale softening from water migrating to pile toe resulting from the development of negative pore water pressure induced by the fracturing of shale, possible disturbance of weak planes such as joints and steep bedding plane, and foliation angle (Hannigan et al. 2020; Poon et al. 2017). The relaxation A factors of -0.07 for SW shale for H-piles match well with that determined for H-piles from Hannigan et al. (2020). This agreement strongly suggested that piles driven in SW shales likely experience relaxation in q_b and construction control should be included to determine the relaxation in end bearing.

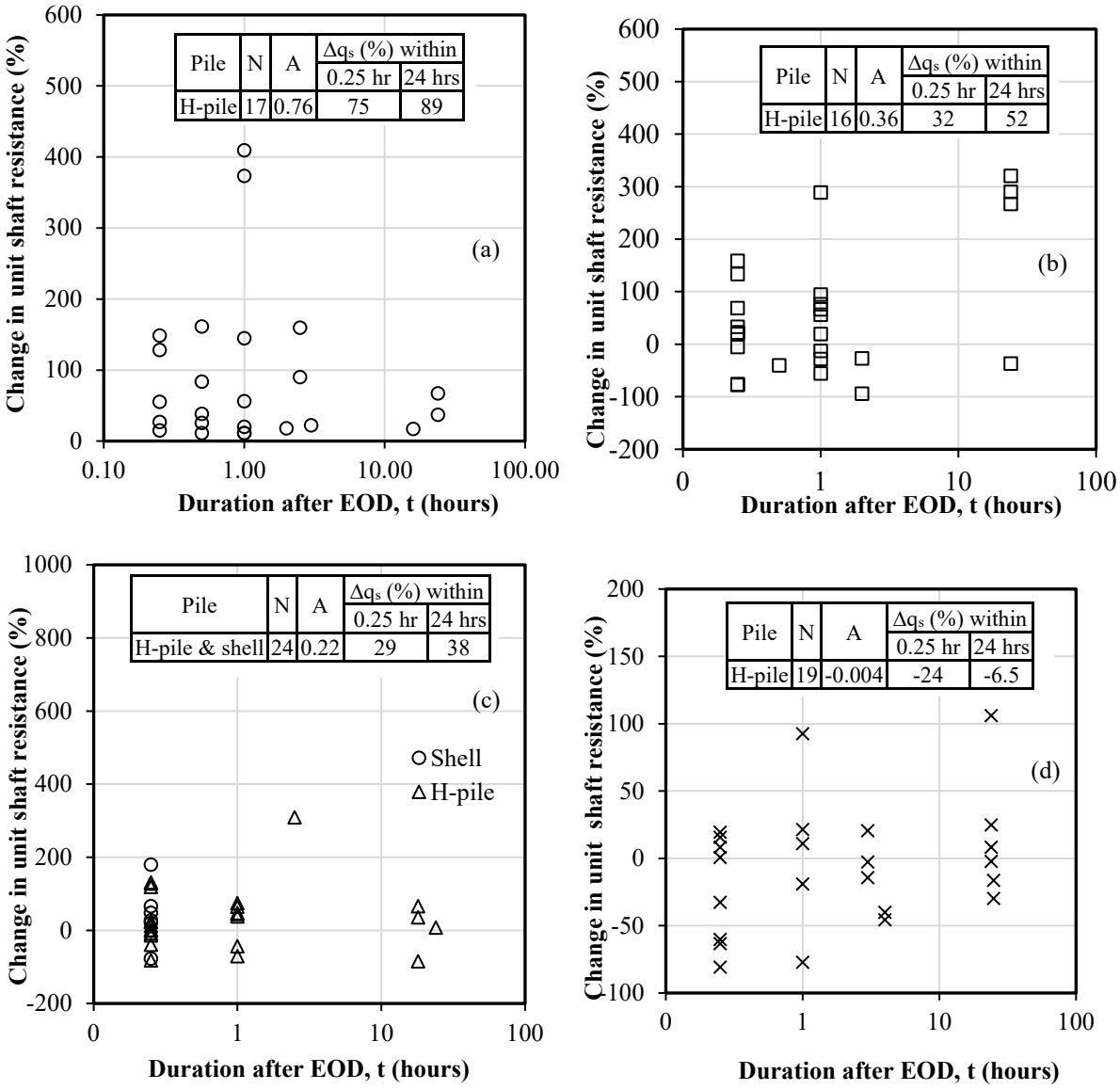

Figure 4.6 Percent change in the unit shaft resistance with time in logarithmic scale: (a) SS shale, (b) HW shale, (c) MW shale, (d) SW shale

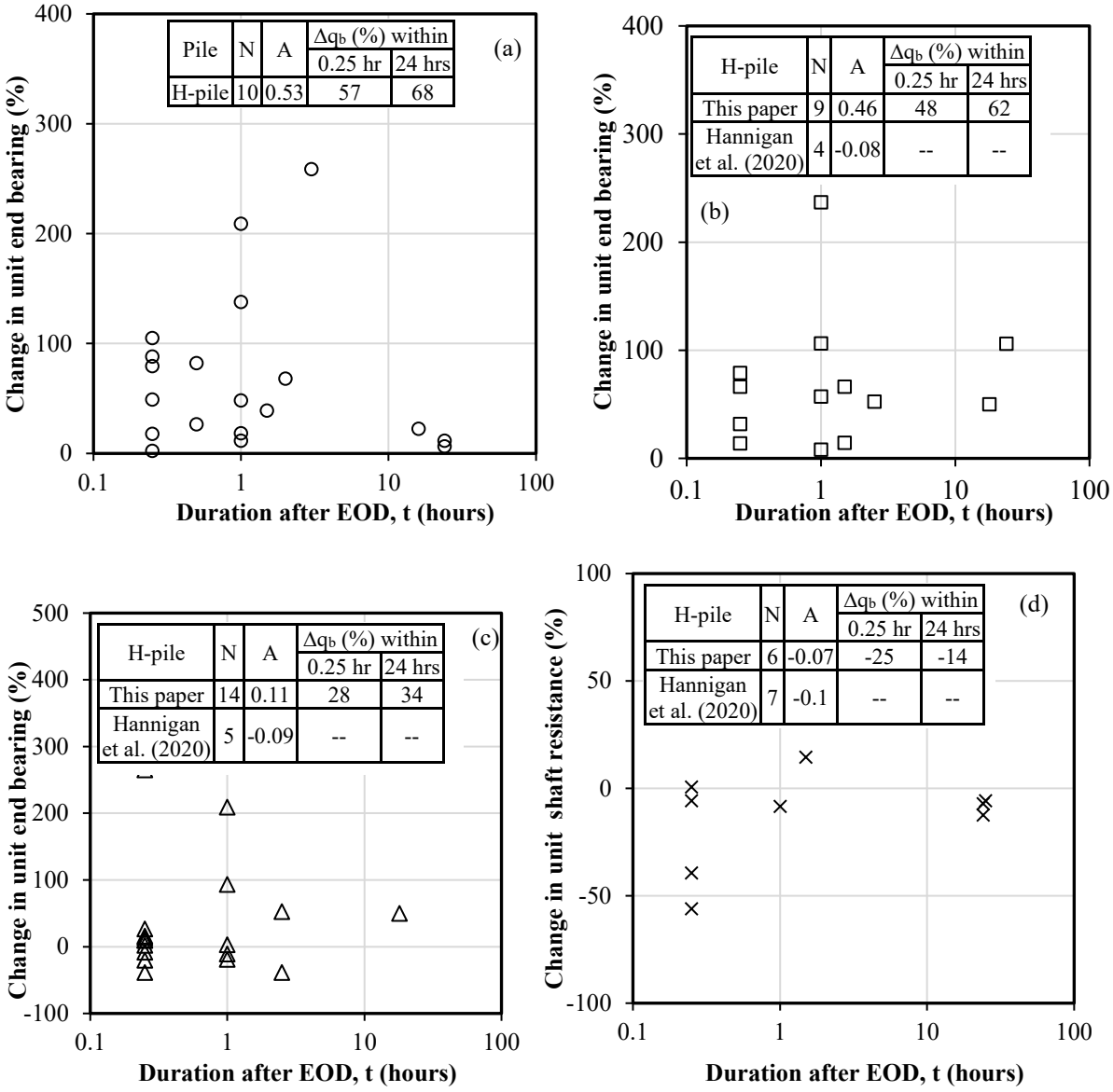

Figure 4.7 Percent change in the unit end bearing with time in logarithmic scale: (a) SS shale, (b) HW shale, (c) MW shale, (d) SW shale

5. IMPROVE WAVE EQUATION ANALYSIS

5.1 Introduction

Shale is a commonly encountered argillaceous bedrock that supports heavy structures such as bridges. Shale is a transition geomaterial harder than soil and softer than rock, and has been considered as a problematic material due to its degradation of shear strength and shrink-swell potential (Yagiz 2001). Furthermore, challenges with characterizing shale properties are often encountered due to the difficulties with classifying, sampling, and testing shales (Martin 2015). The absence of reliable design methods and measured shale properties has hindered the accurate prediction of geotechnical resistance of driven piles in shale (Terente et al. 2015). Although Adhikari et al. (2020b) and Irvine et al. (2015) have developed recommendations for piles in weak rocks, static analysis methods for predicting pile resistances in shale during a design stage have yet to be established. Treating shale as a soil-like material results in underprediction of pile resistances and could lead to several construction challenges such as early pile refusal and pile damage (Ng et al. 2019, n.d.; Ng and Sullivan 2017a; b). Pile performance in shale is often evaluated during the construction stage using dynamic testing, including the Pile Driving Analyzer (PDA) along with signal matching analysis using Case Pile Wave Analysis Program (CAPWAP) (Long 2016). However, the signal matching analysis cannot be performed unless a test or production pile is instrumented with PDA sensors and driven by a pile hammer during construction. To determine a desired penetration depth that achieves a target pile resistance prior to construction, pile driving analysis using the 1D Wave Equation Analysis Program (WEAP) has been conducted to establish pile driving and acceptance criteria. Furthermore, because of the higher cost associated with conducting a pile load test, WEAP has been widely used as an economical construction control method.

Goble and Rausche (1976) developed the WEAP program, while Hirsch et al. (1976) developed the Texas Transportation Institute (TTI) program, based on a mathematical model for 1D wave propagation proposed by Smith (1960). This type of program simulates pile penetration for each hammer blow and determines ultimate pile resistance (R_U), compressive and tensile stresses in a pile, pile drivability, and pile integrity through the modeling of driving system, pile, and geomaterials. The bearing graph is one of the essential outputs of WEAP that determines the R_U as a function of blow count. The bearing graph is influenced by pile type, driving system, percent and distribution of shaft resistance, and the dynamic soil parameters: damping and quake (Adhikari et al. 2019; Ashford and Jakrapiyanun 2001; Bartoskewitz and Coyle 1970; Korb and Coyle 1969; Pile Dynamics 2010). The establishment of pile acceptance criteria depends on proper selection of damping and quake values in the bearing graph analysis. While the modeling of pile and driving systems has been well studied, damping and quake values are neither intrinsic geomaterial properties nor measurable from laboratory tests. Using historical pile load test data, damping and quake values have been developed for piles in soils, but not for shales.

Pile drivability on soil has been extensively investigated to predict geotechnical resistance and distribution, pile stress, hammer blow count, and hammer performance during pile installation (Doherty and Igoe 2013; Rausche et al. 2009; Schneider and Harmon 2010). Past studies followed a back-analysis procedure to determine dynamic soil parameters by matching the R_U from WEAP with the measured pile resistance from static load tests (Coyle et al. 1973; Raines et al. 1992; Rausche et al. 1997) or dynamic load tests (Iskander and Stachula 2002; Ta and Hammann 2013). Adhikari et al. (2019) evaluated the performance of WEAP on 26 H-piles driven into soil-based IGM and rock-based IGMs that include mostly sandstone and claystone. The toe quake value is recommended as a ratio of pile dimension (D) to 120 for piles driven into the soil-based IGMs and 0.04 inches for piles driven

into rock-based IGM (Adhikari et al. 2019). However, none of these studies provides recommended damping and quake values for driven piles in shale.

A comprehensive wave equation analysis of piles driven in shale is developed using GRLWEAP software version 2010-4. A parametric study is conducted to determine the influence of quake and damping on the pile responses in shale. The shaft damping (J_s) and toe damping (J_t) factors for shales are back-calculated using 32 test pile data from Kansas, USA, by matching pile resistances from WEAP and CAPWAP. The performance of WEAP based on our proposed damping factors is evaluated using 46 test pile data from Kansas, Wyoming, and Iowa. Load and Resistance Factor Design (LRFD) resistance factors and efficiency factors for the default and two proposed WEAP methods are calibrated for piles in shales using three probability-based methods to achieve target reliability indices. Finally, an economic impact study demonstrated the additional costs incurred using the default WEAP method and the economic benefits of the proposed WEAP methods. The SI version of this chapter can be found in the article published by Islam et al. (2022).

5.2 Summary of Test Pile Data

A total of 71 historical test pile data from 16 different bridges of nine projects in Kansas constructed from 2010 through 2017 are collected from KDOT. Of the 71 test piles, 32 steel H-piles summarized in Table 5.1 are usable with complete pile, geomaterial, hammer, driving, and load test information for WEAP analysis. The overburden soil layers include sand, clay, silt, and mixed soil, and all the bearing layers are shale. Furthermore, the shale layers are classified as soil-based shales and rock-based shales (soft to hard and slightly weathered to highly weathered shales) based on the weathering conditions described in bore log reports. The unconfined compressive strengths (q_u) of shale layers vary between 3.02 ksf and 52.3 ksf, total pile embedment lengths (L_{EMB}) from 33 to 105 ft, and pile penetrations in shale (L_{Shale}) from 3.4 to 30.1 ft. All test piles are driven using diesel hammers with stroke heights (h_s) varying from 5.5 to 9 ft and blow counts at the end of driving (EOD) from 17 to 640 blows per ft.

5.3 Prediction Study

A detailed parametric study is conducted to investigate the effect of input parameters on the bearing graph and R_U determination. Figure 5.1 shows a typical hammer-pile-geomaterial profile and the default inputs used in this prediction study. A steel HP 12×74 pile with a total pile length of 60 ft is used. Moreover, no soil plugging is assumed for steel H-piles in the analysis. The overburden layer consists of sand with SPT (standard penetration test) *N*-value of 30, and the bearing layer is a moderately weathered shale (MW) with a q_u value of 84 ksf. The default WEAP predicts the unit shaft resistance (q_s) of the sand layer using the relationship: $\hat{q}_s = k_o \tan(\delta)\, \sigma'_v$, where k_o is the coefficient of lateral earth pressure at rest, δ is the pile-geomaterial friction angle, and σ'_v is the effective vertical stress (Pile Dynamics 2010). The q_s and unit end bearing (q_b) of the MW shale layer are predicted using the proposed Equations 3 and 6, respectively (Islam 2021), and manually input into WEAP. The WEAP generated 50% shaft resistance along the total pile length as shown in the Figure 5.1. A Delmag D30-32 hammer with 80% hammer efficiency, ram weight (W_R) of 6.6 kips, and h_s of 6.5 ft is used to generate the bearing graph. The hammer cushion area of 226 inches^2 and helmet weight of 1.94 kips are used as per manufacturer recommendations. The analysis is conducted at a fixed h_s with the variable pressure adjustment option available in WEAP. The program iteratively adjusts combustion pressure in such a way that the upstroke equals the down stroke (Pile Dynamics 2010). The dynamic soil parameters generated by the WEAP are shown in Figure 5.1. During the study, only one parameter is changed at a time while other parameters remained constant.

Figure 5.2 shows the effect of damping factors and quake values on the bearing graph and R_U determination as a function of blow count. Figures 5.2a and 5.2b show that the R_U increases with the decrease in J_s and J_t of shale from 0.2 s/ft to 0.05 s/ft for the same blow count. This observation agrees with this relationship: total pile resistance = dynamic pile resistance + static R_U. The dynamic soil resistance decreases proportionally with the decrease in damping factors and yields a higher static R_U for the same total pile resistance. Figure 5.2c shows that shale with smaller shaft quake (Q_s), indicating a stiffer geomaterial, exhibits a higher shaft resistance along the pile and results in a higher R_U for the same blow count (Authier and Fellenius 1980). On the other hand, Figure 5.2d shows a minimal effect of toe quake (Q_t) on the bearing graph because of the 50% shaft resistance used in this study. However, the effect of Q_t could be more prominent on the end bearing piles where most of the resistance acts along the pile toe compared with the friction piles where most of the resistance acts along the shaft (Hannigan et al. 2006). The toe quake is not only a function of pile size and material, but also depends on the densification or loosening due to driving, geomaterial stiffness, and strength (Rausche et al. 2008). The effect of dynamic parameters on the wave equation results highly depends on the percent shaft resistance. For friction piles, emphasis should be given on the selection of shaft quake and shaft damping rather than the toe quake and toe damping. The above parametric study shows that the dynamic soil parameters, except Q_t, influence the bearing graph and R_U prediction for piles with 50% or more shaft resistance and other details of the hammer-pile-soil conditions analyzed.

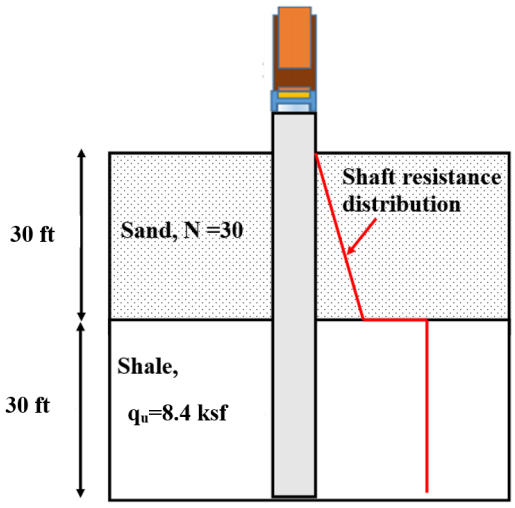

Pile Section	HP 12×74
Hammer Type	Delmag D30-32
Hammer Cushion Area	226 in^2
Hammer Cushion Modulus	100 ksi
Hammer Cushion Thickness	4.25 in
Helmet Weight	1.94 kips
Stroke Height (h_s)	6.5 ft
Overburden Layer	Sand
Shaft Damping (J_s)	0.05 s/ft
Toe Damping (J_t)	0.15 s/ft
Shaft Quake (Q_s)	01 in
Toe Quake (Q_t)	01 in
Shaft Resistance	50%
End Bearing	50%

Figure 5.1 A pile-geomaterial profile and default values used in the prediction study

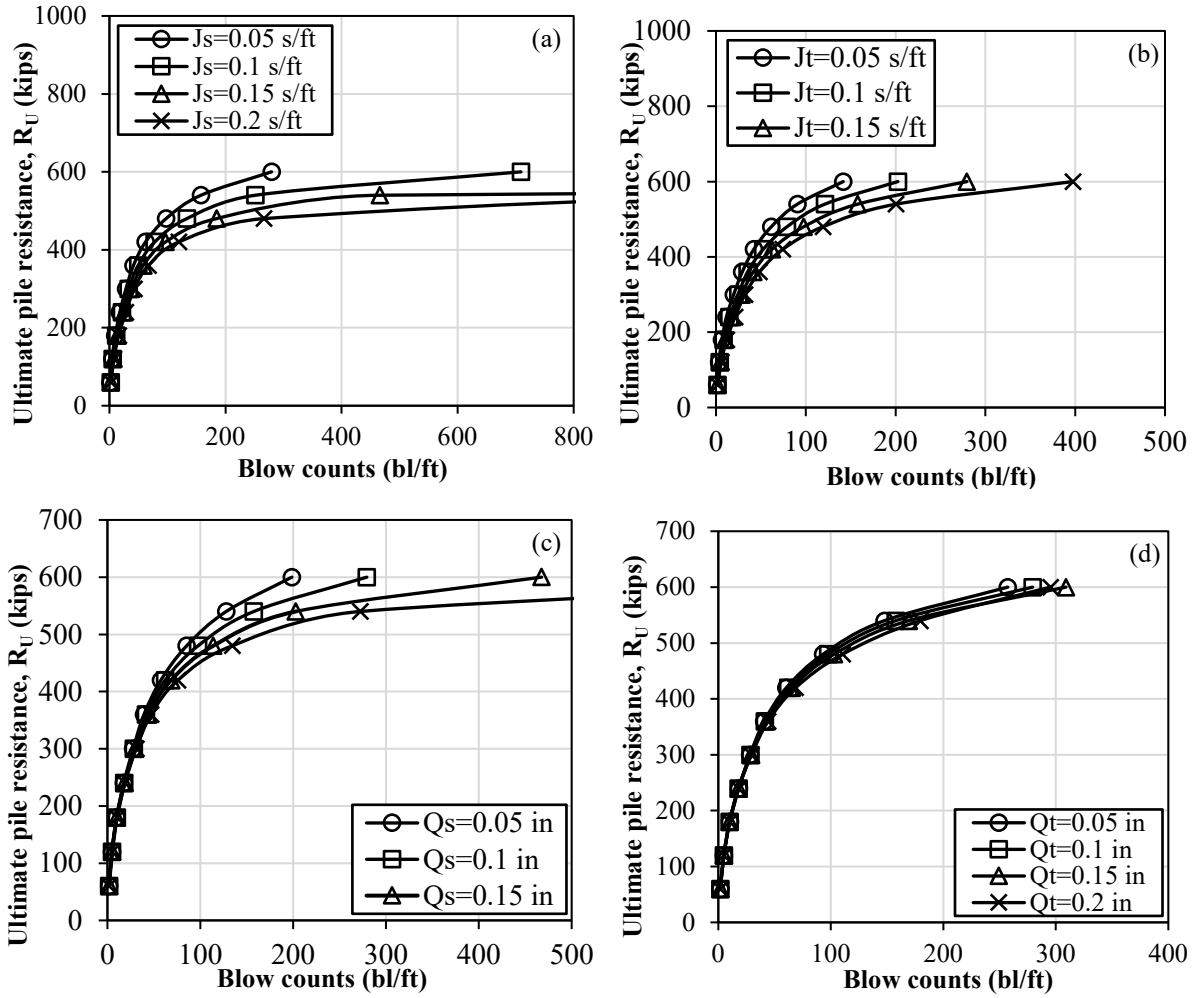

Figure 5.2 Effect of (a) shaft damping J_s, (b) toe damping J_t, (c) shaft quake Q_s, and (d) toe quake Q_t on the ultimate pile resistance prediction from the bearing graph analysis

5.4 Proposed WEAP Methods

A back-analysis procedure is adopted to develop recommended damping factors for steel H-pile in shale by matching WEAP predicted R_U for the observed blow count with the pile resistance determined from CAPWAP. A total 32 usable test pile data collected from Kansas are used in this study (Table 5.1). The hammer models provided in KDOT reports are used while helmet weight, pile cushion, and hammer cushion are selected as per manufacturer recommendations. The *N*-value based (SA) procedure is adopted in this study as it allows direct input of geomaterial properties and gives a more detailed distribution of static resistance than the soil type based (ST) method. Two WEAP methods, denoted as WEAP-SA-R and WEAP-UW-R, are proposed using the recommended back-calculated damping factors for shale. The R_U results from those methods are compared with those from the current default geomaterial input procedure and dynamic parameters in WEAP, denoted as WEAP-SA-D.

Table 5.1 Summary of 32 historical steel H-pile data from Kansas and results of WEAP analysis

Pile ID	County in Kansas	Steel H-pile	Pile location	L_{EMB} (ft)	L_{Shale} (ft)	Overburden geomaterial	Shale Type	q_u[a] (ksf)	RQD (%)	Pile hammer	h_s (ft)	Blow count at EOD (bl/ft)	R_{tc} (kips)	Static Pile Resistance				Back-calculated J_s or J_t (s/ft)	
														WEAP-SA-R		WEAP-UW-R			
														R_{st} (kips)	% Shaft	R_{st} (kips)	% Shaft	WEAP-SA-R	WEAP-UW-R
1	Sedg-wick	12×63	A-1	81	12.1	sand	SW	27.33	76	Pil. D30-32	7.5	87	479	419	84	716	61	0.131	0.117
2		10×42	P-2-SB	80	6.3	mixed	SS	6.87	92	Del. D19-32	5.5	28	190	263	92	302	84	0.135	0.11
3		12×53	P-3	73	9.8	sand	SS	3.5	76	Del. D30-02	8.7	18	286	255	91	268	78	0.153	0.146
4		12×74	P-6A	69	10.2	sand	SS	7.26	84	Del. D30-02	8.5	20	311	271	86	319	76	0.111	0.098
5		12×53	A-2	87	20.8	mixed	SS	9.2	77	Pil. D30-32	7	40	325	344	88	402	81	0.297	0.266
6		10×42	A-1	80	4.96	Clayey sand	SS	8.1	86	Del. D16-32	8	53	285	248	90	277	82	0.103	0.105
7		12×84	P-3	33	11.1	sand	SS	37.56	69	Pil. D30-32	6.5	25	342	141	50	273	59	0.044	0.044
8		12×63	P-4A	68	6.4	mixed	MW	18.3	90	Del. D30-02	8	36	341	276	75	286	69	0.187	0.181
9		10×42	A-1-NB	105	18.2	sand	MW	6.82	85	Del. D19-32	7.25	60	249	477	91	589	75	0.12	0.118
10		12×53	P-1	73	3.4	Clayey sand	MW	6.95	86	Del. D30-02	7	30	279	258	88	442	52	0.128	0.108
11		12×63	P-6	68	16.2	sand	MW	4.88	76	Del. D30-02	8.75	24	411	241	91	485	59	0.01	0.025
12		10×42	P-1-NB	84	11	sand	MW	17.03	87	Del. D19-32	6.5	51	280	300	85	485	65	0.052	0.095
13		12×74	P-6B	70	11.8	sand	MW	7.26	84	Del. D30-02	8.75	80	544	276	87	468	53	0.086	0.086
14		12×74	P-2	47	26.8	sand	SW	19.64	78	Pil. D30-32	7.75	34	531	207	66	453	79	0.028	0.028
15		12×63	P-2	59	12.03	sand	HW	7.65	85	Pil. D30-32	8.3	17	270	218	84	273	73	0.2735	0.2
16		12×63	P-9	58	16.5	mixed	SS	3.02	89	Pil. D30-32	7.2	25	421	275	53	352	52	0.12	0.022
17		12×74	P-5	46	18.9	sand	HW	6.9	70	Pil. D30-32	7.8	27	330	161	80	182	60	0.171	0.145
18		12×74	P-7	45	16.7	sand	HW	6.7	98	Pil. D30-32	7.2	23	318	150	79	184	60	0.081	0.084
19		12×53	P-1	53	8.66	mixed	HW	8.6	35	Pil. D30-32	6.5	27	333	265	85	279	72	0.12	0.112
20		12×74	P-3	61	19.76	sand	HW	4.531	86	Pil. D30-32	7.3	26	337	234	92	276	76	0.128	0.122
21		12×63	P-10	47	15.8	sand	SS	6.1	84	Pil. D19-42	8.25	28	338	348	35	290	76	0.058	0.058
22		12×74	P-11	50	16.6	mixed	MW	4.57	67	Pil. D19-42	8.5	32	326	167	91	160	58	0.093	0.092
23		12×74	P-6	35	14.9	sand	HW	20.7	87	Pil. D30-32	7	52	447	146	55	157	45	0.081	0.081
24		12×63	P-4	50	11.5	mixed	MW	3.93	89	Pil. D30-32	7.2	34	391	170	90	331	44	0.119	0.102
25		12×63	P-4	52	25.9	mixed	SW	6.64	93.8	Pil. D30-32	7.2	26	349	196	85	369	42	0.079	0.089
26		12×74	P-8	61	20.5	mixed	MW	6.76	NA	Pil. D30-32	8	34	513	454	38	525	58	0.085	0.054
27		12×74	P-5	54	20.7	mixed	HW	5	78	Pil. D30-32	8.2	28	348	238	71	391	48	0.134	0.134
28	Clay	12×74	P-2	58.4	30.1	mixed	SS	40.6	66	Del. D19-42	9	62	355	284	75	443	75	0.264	0.168
29	Barton	12×63	P-2	72	25.24	silty clay	SS	12.38	96	Del. D19-42	8	102	264	401	84	466	82	0.175	0.175
30		10×42	A-1	82	17.3	mixed	SS	9.11	36	Del. D19-42	7	46	245	400	93	439	88	0.071	0.071
31	Geary	12×63	P-1	47	21.8	Silty clay	SW	41.67	70	Del. 16-32	7.25	640	448	238	71	406	73	0.157	0.126
32		12×63	A-1	60	16.37	Silty clay	SW	52.3	70	Del. 16-32	9	128	413	302	77	422	73	0.009	0.057

A-Abutment; P-Pier; UW-Static analysis equations for shales proposed by authors; SA- SPT N-value based input procedure; D-WEAP default damping factors; R-Recommended damping factors; q_u-unconfined compressive strength; RQD-Rock quality designation; L_{EMB}-embedded pile length; L_{Shale}-embedded pile length in shale; R_{tc}-Total pile resistance from CAPWAP; R_{st}- Static resistance from drivability analysis; Del.-Delmag hammer; Pil.-Pileco hammer; h_s-Stroke height; SS-Soil based shale; HW-Soft & highly weathered shale; MW-Moderately hard & weathered shale; SW-Hard & slightly weathered shale; J_s-Shaft damping factor of shale; J_t-Toe damping factor of shale; and [a] –Average value of all shale layers.

Table 5.2 Mean and one standard deviation of recommended damping factor of shales

Shale type	Sample size	WEAP-SA-R	WEAP-UW-R
Soil-based Shale (SS)	11	0.139 ±0.08	0.115 ±0.02
Highly Weathered Rock-based Shale (HW)	7	0.141 ±0.07	0.125 ±0.04
Moderately Hard & Weathered Rock-based Shale (MW)	9	0.098 ±0.05	0.096 ±0.04
Hard & Slightly Weathered Rock-based Shale (SW)	5	0.081 ±0.06	0.083 ±0.04

UW-Static analysis **equation**s for shales proposed by authors; SA-SPT *N*-value based input procedure; and R-Recommended damping factors.

Table 5.3 Summary of measured and predicted pile resistances in kips for three WEAP methods

Pile ID	Steel H-pile	Pile location	Shale type	$q_u{}^a$ (ksf)	Blow count at EOD (bl/ft)	Driving hammer	WEAP-SA-R		WEAP-UW-R		WEAP-SA-D			R_{tc} (kips)
							R_{st} (kips)	$R_U{}^{1S}$ (kips)	R_{st} (kips)	$R_U{}^{2S}$ (kips)	R_{st} (kips)	J_s s/ft	$R_U{}^R$ (kips)	
1	12×63	A-1	SW	27.36	87	Del. D 30-32	419	487	716	491	419	0.076	494	323
2	10×42	P-2-SB	SS	6.89	28	Del. D 19-32	263	198	302	189	263	0.071	188	190
3	12×53	P-3	SS	3.55	18	Del. D 30-02	255	319	268	297	255	0.088	275	286
4	12×74	P-6A	SS	7.31	20	Del. D 30-02	276	326	325	300	276	0.088	278	311
5	12×53	A-2	SS	9.19	40	Del. D 30-02	344	402	402	376	344	0.103	362	325
6	10×42	A-1	SS	8.15	53	Del. D 16-32	248	284	277	284	248	0.063	299	285
7	12×84	P-3	SS	37.59	25	Del. D 30-02	141	325	273	265	141	0.152	238	342
8	12×63	P-4A	MW	18.38	36	Del. D 30-02	276	382	286	371	276	0.088	346	341
9	10×42	A-1-NB	MW	6.89	60	Del. D 30-32	477	287	589	279	477	0.085	293	249
10	12×53	P-1	MW	6.89	30	Del. D 30-02	258	327	442	302	258	0.061	312	279
11	12×63	P-6	MW	4.80	24	Del. D 30-02	241	370	485	339	241	0.119	291	411
12	10×42	P-1-NB	MW	17.13	51	Del. D 30-32	300	283	485	263	300	0.077	264	280
13	12×74	P-6B	MW	7.31	80	Del. D 30-02	276	564	468	538	276	0.088	516	544
14	12×74	P-2	SW	19.63	34	Del. D 30-02	207	527	453	437	207	0.18	323	495
15	12×63	P-2	HW	7.73	17	Pil. D30-32	218	363	273	324	218	0.1	286	270
16	12×63	P-9	SS	2.92	25	Pil. D30-32	271	366	352	323	271	0.128	291	421
17	12×74	P-5	HW	6.89	27	Pil. D30-32	238	398	216	318	238	0.169	296	330
18	12×74	P-7	HW	6.68	23	Pil. D30-32	150	330	184	288	150	0.16	244	318
19	12×53	P-1	HW	8.56	27	Pil. D30-32	259	351	279	325	259	0.08	309	333
20	12×74	P-3	HW	4.59	26	Pil. D30-32	237	371	277	325	237	0.137	295	337
21	12×63	P-10	SS	6.06	28	Pil. D30-32	348	456	290	389	348	0.139	346	338
22	12×74	P-11	MW	4.59	32	Pil.D30-32	167	387	160	328	167	0.145	259	326
23	12×74	P-6	HW	20.68	52	Pil. D30-32	146	521	157	429	146	0.158	382	447
24	12×63	P-4	MW	3.97	34	Pil. D30-32	170	455	331	397	170	0.124	344	391
25	12×63	P-4	SW	6.68	26	Pil. D30-32	196	407	369	354	196	0.168	261	349
26	12×74	P-8	MW	6.68	34	Pil. D30-32	209	534	525	448	209	0.139	368	513
27	12×74	P-5	HW	5.01	28	Pil. D30-32	238	399	391	337	238	0.169	301	348
28	12×74	P-2	SS	40.52	62	Del. D 19-42	284	454	443	392	284	0.153	392	355
29	12×63	P-2	SS	12.32	102	Del. D 19-42	401	353	466	342	401	0.183	322	264

30	10×42	A-1	SS	9.19	46	Del. D 19-42	400	239	439	231	400	0.138	237	245
31	12×63	P-1	SW	41.77	640	Del. D 16-32	238	468	406	457	238	0.2	362	448
32	12×63	A-1	SW	52.21	128	Del. D 16-32	302	421	422	421	302	0.2	341	413
33	14×73	P-1	SS	39.26	87	APE 19-42	478	452	488	436	455	0.091	457	311
34	12×63	P-3	SW	124.06	120	Del. D 12-42	238	371	565	394	238	0.192	325	475
35	10×42	A-2	SW	124.06	59	Del. D 19-42	232	254	458	262	239	0.164	236	329
36	12×63	P-1	SW	125.94	160	Del. D 12-42	252	356	562	378	252	0.162	320	483
37	12×74	P-2	HW	5.85	27	Del. D 30-02	257	341	302	341	257	0.079	323	413
38	10×42	A-1-SB	SW	17.13	192	Del. D 19-32	491	268	672	264	491	0.083	294	336
39	12×74	P-8	SW	2.92	16	Pil. D30-32	587	278	201	242	587	0.154	198	372
40	12×53	A-1	SW	30.28	48	Del. D 19-42	165	214	205	216	165	0.2	209	341
41[W]	14×73	B-2	MW	7.10	263	ICE 42-S	159	571	541	488	159	0.177	479	337
42 [W]	14×89	P-1	SS	8.15	120	MVE D-19	73	639	93	570	73	0.068	397	500
43[I]	10×57	A-4	SW	11.49	120	Del. D19-42	65	477	417	414	65	0.173	333	413
44 [I]	10×57	A-5	SW	59.52	120	Del. D19-42	65	477	417	414	65	0.173	333	436
45 [I]	10×42	North A.	SW	28.40	160	Del. D19-42	110	487	263	493	110	0.2	350	617[SLT]
46 [I]	10×57	East A.	MW	4.59	173	Del. D22	155	361	286	366	155	0.149	331	306[SLT]

A-Abutment; P-Pier; UW-Static analysis **equation**s for shales proposed by authors; q_u-unconfined compressive strength; SA-SPT *N*-value based input procedure; D-WEAP default damping factors; R-Recommended damping factors; R_{tc}-Total pile resistance from CAPWAP or SLT; R_U-Ultimate pile resistance predicted from WEAP; R_{st}-Static resistance from drivability analysis; J_s-Shaft damping; Del.-Delmag hammer; Pil.-Pileco hammer; ICE-International Construction Equipment; SS-Soil based shale; HW-Soft & highly weathered shale; MW-Moderately hard & weathered shale; SW-Hard & slightly weathered shale; [1]-Mean shaft & toe damping for WEAP-SA-R method from Table 5.2; [2]-Mean shaft & toe damping for WEAP-UW-R method from Table 5.2; [R]-WEAP generated; [S]-Shaft and toe quake=2.5 mm; [W]-Wyoming, [I]-Iowa; SLT-Static load test and a – Average value of all shale layers.

In the proposed WEAP-SA-R, the static resistance (R_{st}) is predicted using geomaterial properties from the SA method. The bearing graph is generated using the proportional shaft resistance and end bearing based procedure available in WEAP. The SPT *N*-value and unit weight are input for cohesionless soil, and undrained shear strength (s_u) is input for cohesive soil. Shale is treated as a fine-grained, clastic sedimentary rock consisting of clay, and q_u is input in the WEAP. A constant Q_s=0.1 inch is chosen for both soils and shale in this study because it falls within the Q_s range proposed by Forehand and Reese (1964) and Ramey and Hudgins (1977) in their parametric studies and is recommended in WEAP for all soils (Schneider and Harmon 2010; Smith et al. 2011; Stevens et al. 1982). Since steel H-piles are assumed as non-displacement piles with no soil plugging, and the percent shaft resistances are mostly greater than 50% (Table 5.1), a constant Q_t=0.1 inch is chosen for shale, which has little effect on the bearing graph and is recommended in Pile Dynamics Inc. (2010). Moreover, the toe resistance is calculated using the steel H-pile toe area rather than the plugged area. For the overburden soil layers, individual J_s factors, 0.2 s/ft for clay, 0.15 s/ft for silt and 0.05 s/ft for sand/gravel, are assigned to each corresponding soil layer via the variable damping input option in WEAP. The remaining J_s and J_t of the shale layer are back-calculated by matching the R_U determined from the bearing graph analysis based on a field measured blow count with the pile resistance obtained from CAPWAP until their difference is less than 0.1%. The matching procedure yielded a different combination of J_s and J_t values for shale while achieving the same target pile resistance in WEAP. Hence, this study recommends the same J_s and J_t in the shale layer (J_s=J_t) to facilitate the application of the proposed WEAP method while improving the R_U prediction. In the proposed WEAP-UW-R, the same damping input options for soils are used, and Q_s=Q_t=0.1 inch is assumed for soils and shale. However, the proposed Equations (4.4) through (4.7) are applied in terms of q_u to predict q_s for four shale types (Islam 2021). The shales are classified into four types, such as soil-based shale (SS), soft & highly weathered shale (HW), moderately hard & weathered shale (MW), and hard & slightly weathered shale (SW), following visual description of shales from the borehole reports of 49 historical test pile data collected from KDOT. The weathering conditions in these shale groups are quantitatively defined as highly weathered, moderately weathered, and slightly weathered in the borehole reports. Equations 4.8 and 4.9 are applied in terms of q_u to predict q_b for soil-based, soft & highly weathered (SS-HW) shale, and moderately hard to hard & weathered to slightly weathered (MW-SW) shale, respectively. Equations 4.4 through 4.9 are applicable for q_u values ranging from 2.1 to 126 ksf and steel H-piles. The predicted q_s and q_b in the shale layer are inputted manually into WEAP using the SA method during the bearing graph analysis. The same J_s and J_t of shale is back-calculated for each test pile by matching the R_U determined from the bearing graph analysis with the pile resistance from CAPWAP. During the application of the proposed WEAP-SA-R and WEAP-UW-R methods, the back-calculated J_s for shale (Table 5.2) and default J_s for overburden soils can be assigned via the variable damping input option in WEAP. Alternatively, a weighted average shaft damping factor ($J_{s\text{-}ave}$) can be calculated using Equation 5.1 with respect to the shaft resistance ($R_{s\text{-}i}$) of each geomaterial layer i and assigned as a single value in the bearing graph analysis.

$$J_{s-ave} = \frac{\sum_{i=1}^{n} R_{s-i} \times J_{s-i}}{\sum_{i=1}^{n} R_{s-i}} \tag{5.1}$$

The WEAP-SA-D method (default WEAP) is included in this study for comparison. In this method, the static pile resistance is input using the SA procedure in bearing graph analysis. WEAP generated J_s ranging between 0.06 and 0.2 s/ft with a mean of 0.43 s/m, Q_s=0.1 inch, Q_t =0.1 inch, and J_t=0.15 s/ft, as recommended in Pile Dynamics Inc. (2010), are used in the bearing graph analysis for the R_U prediction. The program generated quake values in the WEAP-SA-D method that are identical to the other two methods.

5.5 Back-calculated Shale Damping Factors

The back-calculated damping factors of 32 test piles using WEAP-SA-R and WEAP-UW-R are summarized in Table 5.1. The back-calculated damping factors range from 0.009 to 0.297 s/ft for WEAP-SA-R and 0.02 to 0.266 s/ft for WEAP-UW-R. Figure 5.3 compares the back-calculated damping factors with the percent shaft resistance, q_u of shale, total pile resistance from CAPWAP, and L_{EMB}. Since R_{st} does not affect the bearing graph and all other inputs are identical in both methods, different back-calculated damping factors are attributed to the different percent shaft resistances obtained from both methods. A wide variation in back-calculated damping factors is observed in each comparison, and a prediction equation for the damping factors cannot be established because they depend on a combination of pile sizes, overburden soil types, and driving conditions. A similar conclusion is presented in McVay and Kuo (1999) that no prediction equation could be established to quantify the soil dynamic parameters due to a large variation in dynamic soil values involving SPT *N*-value, pile size, and transfer energy of the driving system. Table 5.2 shows that the mean back-calculated damping factors of rock-based shales decreased from highly to slightly weathered conditions. SW shales exhibited lower mean back-calculated damping than that of SS, MW, and HW shales in both methods. Furthermore, SS and HW shales showed almost the same mean damping factors. Higher damping factors of SS and HW shales indicated a relatively softer material and higher dynamic resistance than the MW and SW shales. Hence, the mobilized shear strain in the pile-shale interface will be higher for SS and HW shales than for MW and SW shales if the blow count is similar.

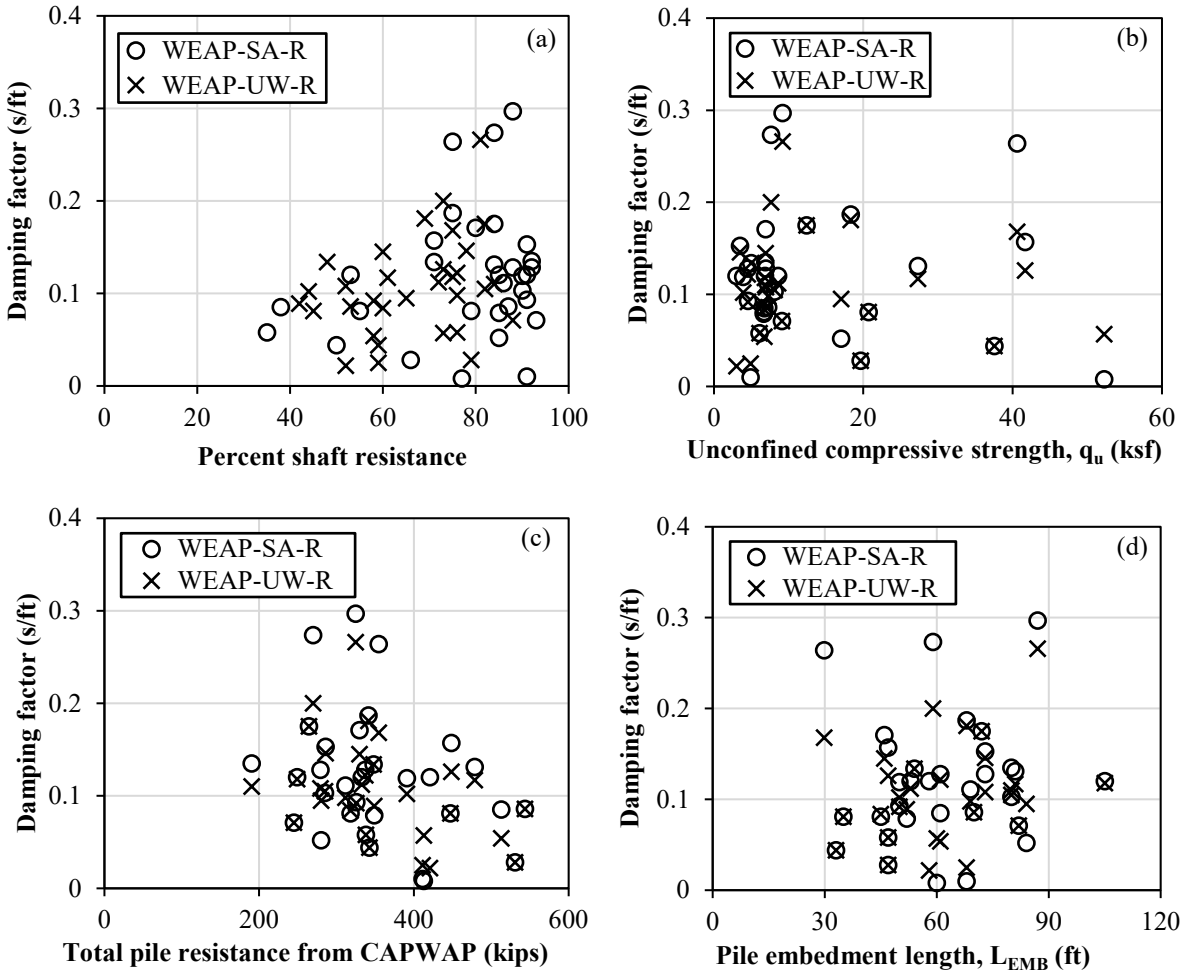

Figure 5.3 Comparison of back-calculated damping factor and (a) percent shaft resistance, (b) unconfined compressive strength of shale, (c) total pile resistance from CAPWAP, (d) pile embedment length

5.6 Comparison of WEAP Analysis Methods

The mean damping factors (Table 5.2) are recommended in the respective WEAP-SA-R and WEAP-UW-R to determine the R_U values of steel H-piles based on the field measured hammer blow count at the EOD (Table 5.3). Including the 32 test pile data from Kansas used in the back-calculation (Table 5.1), along with an additional eight test pile data from Kansas, two from Wyoming, and four from Iowa are added to yield a total of 46 test pile data to compare the performance of the WEAP methods in this study. A total of 44 R_U values determined from each WEAP method are compared with pile resistances from CAPWAP conducted in three states. In addition, R_U values of two test piles, IDs 45 and 46, are also compared with the measured pile resistances from static load tests (SLTs). Test pile ID 45 is located at the north abutment of the US63 replacement bridge over a drainage ditch in Wapello County, Iowa, with a SW shale layer at the pile tip. Test pile ID 46 is at the east abutment of the IA92 bridge replacement in Adair County, Iowa, with an MW shale layer at the pile tip.

Figure 5.4a compares the pile resistances determined from WEAP-SA-R with pile resistances from CAPWAP and SLT. Data points above the one-to-one bias line indicate overprediction, and data points below the one-to-one bias line indicate underprediction. The predicted pile resistances match closely with those from CAPWAP as suggested by a relatively low scatter of points along this line. Considering all 46 test piles, WEAP-SA-R overpredicted R_U, on average, by about 4.2% (i.e., mean bias of $\bar{x}$=0.96) and yields a relatively low coefficient of variation (COV) of 0.21. WEAP-UW-R underpredicted the R_U, on average, by about 2.9% with the lowest COV of 0.2. However, WEAP-SA-D underpredicted the R_U, on average, by about 14.5% with the highest COV of 0.23. Comparing the pile resistances from SLT, WEAP-SA-R and WEAP-UW-R underpredicted R_U, on average, by about 5.7% and 3.8%, respectively, while WEAP-SA-D highly underpredicted R_U by about 25.4%. Comparisons based on CAPWAP and SLT confirmed that WEAP-UW-R provided the most accurate pile resistance prediction with $\bar{x}$ closest to unity. This is attributed to the application of the proposed static Equations (1) through (6) in WEAP-UW-R to yield a more accurate prediction of percent shaft resistance. The difference in the pile resistance predictions by WEAP-SA-R and WEAP-UW-R is attributed to the use of mean damping factors of 0.081 to 0.139 s/ft for WEAP-SA-R and 0.083 to 0.115 s/ft for WEAP-UW-R (Table 5.2) and the different percent shaft resistance.

The CAPWAP results at the beginning of restrike of 31 test piles conducted in Kansas are used to investigate the performance of three WEAP methods in predicting pile resistances in shales. The 31 test piles comprised 49 BOR test results obtained at various elapsed times ranging from 0.25 to 16 hours after the EOD. Using the field observed blow counts and stroke heights at the BOR, these piles are modeled in the three WEAP methods, and the predicted R_U values are compared with those of CAPWAP in Figure 5.5. Figures 5.5a and 5.5b indicate that the WEAP-SA-R and WEAP-UW-R with the mean bias of 0.95 overpredicted the pile resistance by 5.3%. However, WEAP-SA-D with the mean bias of 1.08 underpredicted the R_U by about 7.4% (Figure 5.5c). The lower COV values of 0.13 and 0.14 confirmed the reliability and applicability of WEAP-SA-R and WEAP-UW-R in predicting the pile resistance at BOR.

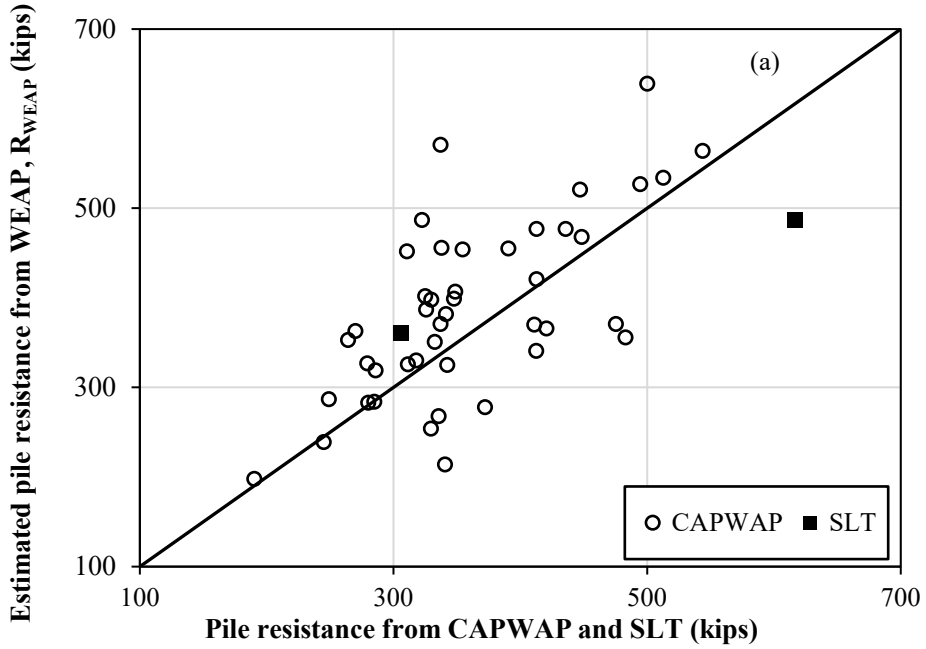

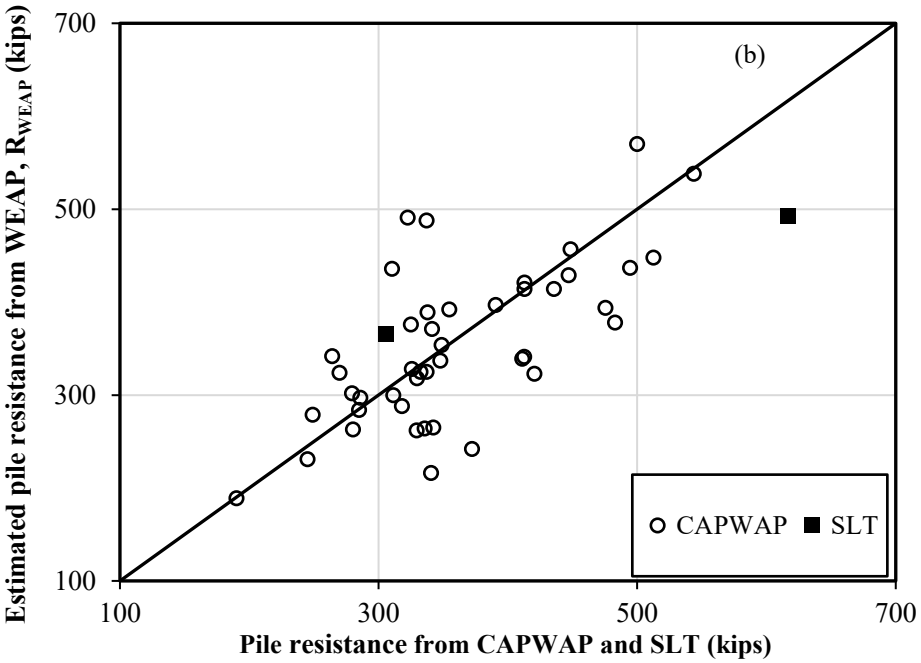

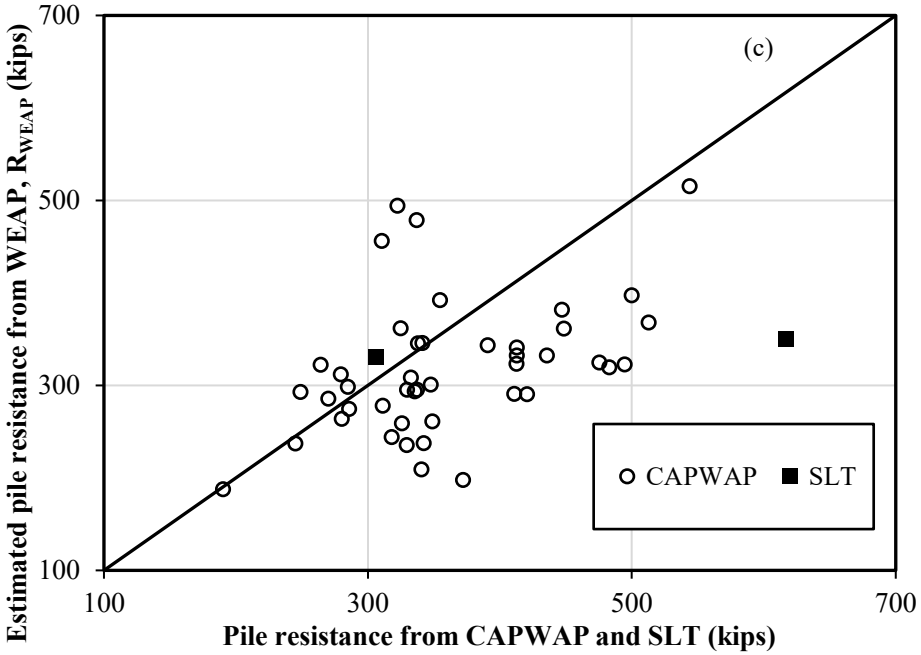

Figure 5.4 Comparing pile resistances from CAPWAP and SLT with predicted pile resistances from (a) WEAP-SA-R, (b) WEAP-UW-R, (c) WEAP-SA-D

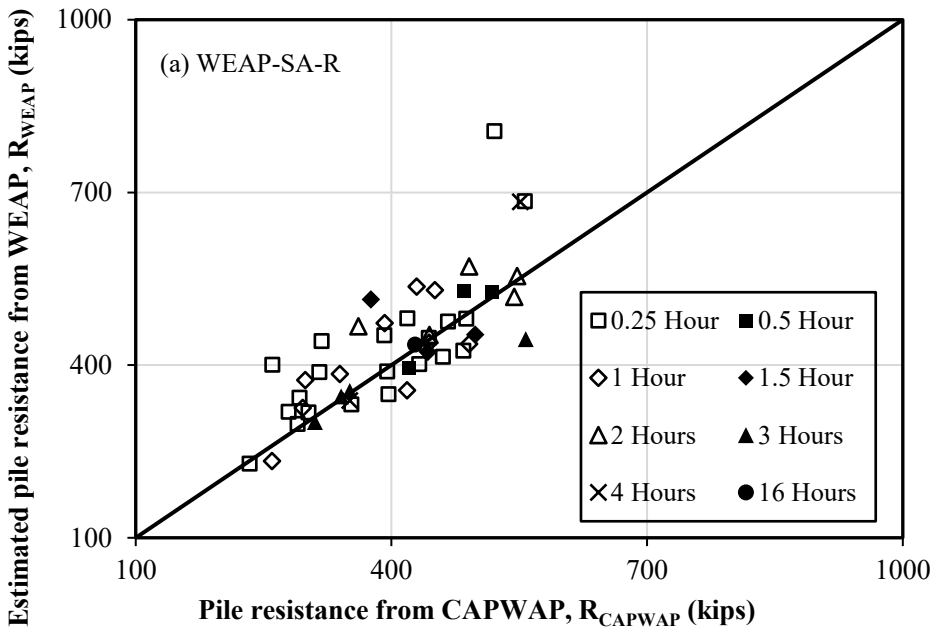
(a) WEAP-SA-R
Estimated pile resistance from WEAP, R_{WEAP} (kips)
Pile resistance from CAPWAP, R_{CAPWAP} (kips)
1000
700
400
100
100
400
700
1000
0.25 Hour
0.5 Hour
1 Hour
1.5 Hour
2 Hours
3 Hours
4 Hours
16 Hours

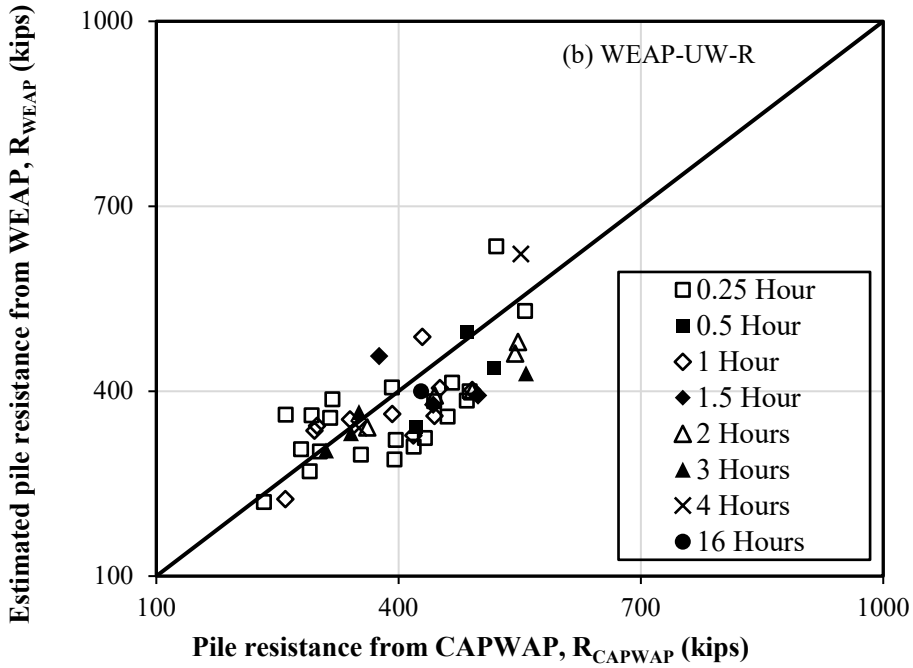
(b) WEAP-UW-R
Estimated pile resistance from WEAP, R_{WEAP} (kips)
Pile resistance from CAPWAP, R_{CAPWAP} (kips)
1000
700
400
100
100
400
700
1000
0.25 Hour
0.5 Hour
1 Hour
1.5 Hour
2 Hours
3 Hours
4 Hours
16 Hours

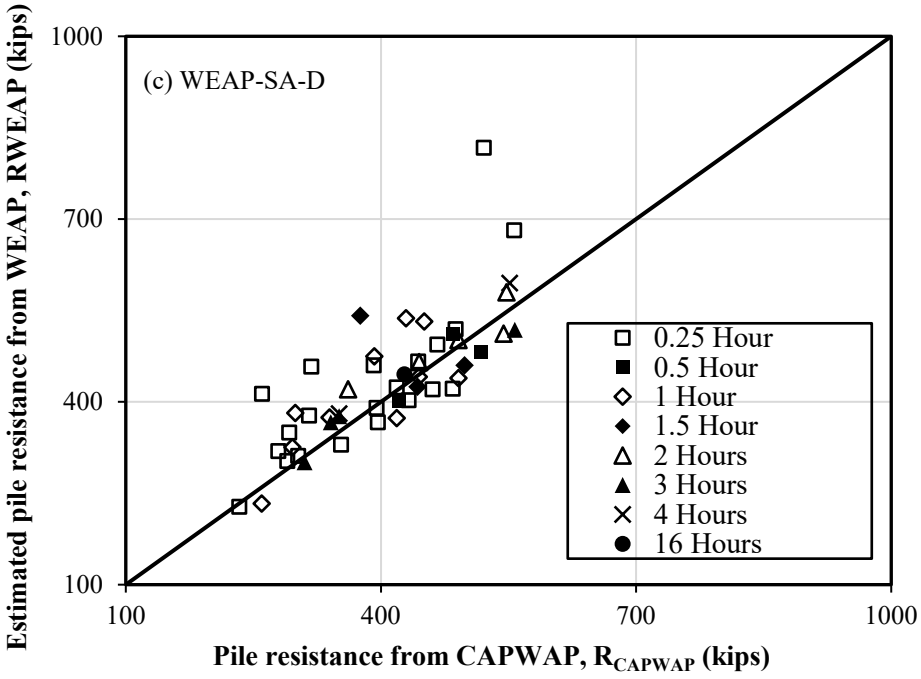

Figure 5.5 Comparing pile resistances at BOR from CAPWAP with predicted pile resistances from (a) WEAP-SA-R, (b) WEAP-UW-R, (c) WEAP-SA-D

5.7 Economic Impact Study of the Proposed and Default WEAP Methods

An economic impact study is conducted to compare the performance of the three WEAP methods in terms of measurable quantities (number of piles and steel weights) for cost estimation with respect to the outcomes from the pile load test during bridge construction. The economic impact study is conducted following the steps by Adhikari et al. (2020b):

- First, total load demand at each pier or abutment location is determined by multiplying the factored load per pile (γQ) with the number of piles per pier or abutment.
- Second, using the reported L_{EMB} of each test pile, factored resistances (φR) per pile are determined for WEAP-SA-R, WEAP-UW-R, and WEAP-SA-D by multiplying the predicted R with the recommended LRFD resistance factors 0.62, 0.68, and 0.73, respectively, based on FOSM described in Chapter 6 (Table 6.5). Similarly, φR are determined for CAPWAP and SLT using the AASHTO (2020) recommended φ values 0.65 and 0.8, respectively.
- Third, the required number of piles to satisfy the LRFD strength limit state ($\gamma Q \leq \varphi R$) is determined by dividing the load demand from step 1 with the φR from step 2 for each WEAP method and pile load test method.
- Fourth, the difference in the number of piles is calculated by subtracting the number of piles for each WEAP method from the number of piles based on the pile load test (Table 5.4). A negative difference indicates the underprediction of pile resistance by WEAP resulting in a higher number of piles than that based on the pile load test.
- Finally, the difference in number of piles is converted to an equivalent weight of steel, which is then normalized by the respective structural load demand (Table 5.4).

The normalized steel weight per load illustrates the performance of WEAP in predicting the required number of piles during construction. The WEAP-SA-R, WEAP-UW-R, and WEAP-SA-D with positive differences underpredicted the number of piles in 24, 28, and 20 cases, respectively, leading to fewer piles allocated in the design phase for bidding. In these cases, the LRFD strength limit state will not be attained with the allocated number of piles if CAPWAP would have been used as a construction control method. Consequently, additional pile penetration or number of piles will be required during construction, resulting in cost overrun. For example, an additional 1,495.2 kg (i.e., 0.2 lb/kips×7476 kips) and 6,578.6 lbs of steel will be required for the pier 2 structure (pile ID 14) using WEAP-SA-R and WEAP-UW-R, respectively, while the highest excess steel quantities of 29,305.9 kg will be realized during construction using WEAP-SA-D.

Excluding the outliers outside the average difference plus two standard deviations (Pile ID 1, 29, and 33), the average differences in steel weight per load of -0.31 lb/kips, -0.13 lb/kips, and -0.54 lb/kips for WEAP-SA-R, WEAP-UW-R, and WEAP-SA-D, respectively, are calculated (Table 5.4). The economic study revealed that all three methods, on average, overpredicted the number of piles and result in excess steel weights delivered during the construction stage. For an average load demand of 20,00 kips per vertical structure, WEAP-SA-R, WEAP-UW-R, and WEAP-SA-D resulted in excess steel weights of 620 lbs, 260 lbs, and 1080 lbs, respectively. Using HP12×63 pile and load demand of 20,00 kips as an example for comparison, WEAP-SA-R, WEAP-UW-R, and WEAP-SA-D will result in excess pile lengths of 9.84 ft, 13 ft, and 17.14 ft, respectively. The lowest excess steel weight per unit load or pile length using WEAP-UW-R is attributed to the more accurate static analysis, Equations (1) through (6), to predict q_s and q_p of shales and the application of back-calculated damping factors for shales in the bearing graph analysis. In contrast, despite having the highest calibrated resistance factors (Table 6.5), the default WEAP-SA-D yielded the highest excess pile length and excess steel weight per unit load. The proposed WEAP-UW-R yielded a minimal excess steel weight, on average, during construction, which will alleviate construction challenges encountered in the current practice, such as higher construction cost and longer duration.

Table 5.4 Summary of economic impact study of the proposed and default WEAP methods

Pile ID	Pile location	γQ per structure (kips)	φR (kips)				Number of piles				Difference in number of piles			Difference in steel weight per unit load (lb/ kips)		
			WEAP-SA-R	WEAP-UW-R	WEAP-SA-D	CAPWAP	WEAP-SA-R	WEAP-UW-R	WEAP-SA-D	CAPWAP	WEAP-SA-R	WEAP-UW-R	WEAP-SA-D	WEAP-SA-R	WEAP-UW-R	WEAP-SA-D
1	A-1	1680	302	334	361	210	5.56	5.03	4.65	8.01	2.45	2.98	3.36	7.45	9.02	10.20
2	P-2-SB	1824	123	129	137	124	14.86	14.19	13.3	14.75	-0.1	0.56	1.46	-0.20	1.08	2.65
3	P-3	7104	198	202	201	186	35.92	35.18	35.43	38.24	2.32	3.07	2.81	1.27	1.67	1.57
4	P-6A	4032	202	204	203	202	19.95	19.76	19.85	19.93	-0.02	0.16	0.08	0.00	0.20	0.10
5	A-2	1854	249	256	264	211	7.44	7.25	7.02	8.78	1.34	1.53	1.76	3.33	3.82	4.41
6	A-1	1782	176	193	218	185	10.12	9.23	8.18	9.62	-0.5	0.4	1.44	-0.98	0.78	2.84
7	P-3	8200	202	180	174	222	40.69	45.5	47.26	36.85	-3.84	-8.65	-10.4	-1.27	-2.94	-3.53
8	P-4A	7182	237	252	253	222	30.32	28.47	28.43	32.36	2.04	3.9	3.93	1.18	2.35	2.35
9	A-1-NB	912	178	190	214	162	5.13	4.81	4.26	5.63	0.51	0.83	1.37	2.45	4.02	6.67
10	P-1	8064	203	205	228	182	39.78	39.27	35.38	44.4	4.63	5.14	9.02	2.26	2.45	4.31
11	P-6	5544	229	231	212	267	24.17	24.05	26.1	20.75	-3.42	-3.3	-5.35	-2.65	-2.55	-4.12
12	P-1-NB	1824	175	179	193	182	10.4	10.2	9.46	10.02	-0.38	-0.18	0.56	-0.69	-0.39	1.08
13	P-6B	5976	350	366	376	353	17.09	16.34	15.88	16.91	-0.18	0.57	1.03	-0.20	0.49	0.88
14	P-2	7476	327	297	236	321	22.88	25.16	31.73	23.25	0.37	-1.9	-8.47	0.20	-0.88	-3.92
15	P-2	6840	225	220	209	175	30.39	31.05	32.8	38.99	8.6	7.94	6.19	4.71	4.31	3.33
16	P-9	5980	227	220	212	273	26.35	27.23	28.19	21.88	-4.47	-5.35	-6.31	-2.75	-3.33	-3.92
17	P-5	7640	247	216	216	214	30.96	35.33	35.42	35.65	4.69	0.32	0.23	2.06	0.10	0.10
18	P-7	7080	205	196	178	207	34.6	36.15	39.68	34.25	-0.35	-1.9	-5.43	-0.20	-0.88	-2.55
19	P-1	7400	218	221	225	216	34	33.48	32.86	34.24	0.24	0.76	1.38	0.10	0.20	0.39
20	P-3	7600	230	221	216	219	33.04	34.39	35.26	34.67	1.63	0.29	-0.58	0.98	0.20	-0.39
21	P-10	4896	283	265	252	220	17.32	18.51	19.4	22.3	4.98	3.79	2.9	3.04	2.26	1.77
22	P-11	4824	240	223	189	212	20.11	21.63	25.48	22.79	2.68	1.16	-2.7	2.06	0.88	-2.06
23	P-6	7760	323	292	279	291	24.02	26.6	27.83	26.71	2.68	0.11	-1.12	0.88	0.00	-0.39
24	P-4	5820	282	270	251	254	20.63	21.56	23.2	22.92	2.29	1.36	-0.29	1.27	0.78	-0.20
25	P-4	5980	252	241	191	227	23.7	24.84	31.35	26.38	2.68	1.53	-4.97	1.47	0.88	-2.75
26	P-8	7820	331	305	269	333	23.62	25.67	29.09	23.47	-0.15	-2.2	-5.63	-0.10	-1.27	-3.24
27	P-5	7900	247	229	220	226	31.93	34.47	35.94	34.95	3.02	0.48	-0.99	1.57	0.29	-0.49
28	P-2	6480	281	267	286	230	23.02	24.31	22.63	28.11	5.09	3.8	5.49	3.43	2.55	3.63
29	P-2	3480	219	233	235	145	15.9	14.96	14.79	23.95	8.05	8.98	9.16	10.49	11.67	11.96
30	A-1	2445	148	157	173	159	16.5	15.56	14.11	15.35	-1.15	-0.21	1.24	-1.57	-0.29	1.67
31	P-1	4400	290	311	264	291	15.16	14.16	16.67	15.1	-0.07	0.94	-1.58	-0.10	0.59	-1.08
32	A-1	1872	261	286	249	268	7.17	6.54	7.51	6.98	-0.2	0.44	-0.54	-0.39	0.88	-1.18
33	P-1	3632	280	296	333	202	12.96	12.25	10.9	18	5.04	5.75	7.1	9.51	10.89	13.44
34	P-3	1809	230	268	237	309	7.87	6.75	7.63	5.86	-2.01	-0.9	-1.78	-3.53	-1.57	-3.14
35	A-2	764	157	178	172	214	4.85	4.29	4.44	3.57	-1.28	-0.72	-0.87	-4.12	-2.26	-2.75
36	P-1	1765	221	257	233	314	8	6.87	7.57	5.62	-2.38	-1.25	-1.94	-4.22	-2.26	-3.43

37	P-2	6048	211	232	236	268	28.61	26.08	25.62	22.56	-6.05	-3.53	-3.06	-5.00	-2.94	-2.55
38	A-1-SB	684	166	180	214	218	4.12	3.81	3.19	3.14	-0.98	-0.67	-0.05	-6.28	-4.31	-0.39
39	P-8	8380	172	165	145	242	48.62	50.92	57.98	34.64	-13.98	-16.29	-23.34	-7.55	-8.73	-12.55
40	A-1	1330	133	147	153	221	10.02	9.06	8.7	6.01	-4.01	-3.05	-2.7	-4.12	-3.14	-2.75
41	B-2	1240	354	332	350	219	3.5	3.74	3.55	5.66	2.16	1.92	2.11	3.43	3.04	3.33
42	P-1	1033	396	388	290	325	2.61	2.67	3.56	3.18	0.57	0.51	-0.38	0.98	0.88	-0.69
43	A-4	1428	296	282	243	268	4.83	5.07	5.88	5.32	0.49	0.25	-0.56	0.39	0.20	-0.49
44	A-5	1428	296	282	243	283	4.83	5.07	5.88	5.04	0.21	-0.03	-0.84	0.20	0.00	-0.69
45	North A.	1218	302	335	256	494	4.03	3.63	4.77	2.47	-0.84	0.15	-2.44	-2.84	-2.16	-4.12
46	East A.	2192	224	249	242	245	9.79	8.81	9.07	8.95	-1.57	-1.17	-0.64	-1.96	-0.59	-0.98
Average (A)														0.30	0.56	0.27
Standard Deviation (SD)														3.42	3.37	4.22
A + 2 × SD														7.15	7.31	8.71
Average[c]														-0.31	-0.13	-0.54

UW-Static analysis equations for shales proposed by authors; SA-SPT *N*-value based input procedure; D-WEAP default damping factors; R-Recommended damping factors; A-Abutment; P-Pier; γQ-Factored load for LRFD; φR-Factored pile resistance; [a]-Potential outlier; and [c]-Statistical parameters calculated by excluding outliers.

6. DEVELOPMENT OF LRFD RESISTANCE FACTORS AND RECOMMENDATIONS

6.1 Introduction

Uncertainties in pile design and construction are incurred from geomaterial sampling, material property estimation, soil disturbance, pile resistance prediction, and field verification. Load and resistance factor design (LRFD) is a probability-based design philosophy used to incorporate uncertainties into the design (Ching and Phoon 2012). LRFD is also known as a reliability-based design (RBD), and it relies on the use of limit states and reliability theory. The reliability theory is used in the determination of factors based on the combined probability of load and resistance looking into the probability of structural failure or the probability of geotechnical failure.

6.2 Calibration of LRFD Resistance Factors

The calibration of LRFD resistance factors is conducted using the First Order Second Moment (FOSM), First Order Reliability Model (FORM), and Monte Carlo Simulation (MCS). The resistance factor (φ) is determined at the target reliability indices (β_T) of 2.33 for a redundant pile group and 3.00 for a non-redundant pile group (Paikowsky et al. 2004; AASHTO 2020). The calibration of φ values requires the statistical summaries: mean and COV along with a best-fit distribution for all random variables involved in a limit state function (Allen et al. 2005). The random variables for this study are pile resistance (R), dead load (Q_D), and live load (Q_L). However, for the dead and live loads, the statistical summaries are presented in Table 6.1. The bias for each observation i is assessed using Equation 6.1:

$$\text{bias}_{(i)} = \frac{y_{(i)}}{\hat{y}_{(i)}} \tag{6.1}$$

where $y_{(i)}$ is the measured resistance for observation i and $\hat{y}_{(i)}$ is the predicted resistance for observation I. The normality of the distribution of the resistance biases is assessed using the Shapiro-Wilk (SW) (1965) test and the Anderson-Darling (AD) (1952) test. If the responses in a sample come from a lognormal distribution, then the logarithm of the responses is assumed to follow a normal distribution. P-values from both SW and AD normality tests are assessed using a level of significance set at 0.05. If the p-value exceeds the level of significance, then there is no evidence against the claim that the responses (original or logarithm) follow a normal distribution.

Table 6.1 Statistical summaries of dead and live loads (Paikowsky et al. 2004)

Statistical parameters	**Dead load (Q_D)**	**Live load (Q_L)**
Mean bias	$\lambda_D = 1.05$	$\lambda_L = 1.15$
Load factor	$\gamma_D = 1.25$	$\gamma_L = 1.75$
Coefficient of variation	$COV_D = 0.1$	$COV_L = 0.2$

6.2.1 First Order Second Moment (FOSM)

FOSM method is used in calibrating LRFD factors through a dataset containing the measured and predicted resistances. The closed form Equation 6.2 is used to calculate φ in terms of mean biases (λ_R, λ_D, and λ_L), dead and live load factors (γ_D and γ_L), and COV bias (COV_R, COV_D, and COV_L) values for R, Q_D, and Q_L (Barker et al. 1991).

$$\varphi = \frac{\lambda_R\left(\frac{\gamma_D Q_D}{Q_L}+\gamma_L\right)\sqrt{\frac{(1+COV_D^2+COV_L^2)}{(1+COV_R^2)}}}{\left(\frac{\lambda_D Q_D}{Q_L}+\lambda_L\right)\exp\left\{\beta_T\sqrt{\ln[(1+COV_R^2)+(1+COV_D^2+COV_L^2)]}\right\}} \quad (6.2)$$

This equation is dependent on the target reliability index and the ratio of dead to live load. The required values of dead load and live load are adopted based on the recommendations by Paikowsky et al. (2004). A dead-to-live load ratio of 2 is chosen for the LRFD calibration (Ng and Sritharan 2016; Haque and Abu-Farsakh 2018). The efficiency of each proposed SA method is evaluated by an efficiency factor ($\varphi/\bar{x}$), which is defined as a ratio of φ to the mean resistance bias ($\bar{x}$) (McVay et al. 2000).

6.2.2 First Order Reliability Model (FORM)

The procedure for the calibration of resistance factor (φ) using FORM is outlined as follows:

- Define the failure equation as the equation used to describe a specific limit state of a system. It is typically the difference between the resistance and load random variables. Failure occurs when the failure equation is less than or equal to zero.
- Choose distribution: This will either be normal or lognormal distribution.
- Choose LRFD factors to analyze: Load factors are typically specified. In FOSM, φ is solved for a target reliability index and the ratio of dead to live load. In FORM, the resistance factor is chosen, and the corresponding reliability index is solved. Hence, there is a need for multiple resistance factors to obtain the target reliability index.
- Partition of the design space: In analyzing the chosen resistance factor, the design space will be partitioned into separate domains.
- Choose representative points for each domain: Equally distributed points within the domain are chosen to define each domain.
- Calculate the initial design point: Each point within each domain is checked individually, starting with the given nominal resistance and dead-to-live ratio.
- Transform into an equivalent normal distribution: An equivalent normal distribution is determined for both the resistance and the load.
- Transform original random variable to standard normal random variables having a mean of 0 and a standard deviation of 1.
- Rewrite the failure equation in terms of the standard normal random variables.
- Compute a new trial design point.
- Calculate the reliability index (β).

6.2.3 Monte Carlo Simulation (MCS)

The procedure for the calibration of resistance factor (φ) using FORM is outlined as follows:

- Generate random numbers for each random variable by using the appropriate statistical summaries. The number of simulations, N, is dependent on the target probability of failure and the coefficient of variation of the results.
- Evaluate the limit state function with the generated values and assume a trial resistance factor, φ.
- Record the number of failures ($g \leq 0$) N_f. The probability of failure, P_f, and reliability index, β_T, can then be calculated as in Equations 6.3 and 6.4:
    - $P_f = \frac{N_f}{N}$ (6.3)

- $\beta_T = \varphi^{-1}(1 - P_f)$ (6.4)
- If the calculated reliability index is different from the target reliability index, β_T, a new trial resistance factor should be assumed. The process is repeated until β_T is achieved.

6.3 Resistance and Efficiency Factors for Fine-Grained Soil-based IGM

The fine-grained IGMs (FG-IGMs) are divided based on their grain size and plasticity into silt-IGMs (ML-IGM) and clay-IGMs (CL-IGM and CH-IGM). Static analysis (SA) methods are discussed in the previous chapter for the prediction of unit shaft resistance (q_s) for piles driven into ML-IGM, CL-IGM, and CH-IGM are given by Equations 3.7, 3.8, and 3.8, respectively. The prediction of unit end bearing resistance (q_b) for piles driven into FG-IGM is given by Equation 3.10.

The normality test results of the proposed SA methods are presented in Table 6.4. SA methods with P-values greater than 0.05 with smaller or comparable loglikelihood values indicate that the resistance biases are a better fit with a lognormal distribution. The resistance biases of using Equations (3.7) and (3.8) for ML-IGM and CL-IGM, respectively, do not follow a normal distribution at the 0.05 level. The resistance and efficiency factors of the proposed SA methods for the q_s and q_b predictions in FG-IGM for target β_T of 2.33 and 3.0 are calculated using both training and testing datasets and summarized in Table 6.3. Resistance and efficiency factors (φ) determined from the more rigorous FORM and MCS methods are higher than that from FOSM. The φ values for the q_s prediction based on the MCS and β_T of 2.33 are 0.43 for CL-IGM, 0.44 for ML-IGM, and 0.80 for CH-IGM. The relatively high value of φ of 0.80 is attributed to the mean bias of 1.13, which is greater than one and a relatively small COV of 0.24. This indicates that Equation 3.9 provides a consistent q_s underprediction of piles in CH-IGM, which results in a relatively high φ value to compensate for the underprediction, matching the q_s values from CAPWAP and achieving the same target β_T. Similarly, the calibration yields a φ value of 0.57 for the q_b prediction in FG-IGM. Compared with the calibrated φ values for β_T=2.33, all φ values for β_T=3.00 reduce, on average, by about 24%, which is comparable to the 20% reduction recommended in AASHTO (2020). The average efficiency factors based on the MCS method are 0.53 and 0.40 for β_T values of 2.33 and 3.00, respectively. They are higher than the average efficiency factors of 0.45 and 0.33 calculated for the α-method for soil and both steel H- and pipe piles (Paikowsky et al. 2004). The proposed SA methods are compared against existing α-methods. A total of 176 FG-IGM layers are included in the assessment of q_s prediction using the α-method. Table 6.2 shows that the resistance biases of the α-method follow a lognormal distribution. The mean resistance bias of 1.26, and a relatively high COV of 0.66, suggesting that the α-method generally underpredicts q_s by about 21%, and any q_s prediction will possess a relatively high uncertainty. The mean resistance bias of 1.99 indicates that the α-method significantly underpredicts the q_b, on average, by about 50%. The mean resistance biases closer to unity, lower COV values, and higher efficiency factors conclude that the proposed SA methods provide a more accurate and consistent prediction of q_s and q_s of steel H- and pipe piles in FG-IGM than the α-method.

Table 6.2 Summary of normality results of the proposed static analysis methods and existing α-method for the estimation of unit shaft resistance and unit end bearing in the fine-grained soil-based IGM

For unit shaft resistance biases									
Steel pile type	SA method	Geo-material	Sample size	P-value for normality test		P-value for lognormality test		Loglikelihood	
				SW test	AD test	SW test	AD test	Normal	Lognormal
H & pipe pile	Equation (3.7)	ML-IGM	41	0.00	0.00	0.10	0.05	-29.82	-22.19
H & Pipe pile	Equation (3.8)	CL-IGM	92	0.00	0.01	0.18	0.08	-38.26	-31.66
H & pipe pile	Equation (3.9)	CH-IGM	43	0.41	0.12	0.26	0.11	-9.97	-10.7
H & Pipe pile	α-method	FG-IGM	176	0.00	0.00	0.35	0.65	-218.59	-178.15
For unit end bearing resistance biases									
H & pipe pile	Equation (3.10)	FG-IGM	27	0.66	0.70	0.10	0.14	-12.11	-13.88
H & pipe pile	α-method	FG-IGM	27	0.24	0.22	0.07	0.05	-34.38	-35.01

SW=Shapiro-Wilk normality test; AD=Anderson-Darling normality test.

Table 6.3 LRFD resistance factors and efficiency factors of the proposed static analysis methods and existing α-method for the estimation of unit shaft resistance and unit end bearing in fine-grained soil-based IGM

SA Method	IGM	Sample size (n)	Mean bias ($\bar{x}$)	COV bias (COV)	FOSM				FORM				MCS			
					β_T=2.33		β_T=3.0		β_T=2.33		β_T=3.0		β_T=2.33		β_T=3.0	
					φ	φ/$\bar{x}$	φ	φ/$\bar{x}$	φ	φ/$\bar{x}$	φ	φ/$\bar{x}$	φ	φ/$\bar{x}$	φ	φ/$\bar{x}$
Unit shaft resistance																
Equation (3.7)	ML-IGM	41	1.07	0.47	0.41	0.38	0.29	0.27	0.44	0.41	0.32	0.30	0.44	0.41	0.31	0.29
Equation (3.8)	CL-IGM	92	0.91	0.41	0.40	0.44	0.29	0.32	0.43	0.47	0.33	0.36	0.43	0.47	0.32	0.35
Equation (3.9)	CH-IGM	43	1.13	0.24	0.69	0.61	0.56	0.50	0.80	0.71	0.66	0.58	0.80	0.71	0.66	0.58
α-method	FG-IGM	176	1.26	0.66	0.31	0.24	0.21	0.16	0.34	0.27	0.22	0.17	0.34	0.27	0.21	0.17
Unit end bearing																
Equation (3.10)	FG-IGM	27	1.07	0.36	0.52	0.49	0.40	0.37	0.57	0.53	0.44	0.41	0.57	0.53	0.43	0.40
α-method	FG-IGM	27	1.99	0.44	0.80	0.40	0.58	0.29	0.88	0.44	0.64	0.32	0.88	0.44	0.63	0.31

COV=Coefficient of variation; φ=Resistance factor; φ/$\bar{x}$=Efficiency factor; β_T=Target reliability index; FOSM=First order second moment; FORM=First order reliability method; MCS=Monte Carlo simulation.

6.4 Resistance and Efficiency Factors for Shale

Shales are classified into soil-based (SS) and rock-based depending on their weathering conditions, mechanical properties, and measured pile resistances. Using those descriptions, the rock-based shale is further classified into three different subgroups: soft & highly weathered shale (HW), moderately hard & moderately weathered to weathered shale (MW), and hard, fresh & slightly weathered shale (SW). New SA methods are proposed in the previous chapter to predict unit shaft resistance (q_s) and unit end bearing (q_b) of piles in shales. The prediction of unit shaft resistance (q_s) for piles driven into SS, HW, MW, and SW are given by Equations 4.4, 4.5, 4.6, and 4.7, respectively. The prediction of unit end bearing resistance (q_b) for piles driven into SS-HW and MW-SW are given by Equations 4.8 and 4.9.

The SW and AD normality tests are conducted to determine an appropriate distribution for modeling resistance biases defined as a ratio of measured pile resistance to predicted pile resistance (Equation 6.1). Table 6.4 shows that neither normal nor lognormal distribution is rejected except q_s for SS shale at which only the lognormal is not rejected, and the comparable loglikelihood values led to the selection of the lognormal distribution following the typical LRFD calibration procedure.

The mean ($\bar{x}$) and COV of resistance bias for each proposed SA equation are calculated and summarized in Table 6.5. Resistance factors and efficiency factors ($\varphi/\bar{x}$) are determined for a target reliability index (β_T), described as the safety associated with a particular probability of failure (p_f). A β_T value of 2.33 (p_f =1%) for a redundant pile group and β_T value of 3.0 (p_f =0.1%) for a nonredundant pile group are adopted (Paikowsky et al. 2004). Table 6.5 generally shows that the $\bar{x}$ values ranging from 0.97 to 1.06 are close to unity, and the COV values from 0.23 to 0.38 are relatively low. In particular, Equation 4.6 for the prediction of q_s in MW shales has the best $\bar{x}$ of 1.02 and the smallest COV of 0.23, which yield the highest φ and $\varphi/\bar{x}$ for all three reliability methods and indexes. Furthermore, Table 6.5 shows that the φ predicted by FOSM is, on average, 10% and 13% lower than that by the FORM and MCS methods for β_T=2.33 and β_T=3.00, respectively. The FORM and MCS methods yield almost identical φ values to the nearest 0.05 for both reliability indexes. The φ values for β_T=3.00 are, on average, 23%, 19%, and 21% lower than that for β_T=2.33 based on FOSM, FORM, and MCS, respectively. These differences agree with the 20% reduction in φ values for β_T=3.00 recommended in AASHTO (2020). The φ values based on the MCS and β_T=2.33 vary from 0.45 to 0.74, which are higher than the 0.35 for α-method and 0.45 for the Canadian Geotechnical Society method (AASHTO 2020). The average $\varphi/\bar{x}$ values based on MCS are 0.6 and 0.47 for β_T values of 2.33 and 3.00, respectively. The average $\varphi/\bar{x}$ of the SA methods for q_s is slightly higher than that for q_b. The $\varphi/\bar{x}$ values of our proposed SA methods are higher than the average $\varphi/\bar{x}$ of 0.45 and 0.33 calculated for the α-method for soils and both steel H-piles and pipe piles, respectively (Paikowsky et al. 2004).

Table 6.4 Summary of normality tests for the proposed static analysis methods for the estimation of unit shaft resistance and unit end bearing in shales

For unit shaft resistance biases									
Steel pile type	SA method	Geo-material	Sample size	P-value for normality test		P-value for lognormality test		Loglikelihood	
				SW test	AD test	SW test	AD test	Normal	Lognormal
H-pile & $12^{3}/_{4}$ shell	Equation (4.4)	SS	27	0.02	0.05	0.18	0.08	NA	-7
H-pile & $12^{3}/_{4}$ shell	Equation (4.5)	HW	23	0.36	0.48	0.38	0.58	-9.1	-8.4
H-pile & $12^{3}/_{4}$ shell	Equation (4.6)	MW	31	0.16	0.23	0.55	0.37	11.1	11.9
H-pile & $12^{3}/_{4}$ shell	Equation (4.7)	SW	35	0.19	0.32	0.21	0.37	27.1	27.9
For unit end bearing resistance biases									
H-pile & $12^{3}/_{4}$ shell	Equation (4.8)	SS-HW	28	0.15	0.23	0.24	0.43	-6.82	-6.8
H-pile & $12^{3}/_{4}$ shell	Equation (4.9)	MW-SW	36	0.16	0.1	0.38	0.23	1.8	4.3

N–Sample size; SS–IGM soil-based shale; HW–Soft & highly weathered shale; MW–Moderately hard & weathered shale; SW–Hard & slightly weathered shale; SS-HW–Soil based, soft & highly weathered shale; MW-SW–Moderately hard to hard & weathered to slightly weathered shale; SW–Shapiro-Wilk normality test; AD–Anderson-Darling normality test; and NA-Not applicable.

Table 6.5 LRFD resistance factors and efficiency factors of the proposed static analysis methods for the estimation of unit shaft resistance and unit end bearing in shales

SA Method	IGM	Sample size (n)	Mean bias ($\bar{x}$)	COV bias (COV)	FOSM				FORM				MCS			
					β_T=2.33		β_T=3.0		β_T=2.33		β_T=3.0		β_T=2.33		β_T=3.0	
					φ	φ/$\bar{x}$	φ	φ/$\bar{x}$	φ	φ/$\bar{x}$	φ	φ/$\bar{x}$	φ	φ/$\bar{x}$	φ	φ/$\bar{x}$
Unit shaft resistance																
Equation (4.4)	SS	27	1.01	0.33	0.51	0.51	0.39	0.39	0.57	0.57	0.45	0.45	0.57	0.57	0.44	0.44
Equation (4.5)	HW	23	0.97	0.38	0.45	0.46	0.34	0.35	0.49	0.51	0.38	0.39	0.49	0.51	0.37	0.38
Equation (4.6)	MW	31	1.02	0.23	0.64	0.63	0.50	0.49	0.73	0.72	0.62	0.61	0.74	0.73	0.61	0.60
Equation (4.7)	SW	34	1.06	0.32	0.56	0.53	0.43	0.41	0.62	0.58	0.50	0.47	0.62	0.58	0.49	0.46
Unit end bearing																
Equation (4.8)	SS-HW	28	0.98	0.32	0.52	0.53	0.4	0.41	0.57	0.58	0.46	0.47	0.57	0.58	0.45	0.46
Equation (4.9)	MW-SW	36	1.02	0.29	0.57	0.56	0.45	0.44	0.64	0.63	0.52	0.51	0.64	0.63	0.51	0.50

7. SUMMARY, CONCLUSIONS, AND RECOMMENDATIONS

7.1 Summary

The report presents the details on the development of LRFD recommendations for piles driven into IGMs, specifically for fine-grained IGM (FG-IGM) and shale. A classification method is first proposed for IGMs. Thereafter, static analysis (SA) methods for predicting pile resistances in the IGMs are developed. In addition, the changes in shaft resistance (q_s) and end bearing (q_b) as a function of time and undrained shear strength (s_u) are investigated for FG-IGM and different weathered shales in terms of setup A factors. The report also considered the effect of weathering on the driven pile resistance predictions and the investigation of time-dependent pile responses in shales. The accuracy of the dynamic analysis method for pile resistance measurement in IGM is validated and improved. An economic impact study is conducted to compare the performance of the dynamic analysis method in terms of the number of piles, pile lengths, and steel weights. LRFD resistance factors for piles in IGMs are developed. Finally, changes and improvements to current pile design and construction practices are recommended.

7.2 Conclusions

The following conclusions are drawn from this study:

- A classification method is proposed to differentiate fine-grain soil and FG-IGM. Fine-grained, soil-based geomaterials with $s_u \geq 2.7$ ksf are classified as FG-IGM so that the uncertainties associated with the design methods and characterization of IGM can be addressed during pile design. To further improve the prediction accuracy of q_s in FG-IGM, FG-IGM is categorized into silt-based IGM and clay-based IGM based on grain size. Both silt-based IGM and clay-based IGM are further categorized based on plasticity.
- Shales are classified into soil-based shale and rock-based shale based on the field description. The soil-based (SS) shale includes soft to hard clayey shale and silty shale. Depending on the weathering conditions and engineering properties, rock-based shales are further classified into soft & highly weathered shale (HW), moderately hard & weathered shale (MW), and hard & slightly weathered shale (SW).
- The comparisons of q_s and s_u for all FG-IGM types show that q_s increase with the increase in s_u, and the increase in q_s reduces when the s_u is greater than about 10 ksf, especially in the clay-based IGM.
- The stress-strain behaviors of SS, HW, MW, and SW shales under uniaxial compression indicate unique characteristics in the post-failure region. In the post-failure region, these SS-HW shale groups behave either perfectly elastic-plastic for small strain or more ductile failure with an M/E ratio of less than one. However, the M/E ratios for all MW-SW shales are more than one, which indicates these shales exhibit more brittle failures than the SS-HW shales.
- The q_s of driven piles increase rapidly with q_u and level off at a critical q_u due to slippage along the pile-shale interface and plastic behavior of shale. The q_s of rock-based shales decrease with the increase in weathering conditions. SA methods are proposed for predicting q_s with 0.19 ksf $\leq q_s \leq$ 3.78 ksf and 2.18 ksf $\leq q_u \leq$ 126 ksf for shales with no interbedded rock layers. For predicting q_b SS-HW is applicable for 39 ksf $\leq q_b \leq$ 182 ksf and 3.23 ksf $\leq q_u \leq$ 52 ksf, and MW-SW is applicable for 35 ksf $\leq q_b \leq$ 384 ksf and 3.23 ksf $\leq q_u \leq$ 124 ksf.
- The SS shale exhibits setup while the rock-based shales exhibit both setup and relaxation in q_s. The average setup A factor of 0.76 is determined for steel H-piles in SS shales. Piles in HW shale exhibit a higher setup in q_s with an average A factor of 0.36 and a lower setup factor of 0.22 in MW. Piles in SW exhibit the relaxation in q_s with an average A factor of -0.004. Piles

in the SS and HW shale exhibit setup in q_b with average A factors of 0.53 and 0.48, respectively. Piles in the MW and SW shales exhibit both setup and relaxation in q_b. The MW shale exhibits an average setup factor of 0.11, and the SW shale exhibits an average relaxation factor of -0.07.

- The validation of the proposed SA methods using an independent pile dataset confirms the performance of the proposed SA methods in the prediction of q_s and q_b.
- The proposed SA methods with mean biases closer to unity, smaller COV of resistance biases, and higher efficiency factors provide a more accurate and consistent estimation of q_s and q_b of piles in IGMs than the existing α-method.
- For each proposed WEAP method, a back-analysis procedure is adopted to determine damping factors for H-piles driven into soil-based shales and rock-based shales for three weathering conditions. The back-calculated damping factors ranged from 0.009 to 0.297 s/ft for WEAP-SA-R and 0.02 to 0.266 s/ft for WEAP-UW-R. SS and HW shales exhibit higher mean damping factors, and the mean damping factors decrease with a decrease in weathering conditions (i.e., from HW to SW shales).
- At the EOD condition using the SA input procedure and back-calculated damping factors, WEAP-SA-R overpredicts the R_U, on average, by about 4.2%. WEAP-UW-R underpredicts the R_U, on average, by about 2.9% and has the lowest COV. However, the WEAP-SA-D underpredicts the R_U, on average, by about 14.5% with the highest COV. At the BOR condition, the WEAP-SA-R and WEAP-UW-R overpredict the pile resistance, on average, by 5.3%. However, the WEAP-SA-D underpredicts the pile resistance, on average, by 7.4%. The best R_U prediction from WEAP-UW-R is attributed to the more accurate static analysis to predict q_s and q_p of shales and the application of back-calculated damping factors for shales.
- The economic impact study reveals that the three WEAP methods, on average, overpredict the number of piles and result in excess steel weights during the construction stage. The average excess steel weight per unit load are -0.31 lb/kips, -0.13 lb/kips, and -0.54 lb/kips for WEAP-SA-R, WEAP-UW-R, and WEAP-SA-D, respectively. WEAP-UW-R provides the best construction control method that yields the lowest excess steel weight and the smallest difference in the number of piles.
- LRFD resistance factors of the proposed static analysis methods for the prediction of unit shaft resistance and unit end bearing in FG-IGM ranged between 0.34 – 0.88 at a target reliability index of 2.33 and between 0.21 – 0.66 at a target reliability index of 3.00. For shales, the resistance factors for the estimation of both unit shaft resistance and unit end bearing range are between 0.49 – 0.74 at a target reliability index of 2.33 and between 0.37 – 0.61 at a target reliability index of 3.00**.**

7.3 Recommendations

- While pile setup can be considered in the prediction of q_s, it is recommended that pile setup be neglected in the prediction of q_b.
- The pile construction control method should be included to determine any pile relaxation in FG-IGM and to evaluate the time-dependent q_s response in rock-based shales.
- WEAP methods and the respective LRFD resistance factors can be considered as the construction control method.
- Pile restrike should be performed to close any potential gap below a pile tip.
- Due to the variability of the natural shale materials and time-dependent responses, the calculated average A factors for q_s and q_b are for comparison purposes but are not recommended for design implementation.

REFERENCES

AASHTO. (2020). AASHTO LRFD Bridge Design Specifications 9th Edition U.S. Customary Units. American Association of State Highway and Transportation Officials (AASHTO), Ishington, D.C.

Abu-Farsakh, M. Y., and Haque, N. (2020). "Modified Time Factor to Estimate the Duration of Pile Setup." *Geotechnical and Geological Engineering*, Springer, 38(6), 5787–5804.

Abu-Hejleh, N. M., O'Neill, M. W., Hanneman, D., and Attwooll, W. J. (2005). "Improvement of the geotechnical axial design methodology for Colorado's drilled shafts socketed in weak rocks." *Transportation Research Record*, SAGE Publications Sage CA: Los Angeles, CA, 1936(1), 100–107.

Adhikari, P., Gebreslasie, Y. Z., Ng, K. W., and Wulff, S. S. (2019). "Performance Assessment of Wave Equation Analysis for Driven Steel H-Piles in IGM." *DFI Journal*, 13(1).

Adhikari, P., Ng, K. W., Gebreslasie, Y. Z., and Wulff, S. S. (2020a). "Improved α-and β-Methods for the Estimation of Shaft Resistance of Steel-H Piles Driven into Intermediate Geomaterials." *Geo-Congress 2020: Foundations, Soil Improvement, and Erosion*, Reston, VA: American Society of Civil Engineers, 114–123.

Adhikari, P., Ng, K. W., Gebreslasie, Y. Z., and Wulff, S. S. (2020b). "Static and Economic Analyses of Driven Steel H-Piles in IGM Using the WyoPile Database." *Journal of Bridge Engineering*, American Society of Civil Engineers, 25(5), 4020016.

Adhikari, P., Ng, K.W., Gebreslasie, Z.Y., Wulff, S.S. and Sullivan, T. (2020c). "Geomaterial Classification Criteria for Design and Construction of Driven Steel H-Piles." *Canadian Geotechnical Journal*, 57(4), 616-621.

Agung, P., Pramusandi, S., and Damianto, B. (2017). "Identification and classification of clayshale characteristic and some considerations for slope stability." *African Journal of Environmental Science and Technology*, Academic Journals, 11(4), 163–197.

Akaike, H. (1974). "A new look at the statistical model identification." *IEEE transactions on automatic control*, Ieee, 19(6), 716–723.

Allen, T.M. (2005). Development of Geotechnical Resistance Factors and Downdrag Load Factors for LRFD Foundation Strength Limit State Design. Final Report FHWA-NHI-05-052, Federal Highway Administration, U.S. Department of Transportation, Ishington, D.C.

Anderson T.W., and Darling, D.A. (1952). "Asymptotic Theory of Certain 'Goodness-of-fit Criteria based on Stochastic Processes." *The Annals of Mathematical Statistics*, 23,193-212.

Ashford, S. A., and Jakrapiyanun, W. (2001). "Drivability of glass FRP composite piling." *Journal of Composites for Construction*, American Society of Civil Engineers, 5(1), 58–60.

ASTM. (2002). *Standard Test Method for Determining Rock Quality Designation (RQD) of Rock Core. ASTM Standard D6032-02*. ASTM International.

ASTM. (2005). *Standard Test Methods for Laboratory Determination of Water (Moisture) Content of Soil and Rock by Mass: ASTM D 2216-05*. ASTM International.

Authier, J., and Fellenius, B. H. (1980). "Quake values determined from dynamic measurements." *Proceedings of the First International Seminar on Application of Stress-Wave Theory to Piles, H. Bredenberg Editor, AA Balkema, Rotterdam*, 197–216.

Barrett, J. W., and Prendergast, L. J. (2020). "Empirical shaft resistance of driven piles penetrating weak rock." *Rock Mechanics and Rock Engineering*, Springer, 53(12), 5531–5543.

Bartoskewitz, R. E., and Coyle, H. M. (1970). *Wave Equation Prediction of Pile Bearing Capacity Compared with Field Test Results*. Research Report 125-5, Texas Transportation Institute, Texas A&M University, College Station, Texas.

Beake, R. H., and Sutcliffe, G. (1980). "Pipe pile drivability in the carbonate rocks of the southern Arabian Gulf." *Proceedings of Conference on Structural Foundations on Rock, Sydney,Australia.*

Rotterdam, Netherlands: A.A. Balkema.
Becker, D., and Moore, I. (2006). *Canadian Foundation Engineering Manual*.
Belbas, R. E. J. (2014). "The capacity of driven steel H-piles in lacustrine clay, till and karst bedrock: a Winnipeg case study." MS thesis, Department of Civil Engineering, University of Manitoba, Winnipeg, Canada.
Bjerrum, L. (1967). "The third Terzaghi lectures; Progressive failure in slopes of overconsolidated plastic clay and clay shales." *Journal of the Soil Mechanics and Foundations Division*, American Society of Civil Engineers, 93(5), 1–49.
Cherblanc, F., Berthonneau, J., Bromblet, P., and Huon, V. (2016). "Influence of water content on the mechanical behaviour of limestone: Role of the clay minerals content." *Rock Mechanics and Rock Engineering*, Springer, 49(6), 2033–2042.
Ching, J., and Phoon, K. K. (2012). "Value of geotechnical site investigation in reliability-based design." *Advances in Structural Engineering*, 15(11), 1935–1945.
CIRIA. (2002). *C574 Engineering in Chalk*. Ciria, London.
Coduto, D. P. (1999). *Geotechnical Engineering: Principles and Practices*.
Coyle, H. M., Foye Jr, R., and Bartoskewitz, R. E. (1973). "Wave Equation Analysis Of Instrumented Test Pile." *Offshore Technology Conference*, Offshore Technology Conference, Houston, Texas.
Deo, P. (1972). "Shales as embankment materials." Purdue University.
Doherty, P., and Igoe, D. (2013). "A Driveability Study of Precast Concrete Piles in Dense Sand." *DFI Journal-The Journal of the Deep Foundations Institute*, Taylor & Francis, 7(2), 3–16.
Eid, H. T. (2006). "Factors influencing determination of shale classification indices and their correlation to mechanical properties." *Geotechnical & Geological Engineering*, Springer, 24(6), 1695.
Erguler, Z. A., and Shakoor, A. (2009). "Quantification of fragment size distribution of clay-bearing rocks after slake durability testing." *Environmental & Engineering Geoscience*, Association of Environmental & Engineering Geologists, 15(2), 81–89.
Forehand, P. W., and Reese, J. L. (1964). "Prediction of pile capacity by the wave equation." *Journal of the Soil Mechanics and Foundations Division*, ASCE, 90(2), 1–26.
Gamble, J. C. (1971). "Durability-plasticity classification of shales and other argillaceous rocks." Ph. D. thesis, University of Illinois.
Goble, G. G., and Rausche, F. (1976). *Wave Equation Analysis of Pile Driving: WEAP Program*. Volume II. User's Manual (No. FHWA/IP-76-14.2 Final Rpt.).
Gu, Y., Wei, H.-L., and Balikhin, M. M. (2018). "Nonlinear predictive model selection and model averaging using information criteria." *Systems Science & Control Engineering*, Taylor & Francis, 6(1), 319–328.
Hannigan, P. J., Goble, G. G., Likins, G. E., and Rausche, F. (2006). *Design and Construction of Driven Pile Foundations Reference Manual–Volume II. Publication No*. FHWA NHI-05-043. National Highway Institute. Federal Highway Administration.
Hannigan, P., Ryberg, A., and Moghaddam, R. . (2020). "Identification and quantification of pile relaxation." *Proceedings of DFI 44th Annual Conference on Deep Foundations*, Chicago, IL.
Haque, M. N., Abu-Farsakh, M. Y., Tsai, C., and Zhang, Z. (2017). "Load-testing program to evaluate pile-setup behavior for individual soil layers and correlation of setup with soil properties." *Journal of Geotechnical and Geoenvironmental Engineering*, American Society of Civil Engineers, 143(4), 4016109.
Hawkins, A. B., and McConnell, B. J. (1992). "Sensitivity of sandstone strength and deformability to changes in moisture content." *Quarterly Journal of Engineering Geology and Hydrogeology*, Geological Society of London, 25(2), 115–130.
Hopkins, T. C., and Deen, R. C. (1984). "Identification of shales." *Geotechnical Testing Journal*, ASTM International, 7(1), 10–18.
Hsu, S.-C., and Nelson, P. P. (2002). "Characterization of eagle ford shale." *Engineering Geology*,

Elsevier, 67(1–2), 169–183.
Irvine, J., Terente, V., Lee, L. T., and Comrie, R. (2015). "Driven pile design in weak rock." *Proc. Int. Symp. on Frontiers in Offshore Geotechnics III*, ISFOG 2015, 569–574.
Iskander, M. G., and Stachula, A. (2002). "Wave equation analyses of fiber-reinforced polymer composite piling." *Journal of Composites for Construction*, American Society of Civil Engineers, 6(2), 88–96.
Islam, M. S. (2021). "Pile behaviors in shales through full-scale static load testing, dynamic testing, and finite element analysis." MS thesis, Dept. of Civil and Architectural Engineering, Univ. of Wyoming.
Islam, M. S., Ng, K. W., and Wulff, S. (2022a). "Prediction of Driven Pile Resistances in Shales Considering Weathering and Time Effects." *Canadian Geotechnical Journal*, (ja).
Islam, M. S., Ng, K., and Wulff, S. S. (2022b). "Improved Wave Equation Analysis of Steel H-Piles in Shales Considering LRFD and Economic Impact Studies." *Journal of Bridge Engineering*, *27*(6), 04022039.
James, G., Witten, D., Hastie, T., and Tibshirani, R. (2013). *An Introduction to Statistical Learning*. Springer.
Kivi, I. R., Ameri, M., and Molladavoodi, H. (2018). "Shale brittleness evaluation based on energy balance analysis of stress-strain curves." *Journal of Petroleum Science and Engineering*, Elsevier, 167, 1–19.
Korb, K. W., and Coyle, H. M. (1969). *Dynamic and Static Field Tests on a Small Instrumented Pile*. Texas Transportation Institute, Texas A & M University.
Kulhawy, F. H., and Mayne, P. W. (1990). *Manual on Estimating Soil Properties for Foundation Design*. Electric Power Research Inst., Palo Alto, CA (USA); Cornell University, Ithaca
Likins, G. E., and Hussein, M. (1984). "Relaxation Of H Piles In Shale." *Lecture notes, Pile Driving Analyser Users Days, Stockholm*.
Likins, G., and Rausche, F. (2004). "Correlation of CAPWAP with static load tests." *Proceedings of the Seventh International Conference on the Application of Stresswave Theory to Piles*, Citeseer, 153–165.
Long, J., and Anderson, A. (2012). *Improved Design for Driven Piles on a Pile Load Test Program in Illinois*.
Long, J., and Anderson, A. (2014). *Improved Design for Driven Piles Based on a Pile Load Test Program in Illinois: Phase 2.* Illinois Center for Transportation.
Long, J. H. (2016). *Static Pile Load Tests on Driven Piles into Intermediate-Geo Materials.* University of Illinois at Urbana-Champaign. Dept. of Civil Engineering.
Long, J., and Horsfall, J. (2017). "Static Pile Load Tests on Driven Piles in Intermediate Geo Materials." Project 0092-12-08, Research Brief, Wisconsin Highway Research Program, February, Madison, WI.
Long, J. H., Kerrigan, J. A., and Wysockey, M. H. (1999). "Measured time effects for axial capacity of driven piling." *Transportation Research Record*, SAGE Publications Sage CA: Los Angeles, CA, 1663(1), 8–15.
Martin, C. D. (2015). "Behaviour of shales in underground environments." *13th ISRM International Congress of Rock Mechanics*, Montreal, Canada.
Masud, N. B., Ng, K. W., Wulff, S. S., and Johnson, T. (2022). "Driven Piles in Fine-Grained Soil-Based Intermediate Geomaterials." *Journal of Bridge Engineering*, *27*(6), 04022037.
McVay, M. C., and Kuo, C. L. (1999). *Estimate Damping and Quake by Using Traditional Soil Testing*. Department of Civil Engineering, University of Florida, Gainesville, FL, USA.
Mohamadi, M. (2015). "Experimental and Constitutive Investigation of the Thermo-Hydro-Mechanical Behavior of Shales: A Case Study of the Colorado Clay Shale." University of Calgary (Canada).
Mokwa, R. L., and Brooks, H. (2008). *Axial Capacity of Piles Supported on Intermediate*

Geomaterials. Montana. Dept. of Transportation. Research Programs.
Morgano, C. M., and White, B. A. (2004). "Identifying soil relaxation from dynamic testing." *Proceedings of the Seventh International Conference on the Application of Stresswave Theory to Piles*, 415–421.
Morton, T. S. (2012). "Assessing Driven Steel Pile Capacity on Rock Using Empirical Approaches."
Ng, K., Adhikari, P., and Gebreslasie, Y. Z. (2019). *Development of load and resistance factor design procedures for driven piles on soft rocks in Wyoming*. Wyoming. Dept. of Transportation.
Ng, K., and Sullivan, T. (2017a). "Challenges and recommendations for steel H-piles driven in soft rock." *Geotech. Eng.*, 48(3), 1–10.
Ng, K. W., Roling, M., Abdel Salam, S. S., Suleiman, M. T., and Sritharan, S. (2013a). "Pile setup in cohesive soil. I: Experimental investigation." *Journal of Geotechnical and Geoenvironmental Engineering*, American Society of Civil Engineers, 139(2), 199–209.
Ng, K. W., Suleiman, M. T., and Sritharan, S. (2013b). "Pile setup in cohesive soil. II: Analytical quantifications and design recommendations." *Journal of Geotechnical and Geoenvironmental Engineering*, American Society of Civil Engineers, 139(2), 210–222.
Ng, K. W., and Sullivan, T. (2017b). "Recent development of load and resistance factor design (LRFD) for driven piles on soft rock." *Geo-Risk 2017*, 307–316.
Ng, K. W., Yasrobi, S. Y., and Sullivan, T. A. (n.d.). "Current Limitations and Challenges of Driven Piles in Rock as Demonstrated using Three Case Studies in Wyoming." *IFCEE 2015*, 500–517.
Paikowsky, S. G. (2004). *Load and Resistance Factor Design (LRFD) for Deep Foundations*. Transportation Research Board.
Paikowsky, S. G., Birgisson, B., McVay, M., Nguyen, T., Kuo, C., Baecher, G., Ayyub, B., Stenersen, K., O'Malley, K., and Chernauskas, L. (2004). "Load and resistance factor design (LRFD) for deep foundations, NCHRP Report 507." *Transportation Research Board, Ishington, DC*, 76.
Peiris, T. A., Morris, B., Kelly, R., and Chan, K. (2010). "Methodology to demonstrate pile capacity in relaxing ground."
Pile Dynamics, I. (2010). *GRLWEAP Manual for Windows*. 30725 Aurora Road, Cleveland, OH 44139 USA: PDI.
Poon, B., McKay, G., Chan, K., and Castañeda, L. R. (2017). "Dynamic load testing of 2 meter steel tubular piles driven into foliated phyllite bedrock." *Proceedings of DFI-PFSFPiled Foundation and Ground Improvement Technology for the Modern Building and Infrastructure Sector*.
Raines, R. D., Ugaz, O. G., and O'Neill, M. W. (1992). "Driving characteristics of open-toe piles in dense sand." *Journal of Geotechnical Engineering*, American Society of Civil Engineers, 118(1), 72–88.
Ramey, G. E., and Hudgins, A. P. (1977). "Sensitivity and Accuracy of the Pile Wave Equation." *Ground Engineering*, 10(7), 45–47.
Rausche, F., Nagy, M., and Likins, G. (2008). "Mastering the art of pile testing." *In Proceedings of the 8th International Conference on the Application of Stress Wave Theory to Piles, J. A. Santos, 1932*, Lisbon, Portugal, September 810. Amsterdam, The Netherlands: IOS., 19–32.
Rausche, F., Nagy, M., Webster, S., and Liang, L. (2009). "CAPWAP and refined wave equation analyses for driveability predictions and capacity assessment of offshore pile installations." *International Conference on Offshore Mechanics and Arctic Engineering*, 375–383.
Rausche, F., Thendean, G., Abou-matar, H., Likins, G. E., and Goble, G. G. (1997). *Determination of pile driveability and capacity from penetration tests.Volume I*. Report No. FHWA-RD-96-179, McLean, Va.: Federal Highway Administration.
Rehnman, S., and Broms, B. B. (1971). "Bearing capacity of piles driven into rock." *Canadian Geotechnical Journal*, NRC Research Press, 8(2), 151–162.
Samson, L., and Authier, J. (1986). "Change in pile capacity with time: case histories." *Canadian Geotechnical Journal*, NRC Research Press, 23(2), 174–180.
Schneider, J. A., and Harmon, I. A. (2010). "Analyzing drivability of open ended piles in very dense

sands." *DFI Journal-The Journal of the Deep Foundations Institute*, Taylor & Francis, 4(1), 32–44.
Schwarz, G. (1978). "Estimating the dimension of a model." *The Annals of Statistics* 6 (2), 461–464." *URL: http://dx. doi. org/10.1214/aos/1176344136*.
Skov, R., and Denver, H. (1988). "Time-dependence of bearing capacity of piles." *Proc. Third International Conference on the Application of Stress-Wave Theory to Piles. Ottawa*, 25–27.
Smith, E. A. (1960). "Pile-driving analysis by the wave equation." *American Society of Civil Engineers Transactions*, 86(4), 35–61.
Smith, T., Banas, A., Gummer, M., and Jin, J. (2011). *Recalibration of the GRLWEAP LRFD resistance factor for Oregon DOT. No. FHWA-OR-RD-11-08).* Research Unit, Oregon Department of Transportation.
Soliman, M., Walter, D., Crabtree, B., and Lee, A. (2018). "Driven Steel Piles in Clay Shale on Northeast Anthony Henday Drive in Edmonton." *71st Canadian Geotechnical Conference and the 13th Joint CGS/IAH-CNC Groundwater Conference*, Edmonton, Alberta, Canada.
Stark, T. D., Long, J. H., and Assem, P. (2013). *Improvement for Determining the Axial Capacity of Drilled Shafts in Shale in Illinois.* Illinois Center for Transportation.
Stevens, R. F., Wiltsie, E. A., and Turton, T. H. (1982). "Evaluating pile driveability for hard clay, very dense sand, and rock." *Proceedings of the 14th Annual Offshore Technology Conference*, Houston, USA, 465–469.
Ta, A.-N., and Hammann, M. (2013). "Application Of Adjusted Wave Equation Analysis For Optimized Pile Acceptance Criteria." *Advances in Soil Mechanics and Geotechnical Engineering*, 230–233.
Talal, A.-B. (2013). "The impact of water content and ionic diffusion on the uniaxial compressive strength of shale." *Egyptian Journal of Petroleum*, Elsevier, 22(2), 249–260.
Team, R. C. (2013). "R: A language and environment for statistical computing." Vienna, Austria.
Terente, V., Irvine, J., Comrie, R., and Crowley, J. (2015). "Pile driving and pile installation risk in weak rock." *Proceedings of European Conference on Soil Mechanics & Geotechnical Engineering XVI*, September 2015, Edinburgh, UK, DOI:10.1201/b18442-73, 1187–1192.
Thompson, C. D., and Thompson, D. E. (1985). "Real and apparent relaxation of driven piles." *Journal of Geotechnical Engineering*, American Society of Civil Engineers, 111(2), 225–237.
Tomlinson, M., and Woodward, J. (2014). *Pile Design and Construction Practice*. CRC Press.
Tutluoğlu, L., Öge, İ. F., and Karpuz, C. (2015). "Relationship between pre-failure and post-failure mechanical properties of rock material of different origin." *Rock Mechanics and Rock Engineering*, Springer, 48(1), 121–141.
Underwood, L. B. (1967). "Classification and identification of shales." *Journal of the Soil Mechanics and Foundations Division*, ASCE, 93(6), 97–116.
Wang, S. R., Hagan, P., Li, Y. C., Zhang, C. G., Liu, X. L., and Zou, Z. S. (2017). "Experimental study on deformation and strength characteristics of sandstone with different water contents." *Journal of Engineering Science and Technology Review*, 10(4), 199–203.
Yagiz, S. (2001). "Overview of classification and engineering properties of shales for design considerations." *Construction and Materials Issues 2001*, 156–165.
Ziogos, A. (2020). "Investigation of the interface shearing resistance of steel and concrete on different rocks for renewable energy gravity foundation applications." University of Dundee, Dundee, UK.